UNIVERSITÀ DEGLI STUDI DI TRENTO

Dipartimento di Ingegneria e Scienza dell'Informazione

Corso di Laurea in
Ingegneria dell'Informazione e delle Comunicazioni

Elaborato finale

Assessment of Image Quality of Waveform-Encoded Synthetic Aperture Radar Using Real Data

Supervisore
Prof. Lorenzo Bruzzone

Laureando
Luca Dell'Amore

Co-Supervisore
Dr. Michelangelo Villano (DLR)

Anno accademico 2017/2018

Acknowledgments

Alla mia Famiglia

This thesis is the result of seven months of research activity in the Microwave and Radar Institute of the German Aerospace Center (DLR) in Oberpfaffenhofen, Germany. A special thank must go to my supervisor Michelangelo Villano for his wise guide and the professionalism shown during my internship. Moreover, I would also thank Professor Lorenzo Bruzzone for the opportunity given to me and the wonderful experience, as well as all the colleagues, in which I have found friends before working partners.

Trento, February 2019
Luca Dell'Amore

Abstract

Synthetic aperture radar (SAR) remote sensing is very attractive for the systematic observation of dynamic processes on the Earth's surface since it allows high resolution imaging independently of weather conditions and sunlight illumination. Nevertheless, many limitations due to the SAR geometry, such as nadir returns and range ambiguities, typically constrain the *PRF* selection while designing conventional SAR systems, thus limiting both their swath width and their ambiguity performance.

In this context, waveform-encoded SAR is a novel SAR concept based on pulse-to-pulse variation of the transmitted waveform that allows focusing the nadir echo and the range ambiguities and suppressing them through a multi-focus post-processing.

However, the assessment of the ambiguity suppression performance for such a system is not trivial, as the processing involves a non-linear thresholding and blanking approach. This work proposes a novel methodology, which exploits real TerraSAR-X data to accurately simulate the effect of the range ambiguity on the useful signal and allows for a quantitative assessment of the image quality of a waveform-encoded SAR. The method considers different waveform variation schemes on transmit, i.e. cyclically-shifted and up- and down- chirps, as well as a multi-focus post-processing for suppressing range ambiguities. Specifically, a contrast-minimization technique for threshold selection is investigated, as well as the best achievable performance, i.e. optimal threshold.

The results of this work further highlight the potentialities of the waveform-encoded SAR concept and also allow accounting for its ambiguity suppression capability in the design of novel SAR systems, as an increased system design flexibility can be achieved at the reasonable cost of employing different waveforms on transmit.

List of Figures

List of Tables

Contents

1 Introduction

In the last decades, Synthetic Aperture Radar (SAR) remote sensing [13] has become of great interest for the scientific community, because of its capability to provide a high resolution imaging independently from daylight, weather conditions and cloud coverage. In particular, the satellite systematic estimation and long-term monitoring of dynamic processes on the Earth's surface has become very attractive, resulting in the investigation of novel SAR concepts to improve the performance and the flexibility in SAR systems design. In this context, several techniques for achieving high-resolution and wide-swath imaging [16][6][8][1][19] are being investigated, as well as several methods for suppressing nadir returns and range ambiguities, as they typically constrain the *PRF* selection in conventional SAR systems design, thus limiting both the swath width and the ambiguity performance of such systems. In the following, the problem is introduced and the objectives of this work are reported.

1.1 Motivation, Objectives and Structure of the Thesis

A big challenge for future spaceborne remote sensing missions is now turning to the exploitation of novel SAR concepts capable of increasing the ambiguity suppression capabilities of conventional SAR systems, thus reducing the system design complexity. Generally, the radar antenna must be designed in order to avoid azimuth and range ambiguities as well as nadir returns; however, satisfying some system requirements, such as the swath width and the azimuth resolution, is not always possible, as several constraints on the *PRF* selection are assumed while designing the system, in order to control these just mentioned ambiguities.

In this context, the waveform-encoded SAR concept [20][21] has been investigated, based on pulse-to-pulse variation of the transmitted waveform. This novel concept is born for nadir returns suppression [20], exploiting the continuous variation of waveforms on transmit and the use of different matched filters in the processing, thus allowing relaxing the constraints on the selection of an optimized *PRF*. In this thesis, this concept has been extended to the case of range ambiguities suppression [21], yielding to a significant improvement in the image quality, with remarkable benefits in the design of novel SAR systems, as an increased system design flexibility can be achieved at the reasonable cost of employing different waveforms on transmit. Moreover, the practical realization of the technique is quite simple, as only a multi-focus post-processing is required in order to remove range ambiguities, as consequence of continuously changing the transmitted waveform from pulse-to-pulse.

The assessment of the ambiguity suppression performance, thus of the resulting image quality, for such a waveform-encoded SAR system is therefore of great interest for the scientific community, as its range ambiguity suppression capability could be accounted for in the design of novel SAR systems, allowing extending the proposed concept also to the case of high-resolution wide-swath SAR systems. In particular, this work proposes a novel methodology, which exploits real TerraSAR-X data to accurately simulate the effect of the range ambiguity on the useful signal and allows for a quantitative assessment of the ambiguity suppression capability for a typical L-band system, thus motivating the present master thesis. The method has considered different waveform variation schemes on transmit, i.e. cyclically-shifted and up- and down- chirps, as well as a multi-focus post-processing with a thresholding and blanking approach for suppressing range ambiguities. Specifically, a contrast-minimization technique for threshold selection has been investigated, as well as the best achievable performance, i.e. optimal threshold. Moreover, the investigation of the processing performance dependency on the range ambiguity power, as well as on the considered scenario, is an interesting goal for understanding in which situation the proposed method can be more or less efficient.

The thesis is structured as follows. Section 2 provides a short review of the SAR remote sensing basic principles, including the procedure of image formation and the required signal processing to retrieve the data from the received echoes. Also, an introduction to the problem is proposed, focusing on the origin of the main ambiguities due to the SAR geometry, together with a description of the corresponding limitations in SAR system design. The waveform-encoded SAR concept is thus presented in Section 3, followed by a detailed description of the sequences of waveforms used, as well as the explanation of the considered multi-focus post-processing for suppressing range ambiguities. The proposed methodology for quantitative assessing the ambiguity suppression capability of such a system is reported in Section 4. The data set used for the analyses is introduced, as well as a specific explanation of the threshold selection procedure for performance assessment is provided, together with a description of the performance measures used for the evaluations. The results of the simulations with real TerraSAR-X data are discussed in Section 5: an experiment assuming a sample case study is specifically described, also reporting the resulting system and processing performance. Furthermore, the ambiguity suppression capability of this technique is discussed, dependently on the range ambiguity power, as well as on the considered scenario. Finally, conclusions are drawn in Section 6, where an outlook for further research is also provided.

2 Synthetic Aperture Radar Remote Sensing

Synthetic Aperture Radar (SAR) remote sensing is very attractive for the systematic observation of dynamic processes on the Earth's surface since it allows high resolution imaging independently of weather conditions and sunlight illumination. The effective long "synthetic" antenna generated by the coherent reception of the radar echoes allows an improvement of the resolution, while the use of microwaves makes possible all-weather imaging independently of clouds, fog and precipitations. SAR covers several fields of application, ranging from geoscience and climate change research, environmental and Earth system monitoring, 2-D and 3-D mapping, change detection, 4-D mapping (space and time) up to planetary exploration [13].

2.1 Geometry, Image Formation and Processing

SAR exploits the motion of the radar over a target region and provides finer spatial resolution than conventional beam-scanning radars. The antenna is mounted on a forward moving platform, typically a spacecraft or an aircraft. The radar system has a side-looking imaging geometry and transmits electromagnetic pulses with high energy in order to receive the backscattered signal echoes in a sequential way [13]. The radar can be monostatic, if the receiving antenna is the same as the transmitting one, or bi- or multi-static, if the transmitting and receiving antennas are different.

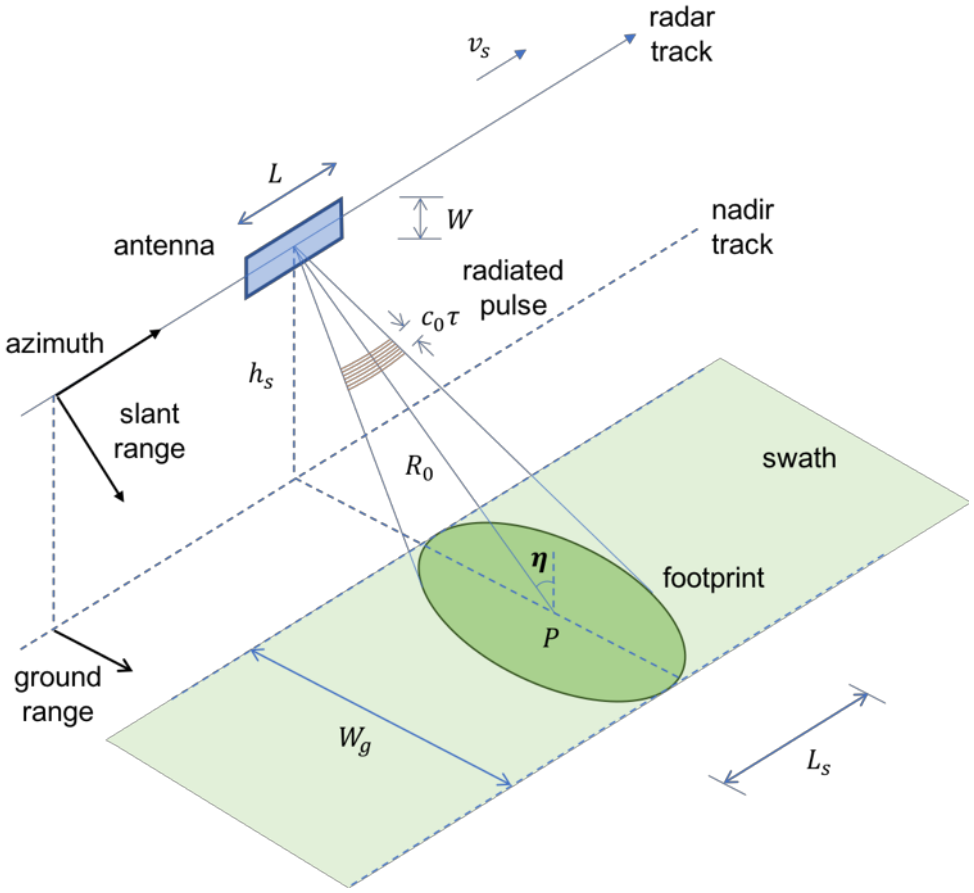

Figure 1: Simplified SAR imaging geometry [17].

Figure 1 shows the simplified SAR imaging geometry. The platform moves with constant speed v_s and at constant height h_s along the azimuth (or along-track) direction. The line-of-sight is denoted as slant range (or cross-track), while its projection on the ground is identified as ground range direction. Usually, the antenna transmits electromagnetic pulses with a constant pulse repetition frequency (*PRF*), which varies depending on the application and the system: it can range from few hundred Hertz considering airborne systems up to few thousands Hertz for spacecrafts. The radiated pulses length along the slant range direction is given by $c_0\tau$, as they travel at constant speed c_0, i.e. speed of light in free space, for a duration τ. As direct implication, also the corresponding echoes are characterized by a duration τ and will return back to the radar with a time delay of $2R_0/c_0$ (Round Trip Time) after transmission, if a point-like scatterer at distance R_0 is considered. Because of the antenna main beam, most of the transmitted energy is directed to the footprint, but only a portion of this energy is backscattered to the radar: specifically, the amplitude and phase of the echo are strictly related to the physical, i.e. geometry and roughness, and electrical properties, i.e. permittivity, of the target. Moreover, the extent of the footprint is directly proportional to the radar wavelength λ and distance R_0 while inversely proportional to the antenna size, both in ground range direction

$$W_g = \frac{\lambda R_0}{W \cos\eta} \tag{1}$$

and along the azimuth one

$$L_s = \frac{\lambda R_0}{L} \tag{2}$$

In particular, η denotes the incidence angle, while λ is the radar wavelength. Generally, this last one determines the penetration efficiency of the electromagnetic pulse: more penetration will occur as the wavelength increases. The most commonly frequency bands used for SAR systems are shown in Table 1 with the corresponding frequency and wavelength ranges. As the platform changes its position, the corresponding footprint moves, covering a strip on the ground denoted as swath. Usually, its extent depends on the application and on the radar system: if the radar antenna is mounted on an aircraft, the swath can range from few kilometers up to 20 km depending on the application, while considering the spacecraft case it varies from 30 to 500 km.

Frequency Band	Ka	Ku	X	C	S	L	P
Frequency [GHz]	40-25	17.6-12	12-7.5	7.5-3.75	3.75-2	2-1	0.5-0.25
Wavelength [cm]	0.75-1.2	1.7-2.5	2.5-4	4-8	8-15	15-30	60-120

Table 1: Commonly used frequency bands for SAR systems and the corresponding frequency and wavelength ranges [13].

Currently, the operating SAR systems are able to acquire in different imaging modes (Figure 2) by changing the orientation of the radiation pattern; in more details, a planar antenna is divided into sub-apertures and the phase and amplitude of each of these ones are controlled by using typically few hundreds transmit/receive modules (TRM). The most common imaging mode is known as Stripmap: the antenna pattern images a single continuous strip on the ground as it is fixed to one single swath. This is the case of the simplified SAR geometry in Figure 1. With SAR, also two other acquisition modes are possible, if a wider swath or a better azimuth resolution are required. In the ScanSAR mode, the antenna pattern successively changes its elevation angle in order to cover multiple sub-swaths; each

of them is illuminated by multiple pulses, but for a shorter time compared to the Stripmap case. The illumination timing is set in order to cyclically repeat the imaging of multiple continuous sub-swaths, thus leading to a degraded azimuth resolution [13]. If a better azimuth resolution is required, another imaging mode known as Spotlight is used: a given target is illuminated over long time by steering the antenna pattern in azimuth. Therefore, a better resolution can be achieved as the radar synthetic aperture increases. However, acquiring in the Spotlight mode results in the impossibility to image a single continuous strip. Hence, changing the imaging mode a better azimuth resolution is limited by the degradation of the swath width and vice versa. This restriction can be overcome by using multi-channel digital beamforming techniques, but this will not be treated in this dissertation.

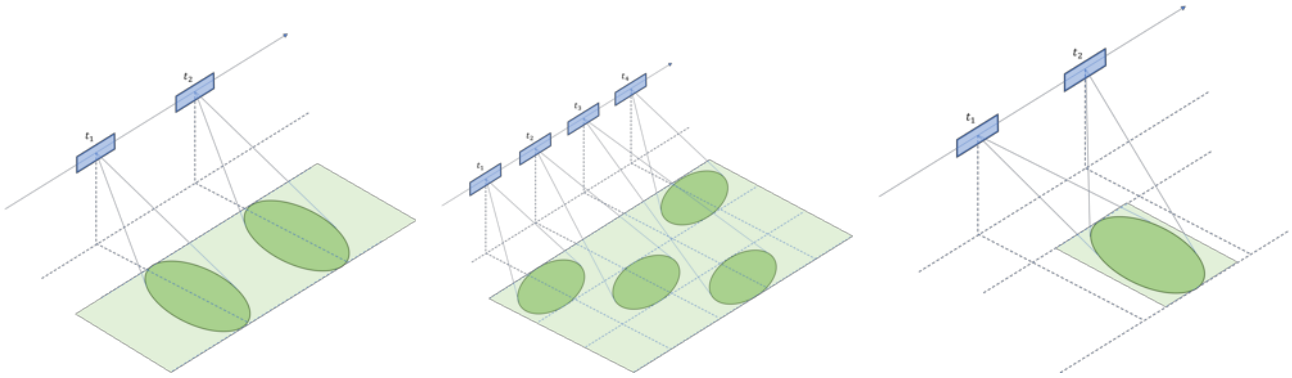

(a) (b) (c)

Figure 2: Illustration of the three different SAR imaging modes. (a) Stripmap. (b) ScanSAR. (c) Spotlight.

The principle of the synthetic aperture was not used until the 50s. In the past, imaging radars, denoted as side-looking airborne radars (SLAR), were characterized by an azimuth resolution which deteriorated as the target range increased. This resolution was directly proportional to the antenna beamwidth $\Theta_a = \lambda/L$ along the azimuth direction and to the slant range distance R_0 of the target from the radar

$$\delta x = \frac{\lambda}{L} R_0 = \Theta_a R_0 \tag{3}$$

where L corresponds to the antenna length. The limitation represented by the low azimuth resolution has been overcome from the beginning of 50s by using coherent radars, able to retain both the amplitude and phase of the echo signal, and exploiting the principle of Doppler beam sharpening [22]. When, in the following years, this concept, based on the Doppler effect, was extended to the principle of the synthetic aperture [3], imaging radars improved their azimuth resolution up to half the azimuth antenna length independently of the target distance.

$$\delta x = \frac{L}{2} \tag{4}$$

Similarly to conventional radars, a sequence of pulses, i.e. electromagnetic waves, is transmitted and the backscattered echoes are then collected by the radar. Specifically, after pulse transmission every pulse repetition interval (*PRI*) seconds, i.e. *PRI = 1/PRF* where *PRF* denotes the pulse repetition frequency, an *echo window* time allows "listening" to the scattered echoes and thus storing the received signals on-board [13]. In the case of SAR, as the platform moves, a coherent radar is required in order to combine the received signals and to construct a much longer virtual aperture, as shown in Figure 3. Therefore, the backscattered echoes are arranged side-by-side in a two-dimensional matrix representing the scene reflectivity, called raw data, whose coordinates correspond to time delay (slant range axis) and pulse number (azimuth axis). The focused SAR data, i.e. the two-dimensional map

of the surface backscatter, is thus obtained after two linear filtering operations along both the range and azimuth dimensions. The different targets appear in the radar image with different intensities depending on the backscattering strength: high backscattered signals appear as bright spots, while flat smooth surfaces are identified as dark areas. As already mentioned, the processing to be applied to the raw data can be split into two separate parts concerning both the range and azimuth dimensions.

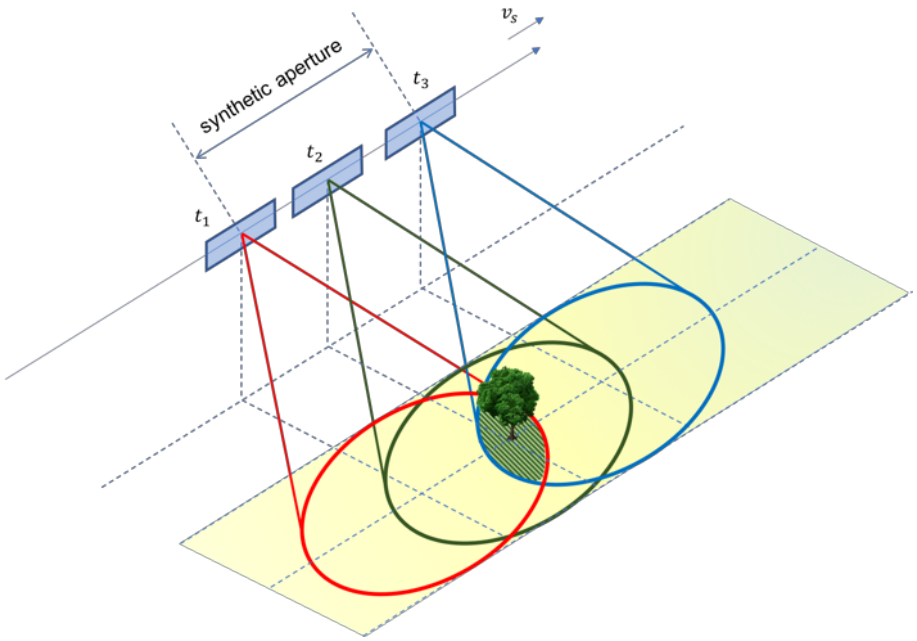

Figure 3: Synthetic aperture generation.

When referring to the slant range dimension, the received echo *r(t)* from a point-like target at distance R_0 from the radar is a delayed, attenuated and phase-shifted version of the baseband waveform *s(t)* radiated by the antenna. Moreover, it is usually corrupted by an additive white Gaussian noise (AWGN) contribution *n(t)*, added at the receiver. Thus, the processing requires the use of a linear, time-invariant filter in order to compress the received energy in slant range and to maximize the output signal-to-noise ratio (*SNR*) of the system. This filter is known as "matched filter" and is characterized by an impulse response

$$h(t) = s^*(-t) \tag{5}$$

where * identifies complex conjugation. As far as the slant range resolution is concerned (Figure 4), it does not depend on the distance between the target and the radar; specifically, two targets can be distinguished only if the last part of the echo from the nearer one is received before the first part of the echo from the more distant target. However, if a rectangular input waveform is employed on transmit, the achievable slant range resolution δR is given by half the distance covered by the radar pulse (the factor 2 appears because of the two-way path from transmission to reception), thus resulting to be proportional to the pulse duration τ, i.e. the shorter the pulse, the better the resolution.

$$\delta R \cong \frac{c_0 \tau}{2} \tag{6}$$

As a consequence, since the pulse duration τ is directly proportional to both the radiated energy and the SNR after matched filtering, a better resolution results of course in a lower SNR. In order to overcome this dependency problem, SAR sensors commonly use linear frequency modulated (LFM)

pulsed waveforms, known as ”chirps”. The chirp signal is a complex signal of the form

$$s(t) = \exp\left(j\pi B\frac{t^2}{\tau}\right)\mathrm{rect}\left(\frac{t}{\tau}\right) \tag{7}$$

and is usually characterized by constant amplitude during the pulse duration τ and quadratic phase variation, with a linear increasing or decreasing frequency depending on up or down chirp. Specifically, the instantaneous frequency changes in a linear manner over time t according to $f_i = k_r t$, where k_r is denoted as chirp rate, yielding the bandwidth $B = k_r\tau$ [13]. In this way, if assuming a large time-bandwidth product $B\tau$, i.e. chirp compression ratio, the achievable slant range resolution δR becomes inversely proportional to the chirp bandwidth according to

$$\delta R = \frac{c_0}{2B} \tag{8}$$

Furthermore, the ground range resolution δR_g can be obtained from δR by considering the incidence angle η

$$\delta R_g = \frac{\delta R}{\sin(\eta)} \tag{9}$$

and therefore varies across the swath, as different incidence angles can be observed inside it [17].

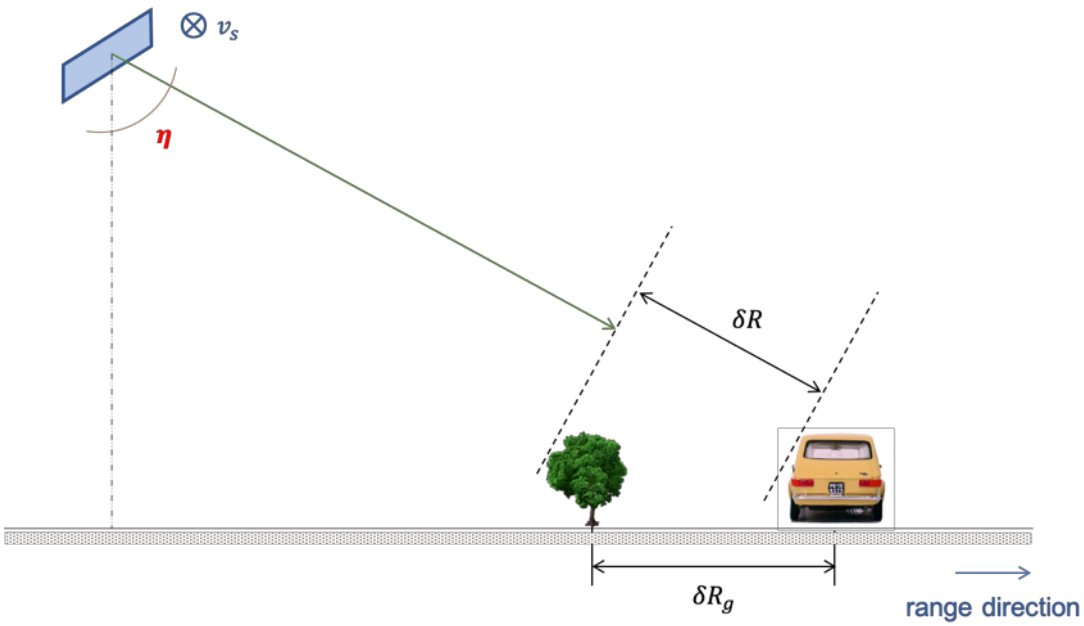

Figure 4: Range resolution. It does not depend on the distance between the target and the radar.

As far as the azimuth dimension is concerned, if no further processing is performed, the resolution δx is provided by the construction of the synthetic aperture, i.e. the path length during which the radar receives echo signals from a point target [13]. Specifically, the extent of the radar beam in azimuth is given by $\delta x = L_s = \frac{\lambda}{L}R_0 = \Theta_a R_0$, leading to a very poor resolution. However, as shown in Figure 5, echoes coming from different azimuth angles φ with respect to the radar track are characterized by different instantaneous Doppler frequency shifts f_D, which can be defined under the assumption of small angle φ as

$$f_D = \frac{2v_s\sin(\varphi)}{\lambda} \cong \frac{2v_s x}{\lambda R_0} \tag{10}$$

From the Doppler analysis, it follows that the azimuth resolution δx is related to the Doppler frequency

resolution δf_D. Using the equation in (10) and assuming the Doppler frequency resolution δf_D to be equal to the reciprocal of the illumination time under the synthetic aperture

$$T_{ill} = \frac{L_s}{v_s} = \frac{\lambda R_0}{v_s L} \tag{11}$$

the azimuth resolution becomes

$$\delta x \cong \frac{\lambda R_0}{2v_s}\delta f_D = \frac{\lambda R_0}{2v_s}\frac{1}{T_{ill}} = \frac{\lambda R_0}{2v_s}\frac{v_s L}{\lambda R_0} = \frac{L}{2} \tag{12}$$

As direct implication, a radar with a shorter antenna "sees" a target on the ground for a longer time, thus constructing an equivalent longer virtual antenna and yielding to a finer azimuth resolution. As the platform moves, the distance between the radar and a target on the ground, described by its coordinates $(x, y, z) = (x_0, 0, \Delta h)$, can be obtained at any time t by simply applying the Pythagoras's theorem

$$R(t) = \sqrt{{R_0}^2 + (v_s t)^2} \approx R_0 + \frac{(v_s t)^2}{2R_0} \quad \text{for} \quad v_s t/R_0 \ll 1 \tag{13}$$

where R_0 denotes the minimum distance in slant range between the radar and the target, at time $t = t_0 = 0$. Furthermore, assuming a distance R_0 much larger than vt during the illumination time T_{ill} allows expanding *R(t)* into a Taylor series and approximating it as in (13) [13]. As a consequence, as the radar footprint passes over the target, the azimuth phase varies in a parabolic way over the two-way path from radar to target, according to $\Delta\varphi(t) = -4\pi\Delta R(t)/\lambda$.

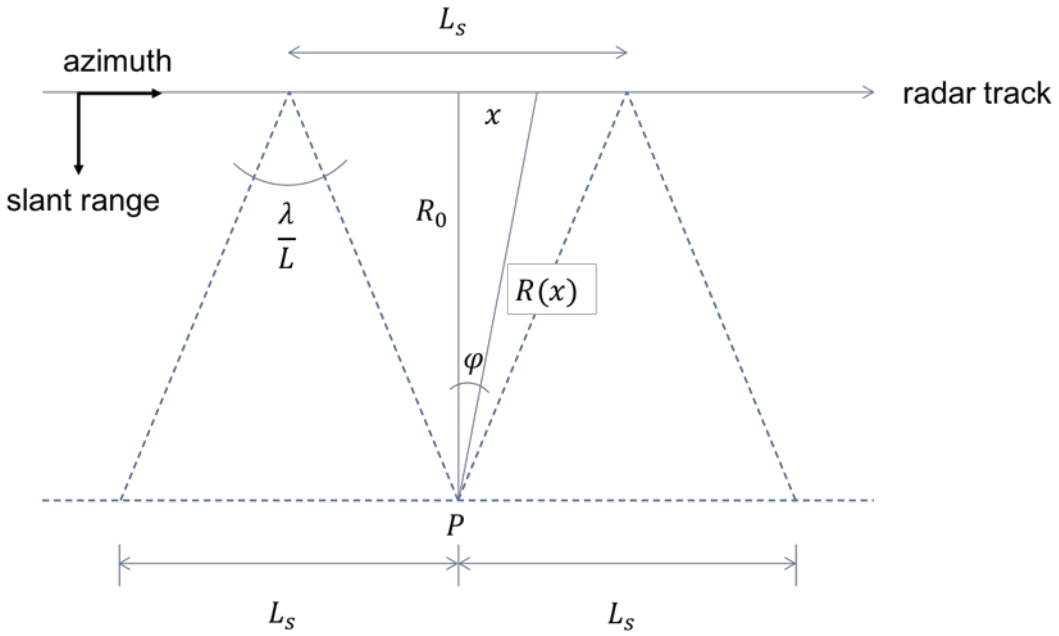

Figure 5: Synthetic aperture [17].

Another implication is related to the phenomenon of *Range Cell Migration* (RCM). Specifically, the response from a fixed scatterer in the range-compressed data results to be curved and spreads over different range cells [17], because of a distance change, given by

$$RCM(t) = \sqrt{R_0^2 + (v_s t)^2} - R_0 \approx \frac{(v_s t)^2}{2R_0} \tag{14}$$

between the radar antenna and any fixed scatterer on the ground, within the synthetic aperture. In

particular, if not corrected, when $RCM_{max} = RCM(t = T_{ill}/2) > \delta R/2$, i.e. the point-like target energy is distributed over several range cells, RCM results in an azimuth defocusing.

During the illumination time T_{ill} and under the synthetic aperture L_s, the echoes energy is received from the target, and it is thus demodulated, sampled and stored inside the SAR signal memory, forming a two-dimensional data matrix (raw data) of complex samples. Each sample is always characterized by real and imaginary parts, representing the amplitude and phase values, respectively. The first dimension of the raw data matrix identifies the range direction (or fast time, alluding to the velocity of the electromagnetic waves travelling at the speed of light); in particular, when the echo from each pulse is received, it is recorded into one line of the SAR signal memory, corresponding to a constant azimuth position. Furthermore, as the platform moves, whenever it travels a distance $v_s \cdot PRI$ the echo from a given target shifts in range, and it is recorded into the next range line of the memory, thus forming the second dimension of the raw data, i.e. the azimuth dimension (or slow time, alluding to the movement of the platform). As it is not possible to get any useful information on the scene from the raw SAR data, a signal processing is required to compress the echoes energy, in order to obtain a focused image. As already mentioned, the processing to be applied can be split into two separate matched filtering operations, along both the range and azimuth dimensions. First of all, the transmitted chirp signals are compressed to short pulses of high resolution: this is done in the frequency domain because of the much lower computational load, as multiplication between each range line and the complex conjugate of the transmitted chirp spectrum (matched filter). Specifically, the matched filter performs a cross-correlation operation between the received signal and a copy of the transmitted one, i.e. pulse or range compression operation, producing an equivalent strong and sharp output of high resolution only when the phase structure of the received signal is well matched with the reference one. This results in a range compressed image revealing only information about the relative distance between the radar system and any point on the ground. The range compressed data is then convolved with the azimuth reference function, i.e. azimuth compression operation, defined as the time reverse complex conjugate of the expected response from a point-like target on the ground, in order to obtain the focused SAR image. As the distance *R(t)* changes within the synthetic aperture, because of the platform movement, also the azimuth phase varies according to $4\pi R(t)/\lambda$. In particular, the frequency variation of the azimuth signal, defined by computing the instantaneous azimuth frequency as the time differentiation of the azimuth phase

$$f_D = -\frac{1}{2\pi}\frac{\partial}{\partial t}\frac{4\pi}{\lambda}R(t) = -\frac{2v_s^2}{\lambda R_0}t \tag{15}$$

results to be similar to that one in the range domain. It is also denoted as Doppler frequency and varies linearly with time t; as shown in (15), the azimuth-frequency rate $2v_s^2/\lambda R_0$ is inversely proportional to the slant range R_0, thus depending on the acquisition geometry. Figure 6 shows the just described SAR processing steps to be applied to the raw SAR data matrix, in order to obtain the focused SAR image.

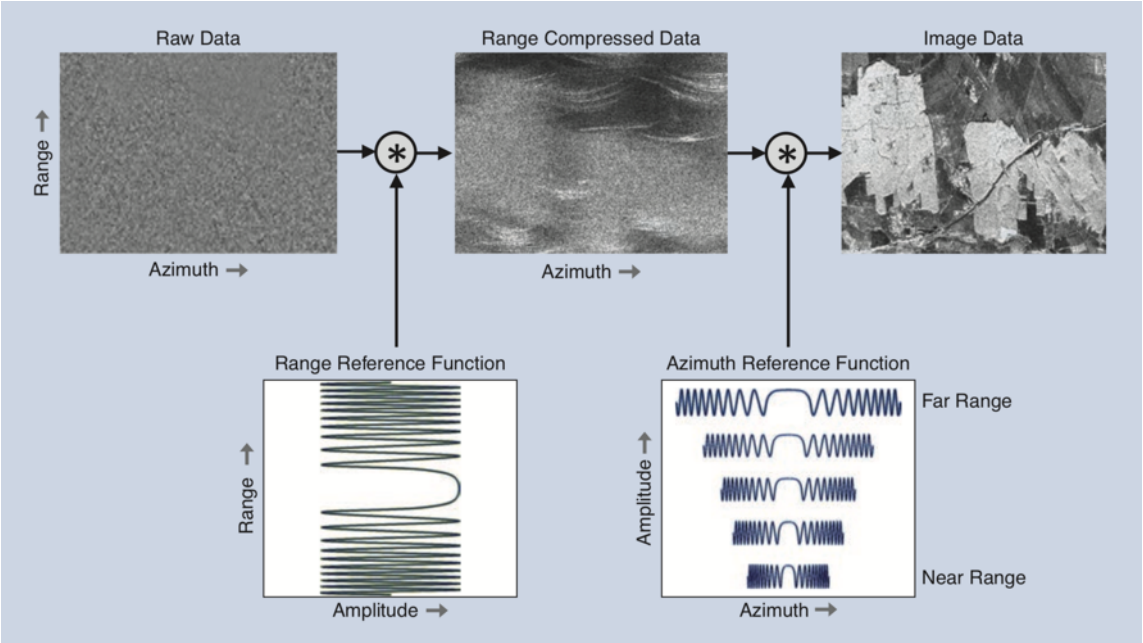

Figure 6: SAR processing steps. Firstly, the range compressed data is obtained after a convolution operation between the raw data and the range reference function, in the time domain. In a second step, the range compressed image is convolved with the azimuth reference function, thus obtaining the focused SAR image. Here, the "$*$" denotes the convolution operation in the time domain [13].

SAR images are typically displayed in terms of intensity values in order to give an information about the reflectivity of the corresponding target on the ground. As a consequence, two additional steps, i.e. calibration and geocoding, are required. Specifically, calibration ensures the coincidence between the intensity values in the raw data and the reflectivity values σ_0 corresponding to the radar cross section normalized to area, while geocoding directly associates the pixels location in the SAR image to the correct position on the ground.

In order to assess the system performance, a quantitative measure of the signal processing quality can be derived by investigating the two-dimensional (2-D) impulse response function (IRF) of the SAR system. It is basically the two-dimensional complex image obtained if only a point-like scatterer is present in the scene. First of all, the 2-D IRF presents a mainlobe which defines the slant range and azimuth resolutions as half-power widths in the two orthogonal directions (slant range and azimuth), respectively. Moreover, also sidelobes are of interest, as they damage the image quality and may mask weak scatterers. As a consequence, two parameters, i.e. the peak sidelobe ratio (*PSLR*) and the integrated sidelobe ratio (*ISLR*), are investigated in order to quantify the signal processing quality; these ones can be reduced by amplitude weighting the transfer function of the matched filters during the processing both in range and azimuth, but degrading the resolution [17].

One of the most challenging aspect of SAR focusing is related to the signal sampling. Along the range dimension, the received echoes are sampled with a sampling rate larger than the transmitted chirp bandwidth according to the Shannon's sampling theorem. In azimuth, of course the sampling rate is equal to the *PRF*; however, as the spatial sample spacing must be smaller than half of the antenna length, i.e. the azimuth resolution,

$$v_s \cdot PRI \leq \frac{L}{2} \tag{16}$$

the employed *PRF* must be larger than the signal Doppler bandwidth, defined as

$$PRF \geq B_D = \frac{2v_s}{L} \tag{17}$$

Therefore, it becomes clear that the sampling frequencies in both range and azimuth dimensions depend on the required resolutions. An improvement of the range resolution results in a larger chirp bandwidth and thus in an increased data rate on board the platform. Differently, a better azimuth resolution leads to a larger Doppler bandwidth and therefore to a higher sampling rate, i.e. higher *PRF*, but reducing the echo window time during which the radar "listens" to the scattered echoes, and thus the swath width.

Typically, SAR images are corrupted by a consistent noise, denoted as *speckle*, due to the presence of many elemental scatterers with a random distribution within a resolution cell. The total complex reflectivity is thus given by the coherent sum of the amplitudes and phases of each elemental scatterer i

$$\Phi = \sum_i \sqrt{\sigma_i} \exp(j\varphi_i^{scatt}) \exp\left(-j\frac{4\pi}{\lambda} R_{0,i}\right) \tag{18}$$

leading to strong backscattering fluctuations from resolution cell to resolution cell. Speckle appears when the radar wavelength is comparable to the surface roughness and is characterized by a multiplicative nature: as its variance increases with the intensity, it cannot be reduced by transmitting a more powerful signal. However, speckle can be attenuated performing a non-coherent averaging of the intensity image [2][14]; this technique is known as *multi-look* and considerably improves the interpretability of the SAR image despite it causes a degradation of the image resolution.

2.2 Range Ambiguities and Nadir Returns

When speaking about SAR, one important limitation has to be considered. As a consequence of the pulsed operation and side-looking geometry, some undesirable echoes coming from different transmitted pulses return back to the radar at the same time of the echos of interest, during the acquisition process. The most common ambiguity corresponds to the nadir returns, i.e. the echoes propagating from the closest point to the radar.

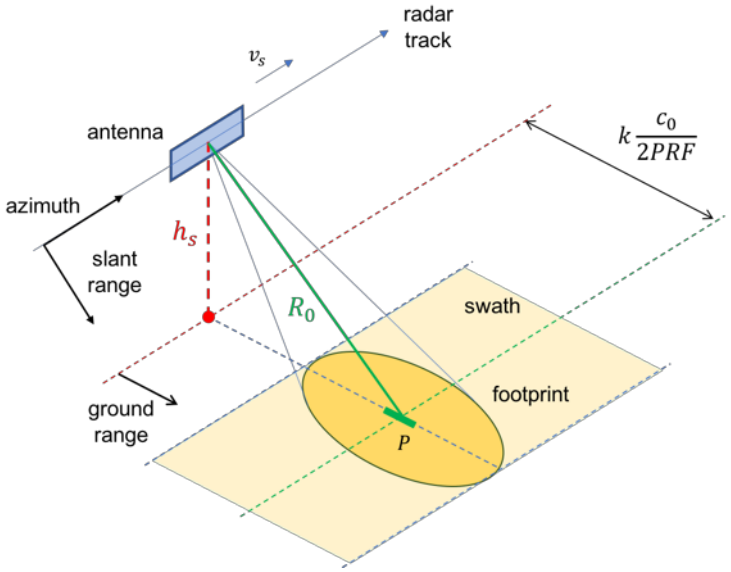

(a)

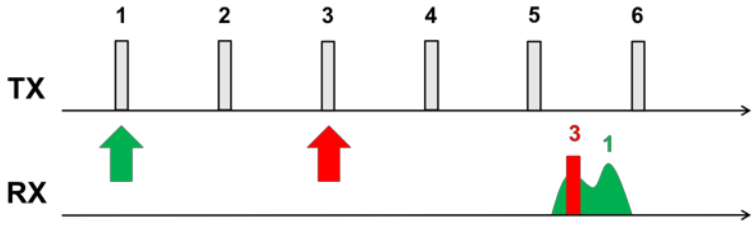

(b)

Figure 7: SAR acquisition geometry (a) responsible for the superimposition (b) between the the swath echos of interest, here in green, and the nadir return, here in red.

Figure 7 shows the simplified SAR acquisition geometry responsible for the superimposition between echos coming from a scatterer placed at the nadir and from a scatterer in the scene at slant range R_0, respectively. In more details, denoting as h_s the platform height, if the following condition

$$R_0 = h_s + k\frac{c_0}{2PRF} \tag{19}$$

is verified, where k is an integer number, the echoes coming from subsequent transmitted pulses and propagating from the nadir arrive back at the radar simultaneously with the echoes of interest. As the nadir echo comes from the shortest slant range R corresponding to a null incidence angle, it may be stronger than the desired returns, strongly corrupting the SAR image quality. The nadir return appears as a bright stripe in the image (Figure 8), with a constant range position, as it always corresponds to the same distance. The nadir interference constraint typically limits both the swath width and the ambiguity performance of the SAR system and is usually avoided by constraining the *PRF* selection in the SAR system design [20].

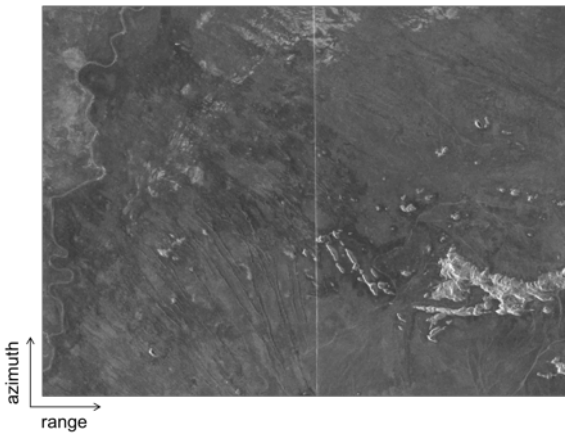

Figure 8: Example of nadir echo in a SAR image, acquired by the TerraSAR-X satellite over Australia. The nadir return is identified by a bright vertical stripe, corresponding to a constant range position, in the middle of the image. The horizontal and vertical axes represent slant range and azimuth, respectively [21].

As well as nadir returns, also the so-called range ambiguities may significantly affect the quality of the acquired SAR image. They correspond to antecedent and subsequent echoes arriving back at the the radar simultaneously with the desired swath return. Figure 9 shows the simplified geometry responsible for the generation of range ambiguities.

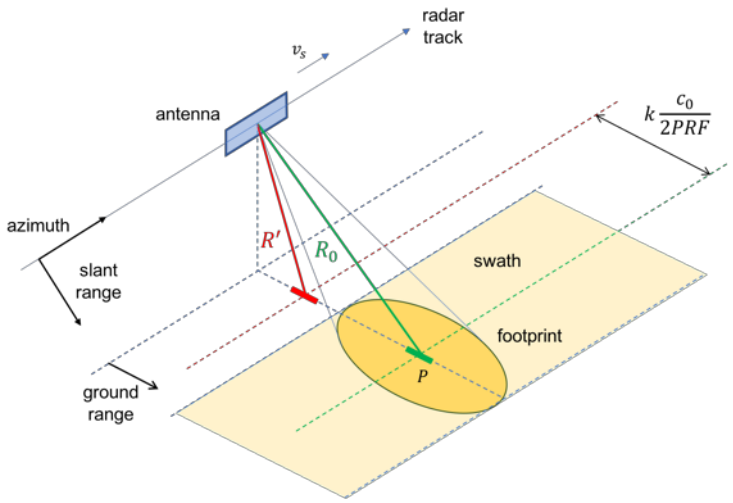

(a)

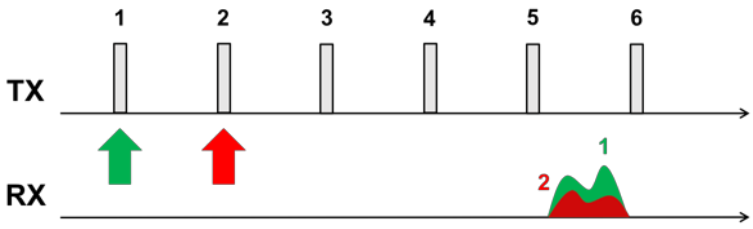

(b)

Figure 9: SAR acquisition geometry (a) responsible for the generation of range ambiguities. In (b), the undesirable echoes (in red) corresponding to the range ambiguity are superimposed to the swath echoes of interest (in green), despite they correspond to a different transmitted pulse.

Differently from nadir returns, where the ambiguous echo comes from only one scatterer placed at the nadir, when being in presence of range ambiguities, the desired swath scene, at slant range R_0 is corrupted by an entire superimposed image, corresponding to slant range positions given by the following equation

$$R^{'} = R_0 + k\frac{c_0}{2PRF} \tag{20}$$

where k is an integer number. For understanding better range ambiguities, Figure 10 shows a very interesting example, where the mountains image is superimposed to the lake one. As the mountains correspond to different ranges, according to (20), compared to the lake, the two scenes result to be superimposed, causing ambiguity and strongly affecting the quality of the acquired image. This phenomenon is mainly relevant for spaceborne SAR systems, where several pulses are transmitted after a given pulse before receiving its echo [17].

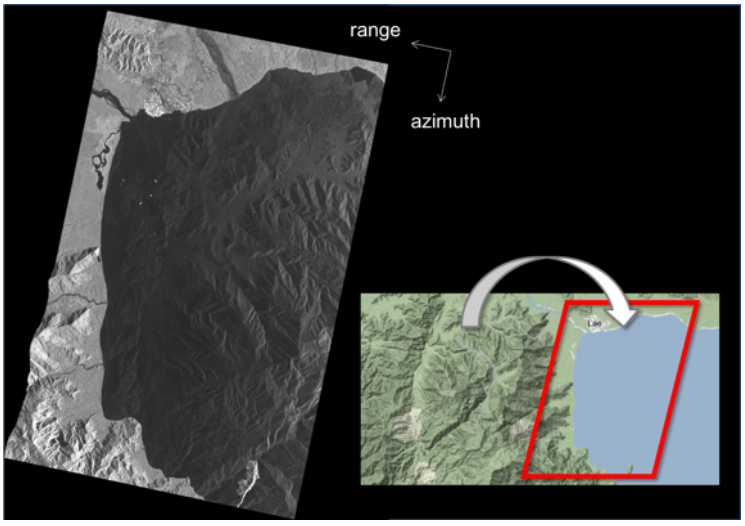

Figure 10: Example of a range ambiguity in a SAR image. Here, the mountains image is superimposed to the lake one, as it corresponds to slant range positions according to (20), thus affecting the final image quality.

2.3 System Design

The design of a SAR system is not a trivial task, as several parameters and requirements are considered. In particular, the radar antenna must be designed in order to avoid azimuth and range ambiguities as well as nadir returns and to satisfy some system requirements, such as the swath width and the azimuth resolution. Firstly, if the desired SAR system is operated in Stripmap mode, the antenna length is selected depending on the required azimuth resolution δx, according to the following equation

$$L = 2\delta x \tag{21}$$

In order to control azimuth and range ambiguities, another constraint on the selected *PRF* must be considered. As the azimuth pattern of a real antenna has sidelobes, the finite sampling of the Doppler spectrum at the *PRF* leads some signal components outside the frequency interval [-*PRF/2, PRF/2*] to be folded back into the main part of the spectrum, giving rise to azimuth ambiguities, i.e. ambiguous signals displaced from the true location of the scatterer [2][10][15]. Azimuth ambiguities are mainly observed in presence of high backscatter regions adjacent to low backscatter regions, e.g. urban area next to a lake [17]. Denoting as v_s the platform speed along the orbit, in order to control them the

selected *PRF* must be chosen higher than the Doppler bandwidth of the system

$$PRF > B_D \tag{22}$$

which corresponds to the range of Doppler frequencies extending across the antenna footprint [5]; it is generally given by

$$B_D = \frac{2v_s}{L} \tag{23}$$

In more details, the selected *PRF* must satisfy a required value of azimuth ambiguity-to-signal ratio (*AASR*), i.e. the ratio of the azimuth ambiguous signal power to the main signal power for an uniform backscatter scene. Also, the *AASR* is strictly related to the processed Doppler bandwidth (PBW) $B_p < PRF$: it is an azimuth low-pass filter of width B_p which is applied to the focused SAR data in order to meet the *AASR* requirement, but degrading the azimuth resolution according to

$$\delta x \cong \frac{v_s}{B_p} \tag{24}$$

As far as range ambiguities are concerned [10], as the swath echo is required to be comprised between two consecutive pulses, the selected *PRF* must be smaller than the time it takes to collect returns from the entire illuminated swath [5]

$$PRF < \frac{c_0}{2W_g \sin\eta} \tag{25}$$

A quantitative measure of the range ambiguities power can be estimated as the ratio between the range ambiguous (preceding and succeeding) signals power and the main signal one, i.e. range ambiguity-to-signal ratio (*RASR*). Differently from the *AASR*, the *RASR* may significantly vary across the swath and has therefore to be evaluated at each slant range within it [17]. Thus, any flexibility in selecting the PRF lies in the lower limit, which seeks to control azimuth ambiguities caused by Doppler aliasing [5]. Starting from the footprint extent along the range dimension

$$W_g = \frac{\lambda R_0}{W\cos\eta} \tag{26}$$

where λ denotes the radar system wavelength, the antenna height can be selected by simply inverting the equation in (26)

$$W = \frac{\lambda R_0}{W_g\cos\eta} \tag{27}$$

Figure 11 shows a simplified illustration concerning the dependency on system parameters and requirements when designing a SAR system. Combining the expression in (26) with the equations expressed in (25) and in (23), another constraint can be derived on the SAR antenna area

$$WL \geq \frac{4v_s\lambda R_0}{c_0}\tan\eta \tag{28}$$

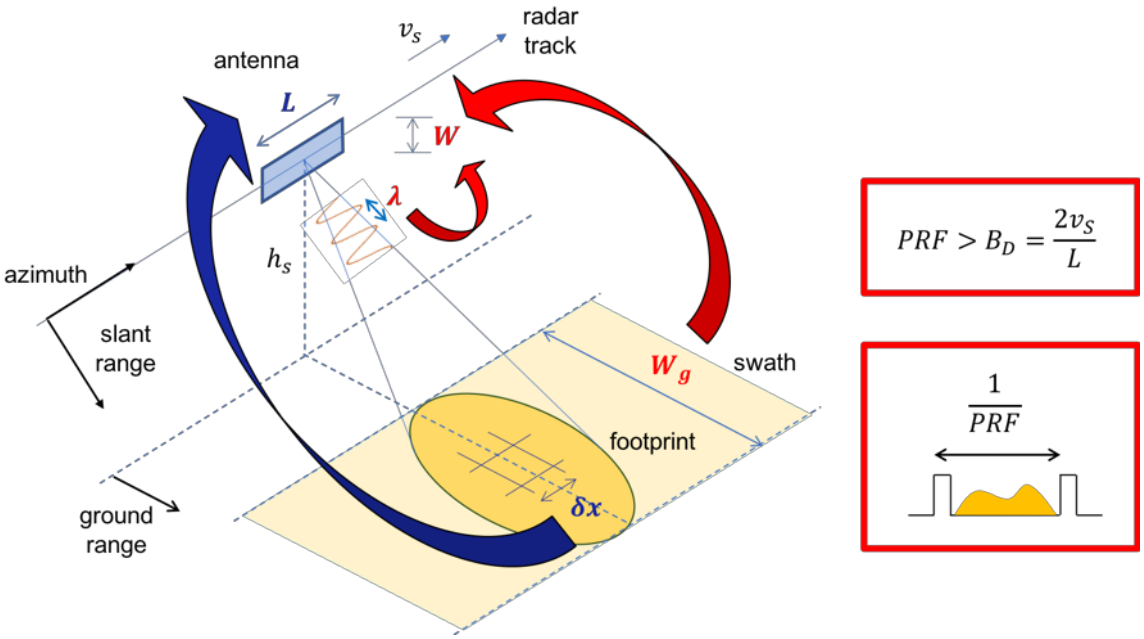

Figure 11: Illustration of the system parameters and requirements dependency in SAR system design.

In practice, the design of a conventional SAR system is a bit more complicated, because on top of range ambiguities also nadir returns have to be taken into account. In order to avoid them, the so-called "diamond diagram" (Figure 12a) can be used: the green and blue zones identify transmit events and nadir returns, respectively, thus the swaths (red stripes) must be placed in the left space. This means that a favorite *PRF*, for instance the optimum one for azimuth ambiguities suppression, cannot really be chosen, as the *PRF* is constrained by transmit events and nadir returns. However, assuming to get rid of nadir returns (Figure 12b), these constraints are significantly relaxed, thus allowing selecting an optimized *PRF*. Therefore, when designing a SAR system the *PRF* must be selected so that the nadir return arrives back while the radar is transmitting; in this way, the nadir return can be strongly attenuated.

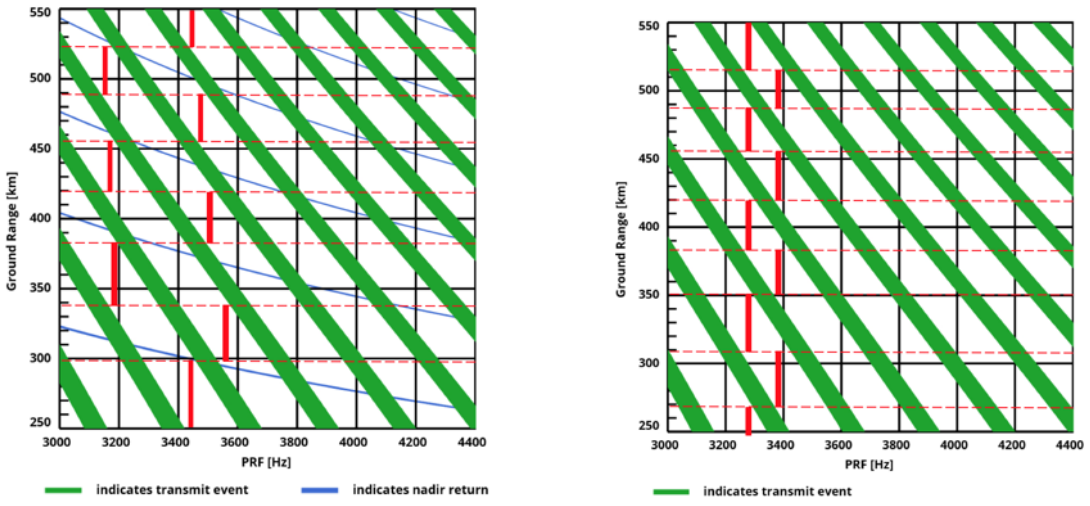

(a) (b)

Figure 12: Diamond diagrams. In (a), the *PRF* is constrained by transmit events and nadir returns, while in (b), as nadir returns are removed, the *PRF* constraints are significantly relaxed. The red stripes indicate some of the swaths, which can be selected.

3 Waveform-Encoded SAR

Waveform-encoded SAR is a novel concept based on pulse-pulse variation of the transmitted waveform that allows focusing the nadir echo and the range ambiguities and suppressing them through a multi-focus post-processing. This technique is born for nadir echo suppression, exploiting the continuous variation of waveforms on transmit and the use of different matched filters in the processing, but in this dissertation it is extended to the case of range ambiguities suppression, yielding an improved image quality with remarkable benefits in the design of novel SAR systems.

3.1 Concept

In order to limit the impact of an echo corresponding to a succeeding transmitted pulse and coming back to the radar simultaneously with the swath return of interest, i.e. range ambiguous echo or nadir return, different and ”orthogonal” waveforms are employed on transmit (Figure 13), so that the ambiguous signal is smeared as a result of the pulse or range compression operation. However, the ambiguous signal, despite it is smeared and therefore less visible, still contributes to the background noise, thus limiting the retrieval of information from a SAR data.

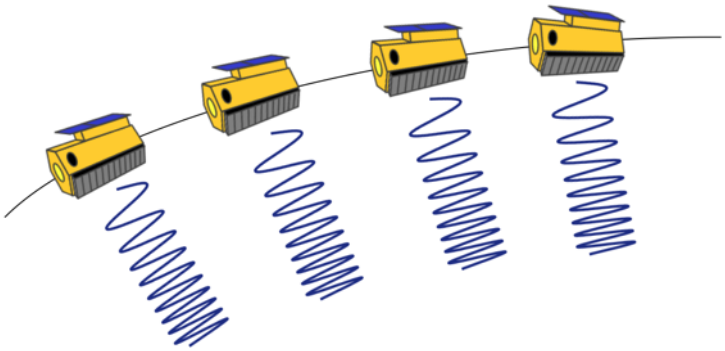

(a)

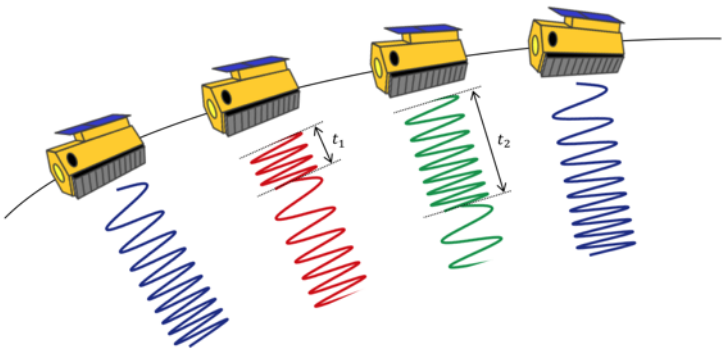

(b)

Figure 13: Simplified illustration of the employed waveforms on transmit for conventional SAR (a) and waveform-encoded SAR (b) systems. In (a), the radar transmits always the same waveform, i.e. a chirp, while a waveform-encoded SAR (b) continuously and periodically changes the waveform on transmit.

As well as waveform diversity on transmit, in order to remove the ambiguous signal this novel technique proposes a multi-focus post-processing. Starting from the acquired raw SAR data, it is focused using a filter matched to the ambiguous signal: therefore, the ambiguity results to be correctly focused and properly located, while the useful signal, i.e. the swath echo of interest, is smeared. This post-processing step is required in order to remove the ambiguity with a negligible corruption of the useful signal, as well as both the nadir return and the range ambiguity are concerned. This latter focused SAR data, where the ambiguous signal has been removed, is then transformed back into raw data through an inverse focusing operation and finally focused again using a filter matched to the useful signal. For such a multi-focus post-processing, a sequence of employed waveforms must be properly selected in order to obtain a focused SAR image, where the ambiguous signal, i.e. the nadir return or the range ambiguity, is significantly attenuated, while the useful signal, i.e. the swath echo of interest, results to be only minimally affected [21]. Figure 14 shows the block diagram of the proposed multi-focus post-processing for such a waveform-encoded SAR system, designed for range ambiguities suppression, if the waveform variation concept is exploited; the useful and ambiguous signals are schematically represented by a tree and a house, respectively.

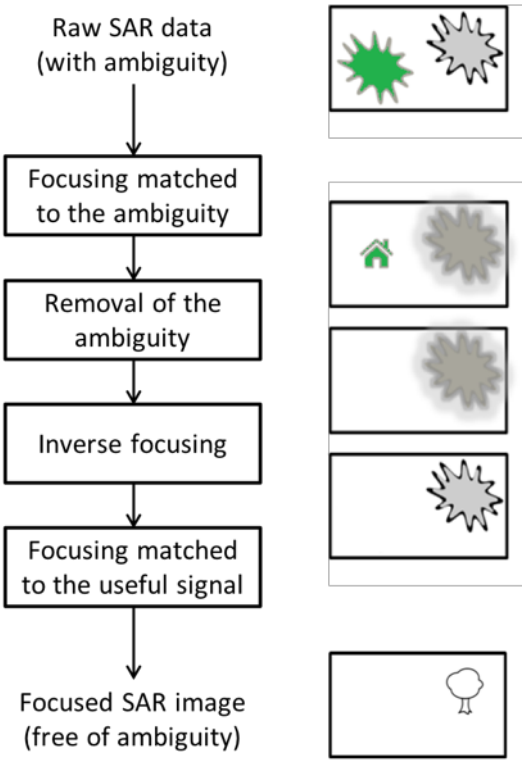

Figure 14: Block diagram of the proposed multi-focus post-processing concerning a waveform-encoded SAR system designed for range ambiguities suppression [21].

3.2 Sequences of Waveforms

In order to implement the proposed waveform-encoded SAR system for range ambiguities suppression, waveform diversity must be kept on transmit, so that a different focusing can be performed for the useful and ambiguous signals, respectively. In particular, as the ambiguous signal comes from succeeding or preceding transmitted pulses, compared to the useful one, transmitting a different waveform from pulse-to-pulse allows focusing the swath echo of interest and the range ambiguity separately. Therefore, while a conventional SAR system always transmits the same waveform, i.e. a

chirp signal of the form

$$s(t) = \exp\left(j\pi B\frac{t^2}{\tau}\right)\text{rect}\left(\frac{t}{\tau}\right) \tag{29}$$

such a waveform-encoded SAR system transmits a properly selected sequence of waveforms, in order to smear in the most uniform way the unfocused signal. However, the continuous variation of the transmitted waveform along the slant range direction may have implications on the pulse or range compression operation, during the image formation process, making the use of different matched filters necessary during the processing. In this dissertation, two waveform variation schemes will be discussed: the first, i.e. cyclically-shifted chirps, are characterized by a quadratic variation of the shift along azimuth and requires to perform an ideal filtering operation during the processing, while the second, i.e. up- and down-chirp alternation, implies the use of two orthogonal waveforms for two succeeding transmitted pulses.

3.2.1 Cyclically-Shifted Chirps

In order to smear in the most uniform way the unfocused signal along range and azimuth directions, cyclically-shifted chirps, i.e. short-term shift-orthogonal waveforms [9], are employed on transmit. They are described by

$$s_k(t) = \begin{cases} e^{j\pi\frac{B}{\tau}\left(t-t_k-\tau\left(\left\lfloor\frac{t+\frac{\tau}{2}-t_k}{\tau}\right\rfloor\right)\right)^2}, & |t| \leq \frac{\tau}{2} \\ 0, & \text{otherwise} \end{cases} \tag{30}$$

where τ and B are the chirp duration and bandwidth, respectively, while t_k is the cyclical shift of the chirp waveform, defined in the interval $-\tau/2 \leq t_k < \tau/2$. In particular, a sequence of waveforms is employed, which repeats periodically, where τ and B remain constant for all the waveforms and t_k is varied from pulse-to-pulse according to the following quadratic law [21]

$$t_k = \frac{k(k+1)}{2B} - \tau\left\lfloor\frac{k(k+1)+B\tau}{2B\tau}\right\rfloor, k = 0..2B\tau - 1 \tag{31}$$

Hence, the quadratic variation of the shift along azimuth is given by the product $k(k+1)$ in (31) and is proportional to the chirp compression ratio $B\tau$. In practice, cyclically-shifted chirps are basically obtained by shifting the conventional, non-shifted chirp by a quantity t_k and translating the last t_k seconds from the end to the beginning; this implies also a cyclical shift in the corresponding time-frequency diagram, as shown in Figure 15a. Figure 15b schematically shows the radio frequency signals and the time-frequency diagrams of a conventional, non-shifted chirp and two cyclically-shifted chirps.

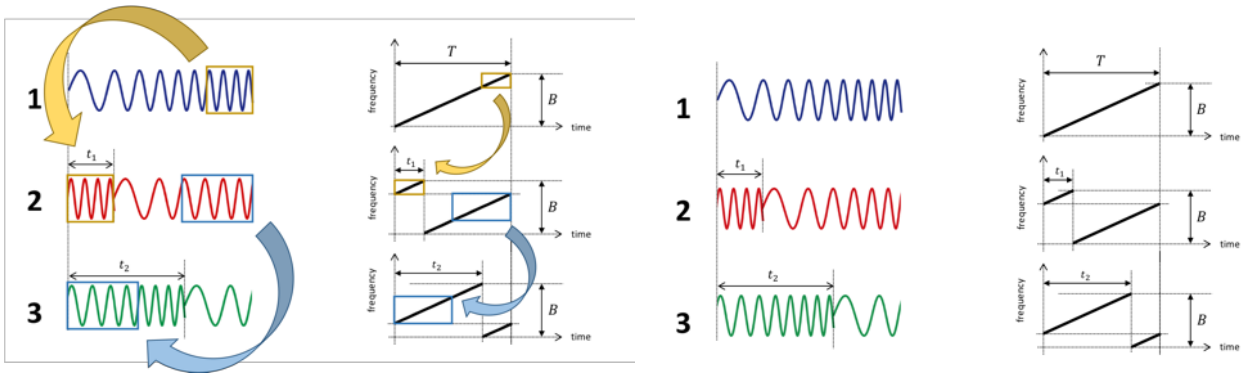

(a) (b)

Figure 15: Schematic representation (b) of the radio frequency signals (left) and time-frequency diagrams (right) of a conventional, non-shifted chirp (blue) and two cyclically-shifted chirps (red and green). (a) shows the schematic procedure for cyclical shifts for both the radio frequency signals and the time-frequency diagrams.

However, the continuous variation of the transmitted waveform from pulse-to-pulse has implications also on the chirp spectrum, which presents a strong oscillation of the frequency components inside the bandwidth (Figure 16d). This implies also a change in the compressed chirp using a matched filter, i.e. the optimal linear filter for maximizing the signal-to-noise ratio (*SNR*). Mathematically, a filter operation is expressed as convolution of an input f with an impulse response function h, giving output

$$g(\tau) = f * h := \int_{-\infty}^{\infty} f(t)h(\tau - t)\,dt \tag{32}$$

where $*$ denotes the convolution operator. In order to make convolution look like autocorrelation, the matched filter $h(t)$ must be given by $h(t) = f^*(-t)$, so that

$$g(\tau) = \int_{-\infty}^{\infty} f(t)f^*(t-\tau)\,dt = \int_{-\infty}^{\infty} f(t^{'}+\tau)f^*(t^{'})\,dt = acf_f(\tau) \tag{33}$$

The second integral in (33) is obtained by the change of variable $t^{'} = t - \tau$, thus autocorrelation amounts to convolution, i.e. (matched) filtering with the time reversed complex conjugate of the original signal [7]. The chirp compression is usually performed in the frequency domain because of the much lower computational load. According to the complex conjugation property in the Fourier transform, the matched filter becomes

$$h(t) = f^*(-t) \Rightarrow H(f) = F^*(f) \tag{34}$$

so that the compression in the frequency domain is simply performed by multiplying the original signal by the filter

$$g(t) = f(t) * h(t) = f(t) * f^*(-t) \Rightarrow G(f) = F(f) \cdot H(f) = F(f) \cdot F^*(f) = |F(f)|^2 \tag{35}$$

As well as cyclically-shifted chirps are concerned, as their spectrum (Figure 16d) deviates from the conventional, non-shifted chirp one (Figure 16c), presenting a strong oscillation of the frequency components inside the bandwidth, the matched filter results to be not the best filter for maximizing the *SNR*. In more details, the normalized compressed chirp (Figure 16f) shows some undesirable sidelobes peaks which damage the image quality and may mask weak scatterers. In order to maximize the *SNR* and thus to obtain the normalized compressed chirp in Figure 16e, the so-called ideal filter [12] must

be employed.

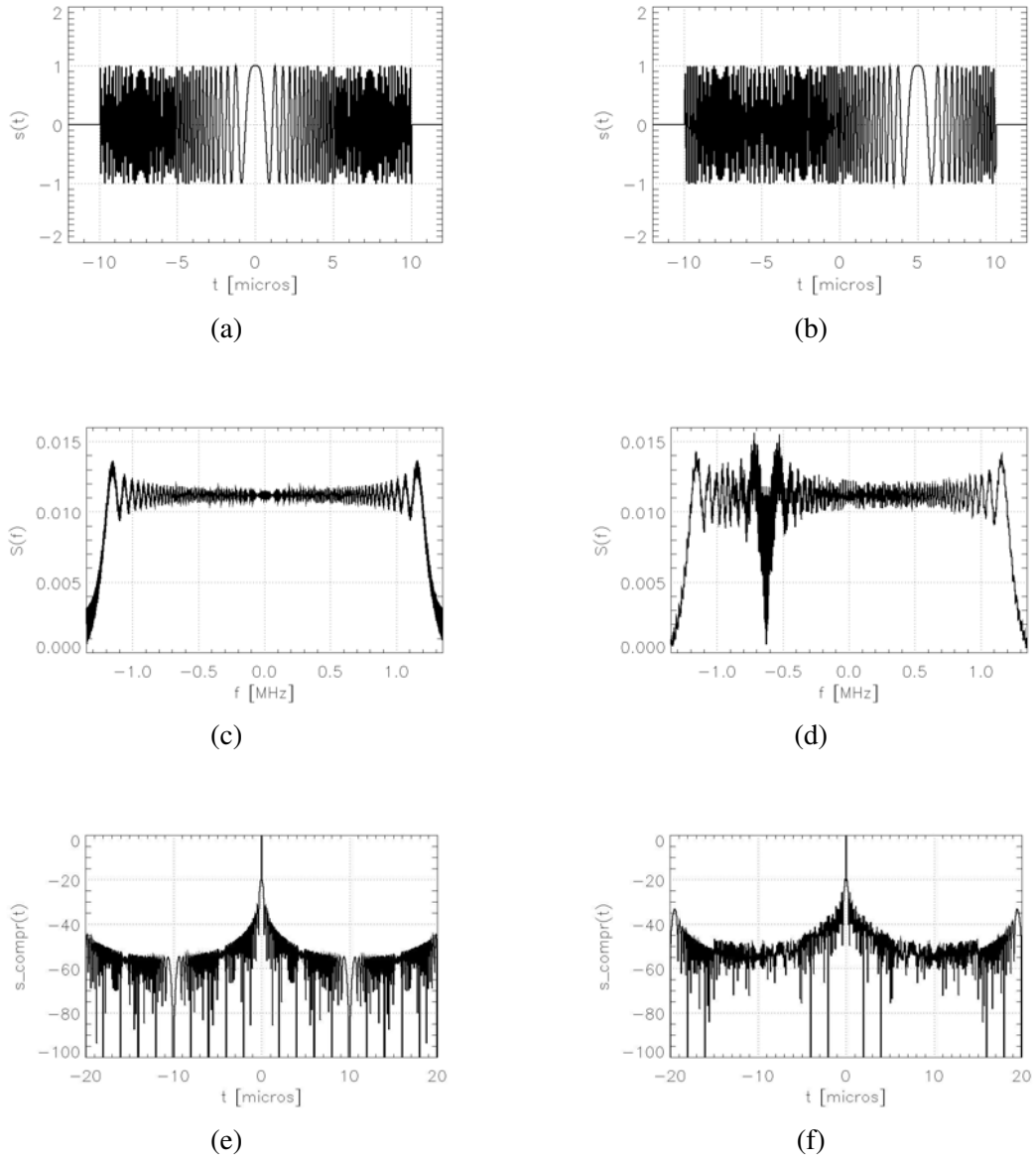

(a) (b) (c) (d) (e) (f)

Figure 16: Graphic representation of the signals (a-b), i.e. real part, spectra (c-d), i.e. absolute value, and autocorrelations (e-f), i.e. normalized compressed signals in dB, of a conventional, non-shifted down-chirp (left) and a cyclically-shifted down-chirp (right).

Denoting as $S_{conv}(f)$ and $S_{shift}(f)$ the conventional, i.e. non-shifted, and cyclically-shifted chirps in the frequency domain, respectively, the compression equation, expressed in (35), leads to a different mathematical result for the two considered waveforms, justifying the differences between Figure 16e and Figure 16f. In particular, as the spectrum of the two signals is different, also the compression will change, according to

$$S_{conv}(f) \cdot H(f) = S_{conv}(f) \cdot S^*_{conv}(f) = |S_{conv}(f)|^2 \tag{36}$$

considering a conventional chirp, and to

$$S_{shift}(f) \cdot H(f) = S_{shift}(f) \cdot S^*_{shift}(f) = |S_{shift}(f)|^2 \tag{37}$$

for a cyclically-shifted one. Hence, a new filter, i.e. the ideal filter, must be defined in the frequency domain, in order to maximize the *SNR* while using cyclically-shifted chirps, thus to obtain the same

compression as in Figure 16e. It is defined [12][21][20] as

$$H(f) = \frac{|S_{conv}(f)|^2}{S_{shift}(f)} \tag{38}$$

in order to satisfy the following expression

$$S_{shift}(f) \cdot H(f) = S_{shift}(f) \cdot \frac{|S_{conv}(f)|^2}{S_{shift}(f)} = |S_{conv}(f)|^2 \tag{39}$$

Keeping the cyclically-shifted chirp in Figure 16b, Figure 17 shows the results of the compression using a matched filter (Figure 17a) and the ideal filter (Figure 17b).

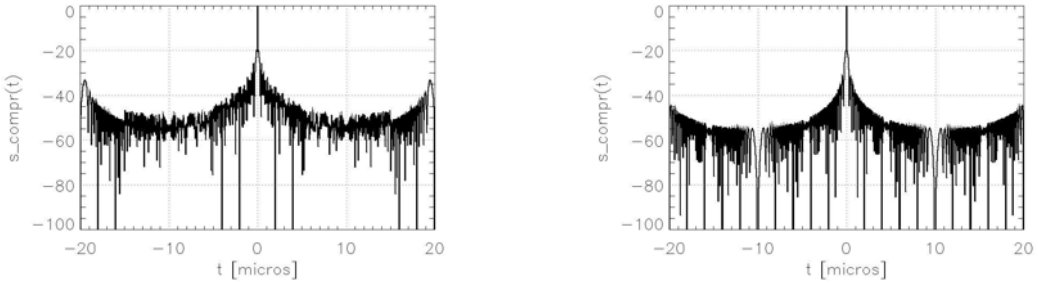

(a) (b)

Figure 17: Comparison between the compression of the cyclically-shifted chirp in Figure 16b using a matched filter (a) and the ideal filter (b). The two plots are normalized and expressed in dB.

3.2.2 Up- and Down-Chirp Alternation

As alternative, the unfocused signal can be smeared only along the range direction, as a result of the pulse or range compression operation, if different, orthogonal waveforms are used for two succeeding transmitted pulses [21][11], i.e. up- and down-chirps alternation. As up- and down-chirps are orthogonal from each other, they have a linearly increasing and decreasing frequency, respectively, as shown in Figure 18.

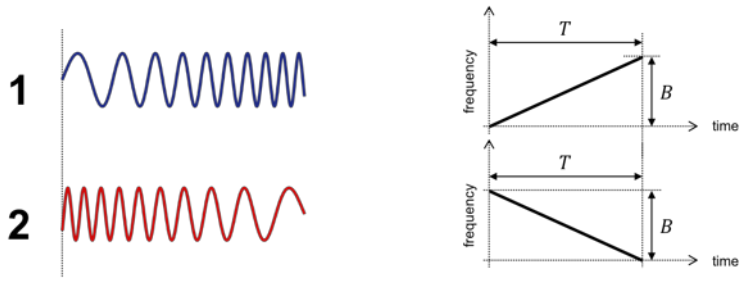

Figure 18: Schematic representation of the radio frequency signals (left) and time-frequency diagrams (right) of up- (blue) and down-chirps (red).

Hence, up- and down-chirps are defined as

$$s(t) = \exp\left(\pm j\pi B \frac{t^2}{\tau}\right) \mathrm{rect}\left(\frac{t}{\tau}\right) \tag{40}$$

where τ and B are the chirp duration and bandwidth, respectively. The two orthogonal waveforms are identified by "+" (up-chirp) and "−" (down-chirp) operators; in practice, this means that the up-chirp phase (Figure 19e) is the negative of the down-chirp one (Figure 19f), and vice versa. Also, this implies that the imaginary parts of the two signals are opposite from each other, as shown in Figure 19c and Figure 19d.

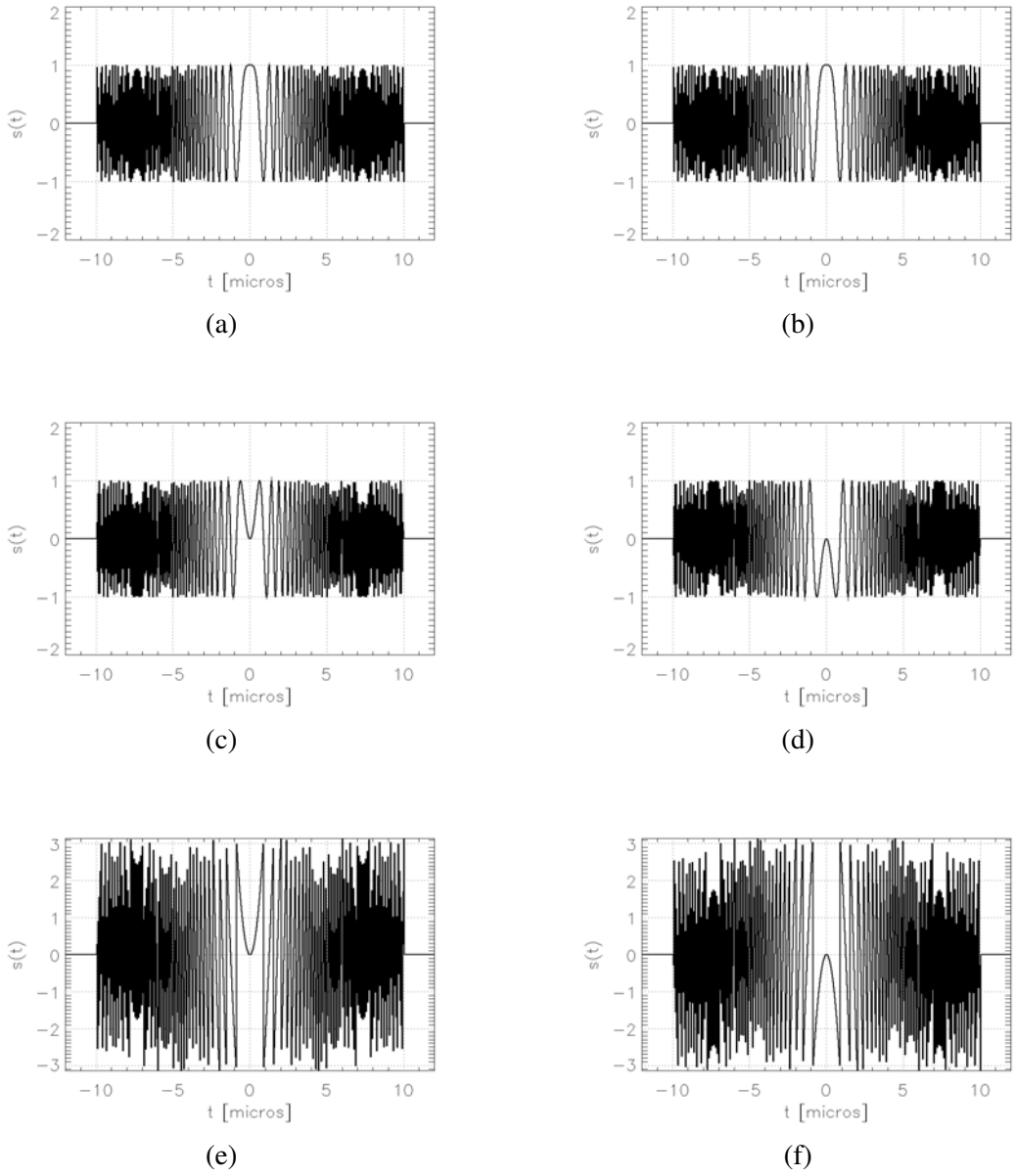

Figure 19: Graphic representation of the real part (a-b), imaginary part (c-d), and phase (e-f) of an up-chirp (left) and a down-chirp (right).

As well as chirp compression is concerned, the ideal filter is not required, as the matched filter allows maximizing the signal-to-noise ratio (*SNR*); in particular, this is due to the behaviour of the spectrum, whose absolute value and phase are symmetric with respect to the y-axis, i.e. *S(f) = S(-f)*. Mathematically, as the up- and down-chirps are complex conjugate from each other, i.e. $s_{up}(t) = s^*_{down}(t)$, their spectra are given by

$$\begin{aligned} s_{up}(t) = s^*_{down}(t) \Rightarrow S_{up}(f) = S^*_{down}(f) \\ s_{down}(t) \Rightarrow S_{down}(f) \end{aligned} \tag{41}$$

They are still complex conjugate from each other, which means that present the same absolute value (Figure 20a) but opposite phase. The matched filters are so defined as

$$\begin{aligned} h_{up}(t) = s^*_{up}(-t) = s_{down}(-t) \Rightarrow H_{up}(f) = S^*_{up}(f) = S_{down}(f) \\ h_{down}(t) = s^*_{down}(-t) \Rightarrow H_{down}(f) = S^*_{down}(f) \end{aligned} \tag{42}$$

According to (35), the compressed signals in the frequency domain are given by

$$\begin{aligned} S_{up}(f) \cdot H_{up}(f) = S^*_{down}(f) \cdot S_{down}(f) = |S_{down}(f)|^2 \\ S_{down}(f) \cdot H_{down}(f) = S_{down}(f) \cdot S^*_{down}(f) = |S_{down}(f)|^2 \end{aligned} \tag{43}$$

thus presenting the same result for both up- and down-chirps (Figure 20b). Figure 20 shows the spectrum absolute value (Figure 20a) and the autocorrelation (Figure 20b), i.e. the normalized compressed signal in dB, corresponding to both up- and down chirps, assuming the same signal parameters.

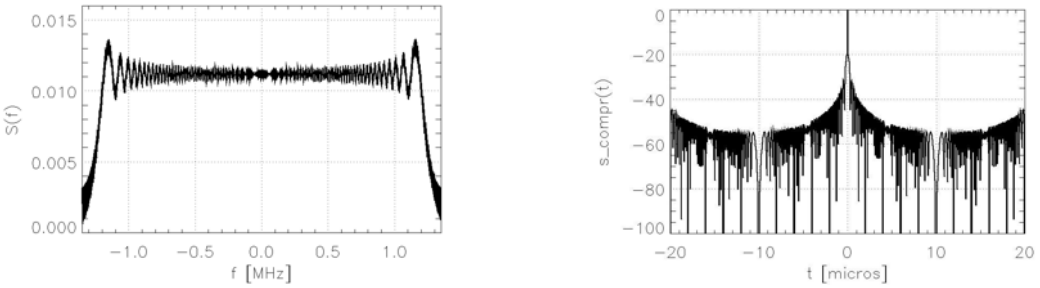

(a) (b)

Figure 20: Graphic representation of the spectrum (a), i.e. absolute value, and autocorrelation (b), i.e. normalized compressed signal in dB, of both up- and down-chirps, assuming the same signal parameters.

However, employing up- and down-chirp alternation allows smearing only odd range ambiguities, i.e. echoes corresponding to odd succeeding or preceding transmitted pulses and coming back to the radar simultaneously with the swath echo of interest, as the even ones correspond to the same transmitted waveforms, compared to the useful signal, thus not allowing the separate focusing between the superimposed received signals.

3.3 Multi-Focus Post-Processing

As well as waveform diversity on transmit, a multi-focus post-processing is required in order to perform a separate focusing for the useful signal, i.e. the swath echo of interest, and the ambiguous one, thus allowing focusing and then suppressing to some extent the ambiguity. While keeping a conventional SAR system without waveform variation and performing a focusing matched to the useful signal, the ambiguity appears as localized, slightly-defocused artifacts. If a waveform-encoded SAR system, i.e. with a continuous pulse-to-pulse variation of the transmitted waveform, is employed, the ambiguous signal is uniformly smeared over the pulse width, i.e. slant range direction, and the synthetic aperture, i.e. azimuth direction, appearing as a noise-like disturbance, as well as some ambiguous energy is suppressed. Similarly to a staggered SAR, in fact, the ambiguous energy is incoherently integrated in azimuth and spread almost uniformly across the Doppler spectrum (Figure 21); therefore, a part of it is filtered out during the SAR processing, if the *PRF* of the system is larger than its processed Doppler bandwidth [21][18]. As cyclically-shifted and up- and down-chirps differently

spread the ambiguous energy across the Doppler spectrum (Figure 21), a different ambiguous energy suppression can be achieved by imposing the same processed Doppler bandwidth.

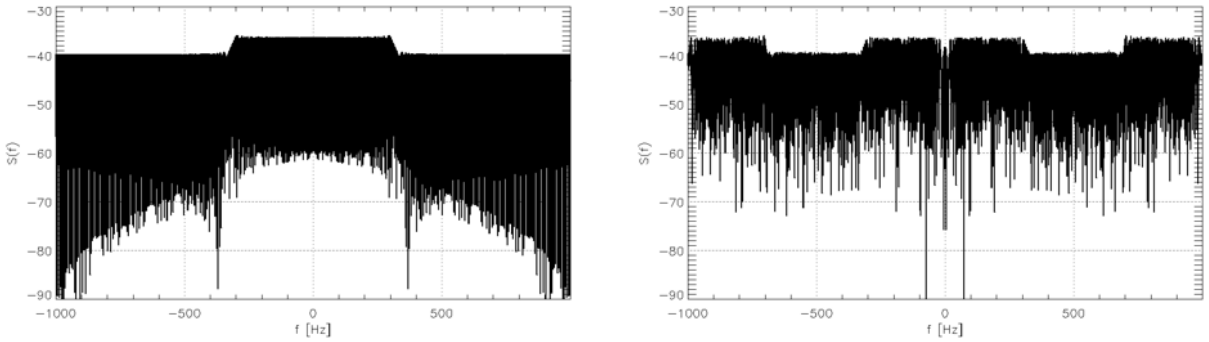

(a) (b)

Figure 21: Graphic representation of the ambiguity Doppler spectrum, if cyclically-shifted (a) or up- and down-chirps (b) are employed.

A further ambiguity suppression can be achieved by means of a dual-focus or multi-focus post-processing, as far as nadir echo or range ambiguities suppression is concerned, respectively; therefore, data are subsequently focused with filters matched to each ambiguous signal, in order to highlight and remove it.

As far as nadir return is concerned, the superimposed raw SAR data, i.e. raw data corresponding to the superimposition between the ambiguity and the swath echo of interest, is first focused using a filter matched to the nadir echo. In case the sequence of waveforms in (30), i.e. cyclically-shifted chirps, is employed, the useful signal, after range compression, is dislocated at different ranges and then smeared over azimuth as a consequence of azimuth compression, while the nadir return is correctly focused and properly located. Hence, the nadir signal can be removed with a negligible corruption of the useful signal. This focused data, where the nadir echo energy has been attenuated, is then transformed back into raw SAR data through an inverse filtering operation and finally focused again with a filter matched to the signal.

The same post-processing can be applied for suppressing range ambiguities in SAR images, despite the range ambiguous echoes are not located at specific known ranges, but can be present at different range and azimuth locations [21]. In such a case, a multi-focus post-processing is required: the processing steps are very similar as for nadir echo suppression, with the difference that the first three steps, i.e. focusing matched to the range ambiguity, removal of the range ambiguous signal, and inverse filtering, shall be repeated for all range ambiguities to be suppressed [21]. Figure 22 shows the block diagram of the proposed multi-focus post-processing, if such a waveform-encoded SAR concept is kept for range ambiguities suppression. The useful and ambiguous signals are schematically represented by a tree and a house, respectively.

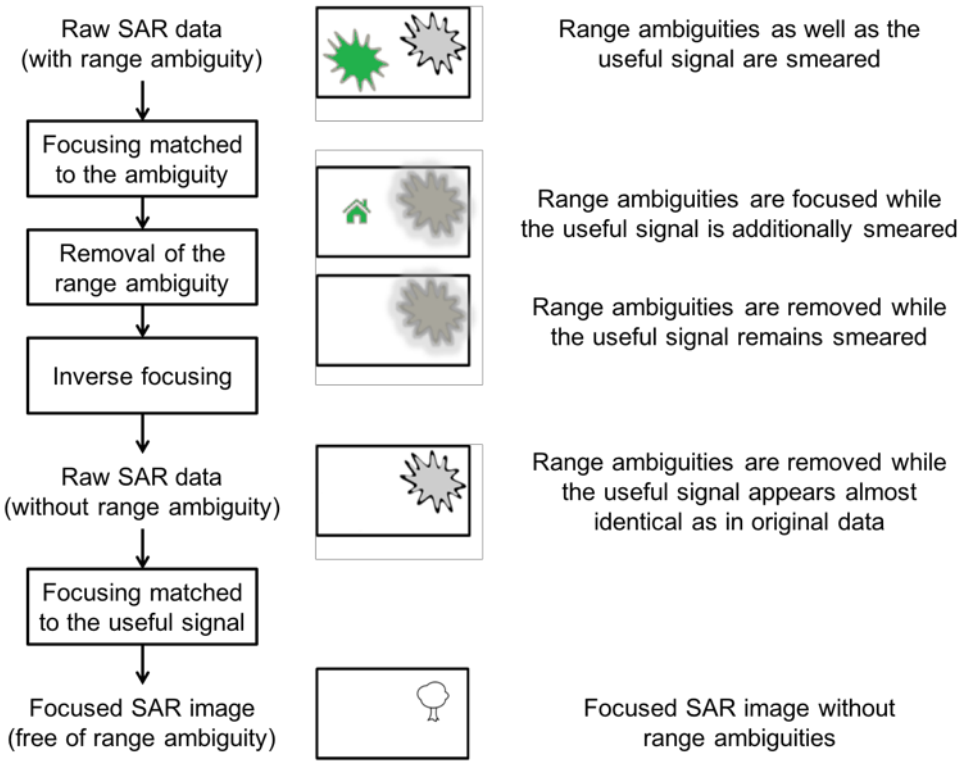

Figure 22: Block diagram of the proposed multi-focus post-processing for such a waveform-encoded SAR system, designed for range ambiguities suppression [21].

3.3.1 Thresholding and Blanking

In order to suppress a nadir return, once the raw data is focused using a filter matched to the nadir echo, i.e. the ambiguity results to be correctly focused and properly located, while the useful signal is smeared, this last one can be simply removed by blanking the pixels, where it is located. Specifically, the nadir return location can be determined from the *PRF*, the orbit information, and a digital elevation model (DEM) of the area of interest [21]. As alternative, an adaptive threshold can be applied to the focused image matched to the nadir return, suppressing this one only if the image is indeed corrupted. This can be considered a better solution, as the level of the smeared nadir echo signal in the SAR image obtained after focusing matched to the useful signal, as consequence of the pulse-to-pulse variation of the transmitted waveform, can be in some cases much lower than that of the thermal noise.

As far as range ambiguities are concerned, the ambiguity removal is more critical because of an entire superimposed ambiguous image. Hence, each range ambiguity can be removed by simply applying an adaptive threshold to the focused image matched to that range ambiguous signal, and then blanking, i.e. setting to zero, all the pixels above that. In particular, assuming for simplicity a single range ambiguity to be superimposed to the useful signal, the thresholding and blanking approach is justified by the analysis of the intensities histograms of the useful and ambiguous signals, after focusing with a filter matched to the range ambiguity. Figure 23 shows these histograms for the sample case study described in Section 5.1, where an urban area is causing range ambiguity on a lake, and assuming the sequence of waveforms in (30), i.e. cyclically-shifted, to be employed on transmit. It can be noticed that the range ambiguous signal contains more pixels with higher intensity compared to the useful signal, despite the total energy of this last one exceeds the total energy of the range ambiguity, as the ambiguous signal is properly focused, while the useful signal is not correctly focused because of a mismatched filter. As suggested by the histograms in Figure 23, the range ambiguity can be significantly attenuated, with a negligible corruption of the useful signal, which

results to be only minimally affected, if an adaptive threshold is properly imposed.

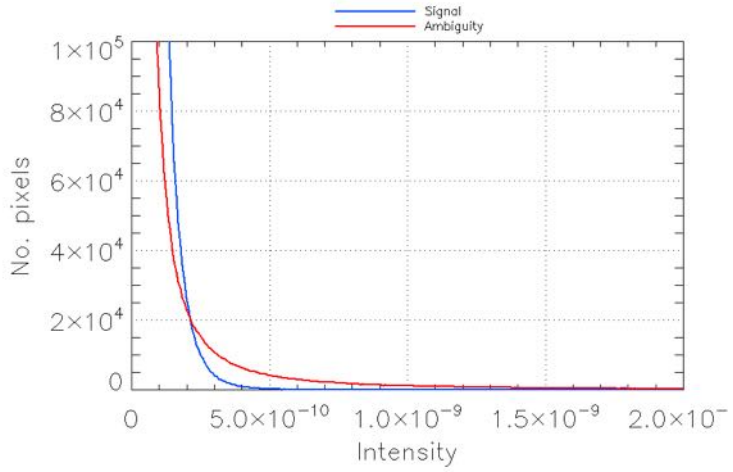

Figure 23: Intensities histograms of the useful and range ambiguous signals, after focusing with a filter matched to the range ambiguity, assuming the sample case study described in Section 5.1.

However, the main issue while dealing with such a thresholding and blanking approach is related to the difficulty of finding an effective criterion for threshold selection; therefore, the assessment of the ambiguity suppression performance for such a system becomes not a trivial task.

3.3.2 Contrast Minimization Method

While keeping the thresholding and blanking approach, an effective criterion for threshold selection is required. Applying for simplicity a single threshold over the full SAR image, the total error (Figure 24) can be evaluated on the focused data matched to the range ambiguity, with reference to the ambiguity-free image as a function of the threshold. In particular, this error can be decomposed into two components, i.e. the residual ambiguous signal and the removed useful signal [21]. Despite the total error minimization could be a criterion for threshold selection (Section 4.1.3), it requires the separate knowledge of the useful and ambiguous signals within the simulation and thus it cannot be applied in practice, as only the sum of them is available.

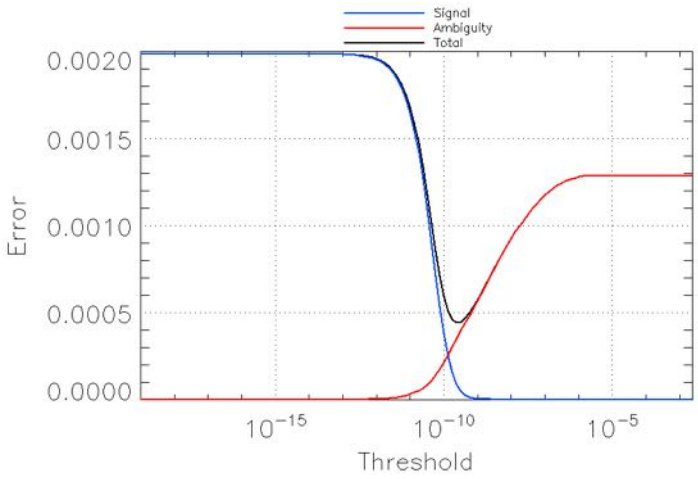

Figure 24: Total error (black) and their components, i.e. residual ambiguous signal (red) and removed useful signal (blue), as a function of thresholds, assuming the sample case study described in Section 5.1 and cyclically-shifted chirps as transmitted waveforms.

As a consequence, a different strategy for threshold selection has to be defined: a simple but effective criterion for selecting an adaptive threshold can be obtained by minimizing the image contrast, defined as the ratio between the standard deviation of the intensities and their mean, after focusing matched to each range ambiguity. The effectiveness of the proposed method is given by the contrast behaviour of the useful and ambiguous images, when focusing using a filter matched to the ambiguity. The continuous pulse-to-pulse variation of the transmitted waveform allows smearing the useful signal over the pulse width, i.e. slant range direction, and the synthetic aperture, i.e. azimuth direction, so that it appears as a noise-like disturbance. Because of the contrast definition, i.e.

$$Contrast(I) := \frac{StdDev(|I|^2)}{Mean(|I|^2)} = \frac{\sigma(|I|^2)}{\mu(|I|^2)} \tag{44}$$

where I identifies the focused superimposed SAR image matched to the ambiguous signal, the focused range ambiguity is characterized by a high image contrast, while the smeared useful signal, as it appears as a noise-like disturbance, i.e. described by similar mean and standard deviation values, presents a low image contrast. Figure 25 shows the contrast as function of thresholds, if the sample case study described in Section 5.1 and cyclically-shifted chirps on transmit are kept. As the threshold decreases, the image contrast decreases as a consequence of the removal of strong and focused ambiguity features; once the ambiguous signal has been removed, a further decrease of the threshold determines an increase in the image contrast, as a consequence of useful signal removal [21]. As is apparent, the threshold which minimizes the contrast (Figure 25) could approximate well the one minimizing the total error (Figure 24).

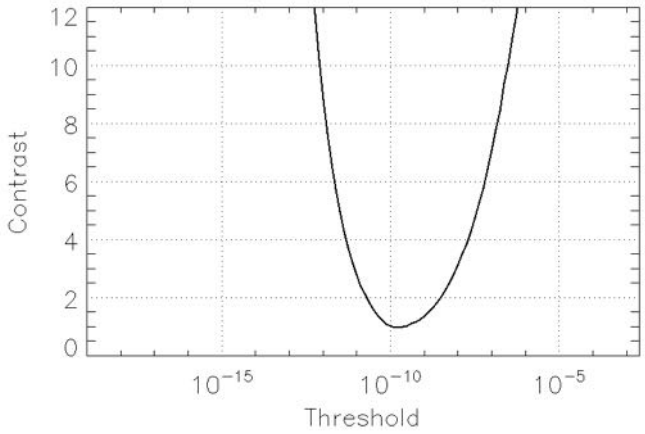

Figure 25: Image contrast as a function of thresholds, after thresholding and blanking on the focused image matched to the range ambiguity, assuming the sample case study described in Section 5.1 and cyclically-shifted chirps as transmitted waveforms.

3.3.3 Considerations on Block Size

Generally, the acquired data is characterized by a very large image size, both in range and azimuth directions; thus, a block-based image processing is required in order to limit the computational load. As a consequence, the optimum block size analysis becomes a challenging, not trivial task, as it of course depends on some system parameters, i.e. synthetic aperture and pulse duration, and could improve the processing performance. While keeping the waveform variation concept, the proposed multi-focus post-processing (Figure 22) can be block-implemented by simply applying a moving window; in particular, better results in terms of ambiguity suppression could be achieved by exploiting a spatially variant threshold. Assuming a fixed block size, a different threshold can be in principle

estimated for each block of pixels by minimizing the image contrast; however, the moving window implementation requires computing the contrast not inside the considered block, but assuming a bigger window centered in it. First of all, the focused image matched to the range ambiguity is divided in blocks; the moving window is thus simply implemented by considering bigger windows, i.e. of one and a half time the inner ones, and centering them in each block (Figure 26b). After performing the thresholding and blanking approach for a set of thresholds, and for each outer window, i.e. the red one in Figure 26b, the threshold obtained by minimizing the image contrast is used for blanking only the pixels inside the corresponding original block, i.e. the blue one. Figure 26b schematically shows the proposed moving window implementation, assuming the sample case study described in Section 5.1 and cyclically-shifted chirps as transmitted waveforms. For the edge blocks, e.g. the blue one in the upper right of Figure 26b, as the range ambiguity is correctly focused and properly located, while the useful signal is smeared also outside the image (as shown in Section 5.1), when defining bigger windows the external pixels are simply neglected, so that the smeared useful signal outside the image cannot be removed.

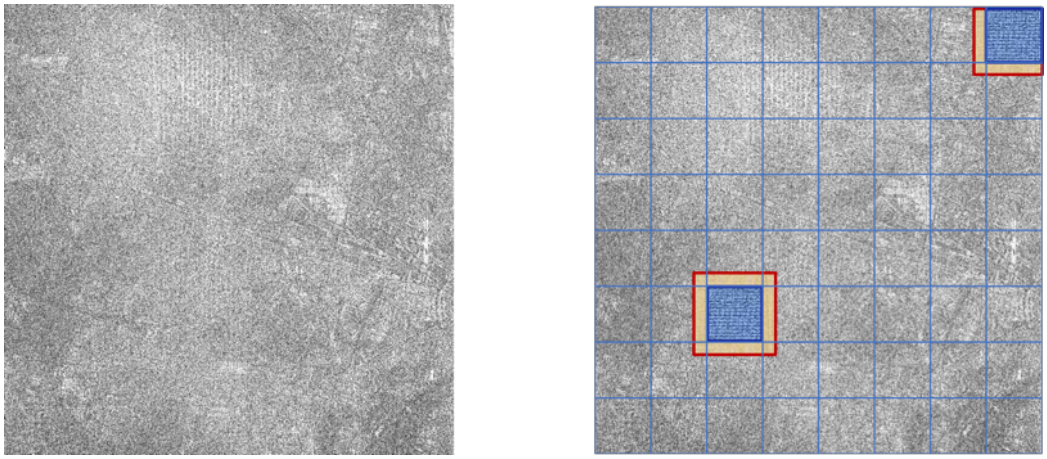

(a) (b)

Figure 26: Focused data matched to the range ambiguity (a), assuming the sample case study described in Section 5.1 and cyclically-shifted chirps as transmitted waveforms. (b) schematically shows the moving window implementation, considering sixty-four blocks and assuming an outer window of one and a half time the inner one. Both the images have the same size, i.e. 4096 x 4096 pixels. The horizontal and vertical axes represent slant range and azimuth, respectively.

The implementation of such a moving window could lead to a further ambiguity suppression and thus to better results, as different spatially variant thresholds are used for performing the blanking operation on each block of pixels. In particular, the goal would be to obtain a threshold-based image (Figure 27b), whose values, i.e. the thresholds values, reflect and thus would be strictly linked to the intensities values of each block of the focused SAR image matched to the range ambiguity (Figure 27a). Hence, a performance improvement could be achieved as a consequence of block-adaptive thresholds, which allow removing the ambiguity depending on the block-based behaviour of the useful and ambiguous signals. Also, this suggests using a small block size, in order to account for small intensities variations, especially in the range ambiguity, as the signal of interest is smeared and thus appears as a noise-like disturbance. However, employing too small blocks could be not a proper choice, because of block-based contrast computation, as successively discussed in Section 5.2.3. Figure 27b shows an example of a threshold-based image, assuming the sample case study in Figure 26 and small processed blocks, i.e. 16 x 16.

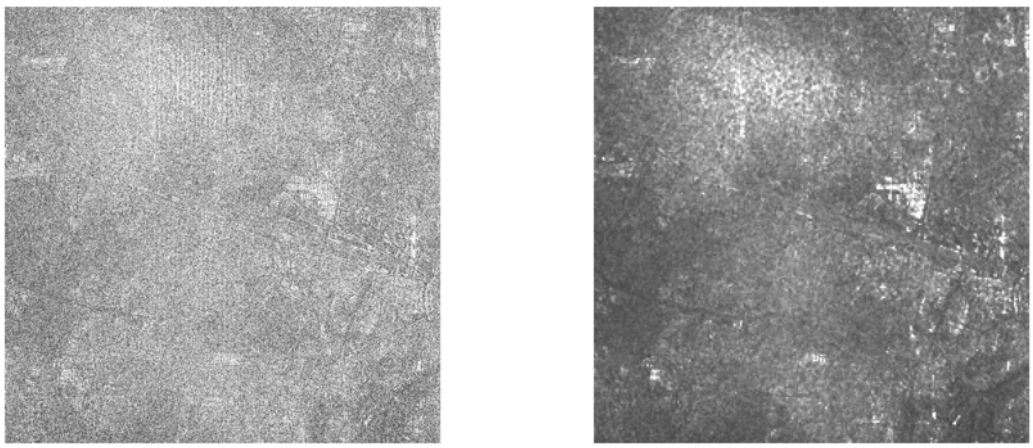

(a) (b)

Figure 27: Comparison between the focused data matched to the ambiguity (a), assuming the sample case study described in Section 5.1 and cyclically-shifted chirps as transmitted waveforms, and the image obtained from the block-based spatially variant thresholds (b), if inner blocks of fixed size, i.e. 16 x 16, and outer windows of one and a half time the inner ones are employed. Both the images have the same size, i.e. 4096 x 4096 pixels. The horizontal and vertical axes represent slant range and azimuth, respectively.

Nevertheless, the proposed considerations on block size depend on the considered system parameters, i.e. synthetic aperture L_s and chirp duration τ; in particular, while focusing the superimposed raw SAR data using a filter matched to the ambiguity, the defocused useful signal, after range compression, is dislocated at different ranges, as a consequence of an uniform smearing over the pulse width τ, i.e. the slant range direction, and then incoherently integrated in azimuth, i.e. over the synthetic aperture L_s, and spread almost uniformly across the Doppler spectrum, because of azimuth compression. The proposed considerations on block size are so strictly related to these two system parameters, and can be reformulated if using different synthetic aperture and pulse duration integration windows.

4 Performance Assessment

Waveform-encoded SAR is a novel SAR concept which allows suppressing, not only smearing, range ambiguities by exploiting a continuous pulse-to-pulse variation of the transmitted waveform. However, despite a further range ambiguity suppression can be achieved by means of a multi-focus post-processing with a contrast minimization-based thresholding and blanking approach, an assessment of the image quality, and thus of the system performance, for such a waveform-encoded SAR system is required, in order to understand the behavior of the proposed contrast minimization method with reference to the best achievable performance which can be obtained by using an optimal threshold. In particular, this work proposes a novel methodology, which exploits real TerraSAR-X data to accurately simulate the effect of the range ambiguity on the useful signal and allows for a quantitative assessment of the image quality of such a system.

4.1 Methodology

The proposed methodology exploits the separate knowledge of the useful and ambiguous signals within the simulation context, in order to accurately simulate the range ambiguity impact on the desired signal and to allow a quantitative assessment of the resulting image quality for such a waveform-encoded SAR system. First of all, simulated raw SAR data are generated for the two separate signals, starting from the complex backscatters of two different parts of a TerraSAR-X image; thus, they are then superimposed to each other to obtain the same raw data as it would be acquired in practice by a SAR system (Section 4.1.2). Hence, the multi-focus post-processing proposed in Section 3.3 is separately performed for the three different simulated raw data, in order to both simulate the effect of the range ambiguity on the useful signal and allow for a quantitative assessment of the proposed thresholding and blanking approach for such a system. In particular, when performing the removal of the range ambiguous signal in the focused superimposed data matched to the ambiguity, the threshold obtained by minimizing a given cost function, i.e. the image contrast or the total error, is used for blanking pixels of both the three simulated images. The analysis considers the two different waveform variation schemes described in Section 3.2, i.e. the employment of cyclically-shifted chirps and an alternation of up- and down-chirps, and aims to assess the proposed contrast minimization method (Section 3.3.2) for threshold selection, as well as the best achievable performance, i.e. optimal threshold. Figure 28 shows the block diagram of the employed methodology for performance assessment, assuming a waveform-encoded SAR system designed for range ambiguities suppression. The resulting image quality of the corrupted desired signal, due to the range ambiguity, is thus evaluated through three difference performance figures, i.e. total error, ambiguity suppression and removed useful signal.

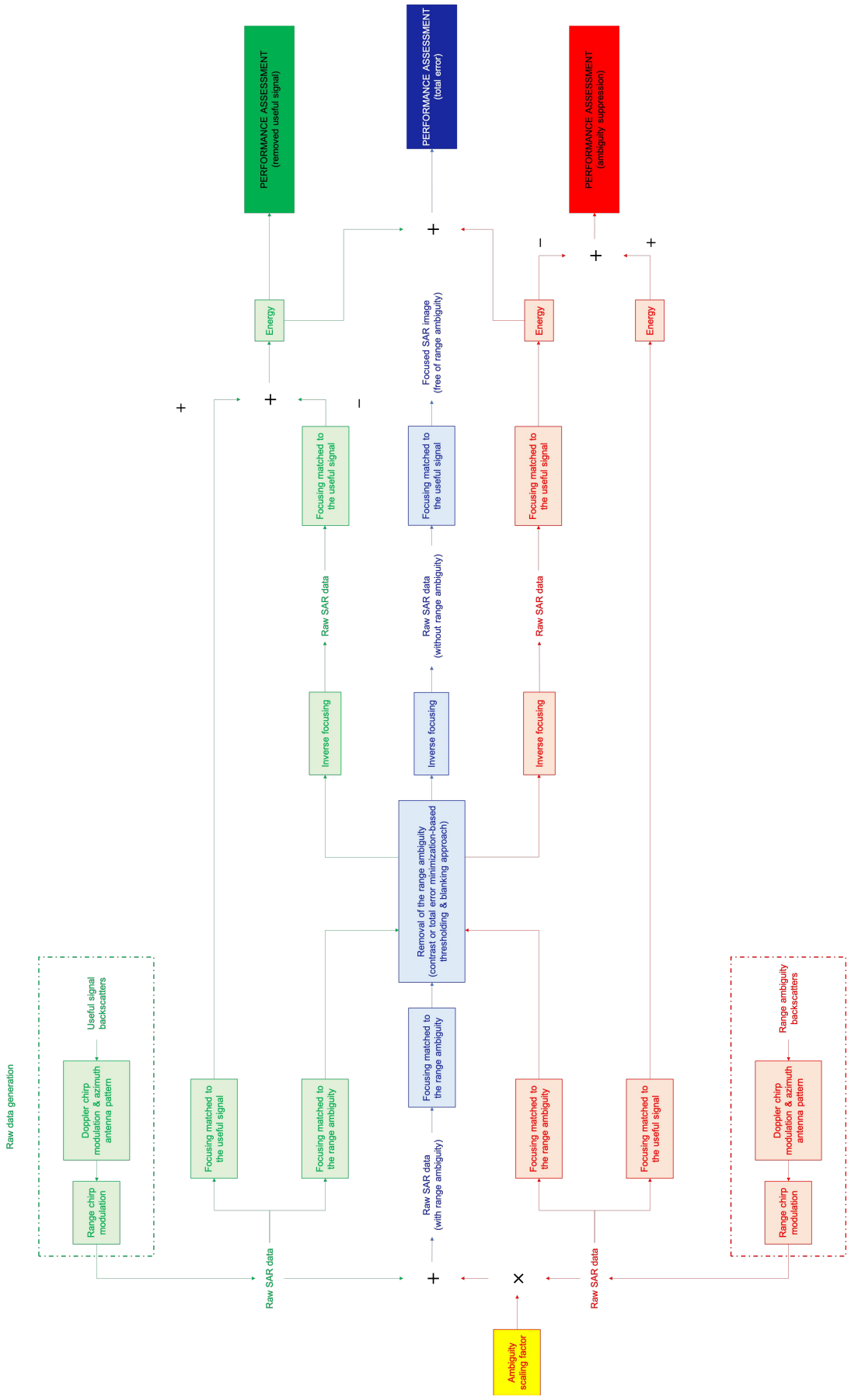

Figure 28: Block diagram of the proposed performance assessment methodology, for a waveform-encoded SAR system designed for range ambiguities suppression.

4.1.1 Data Set Used for the Analyses

The assessment of the system performance, i.e. of the image quality of the superimposed signal resulting from the range ambiguity impact on the desired echo, can be performed only if the useful and ambiguous signals are separately available within the simulation, as shown in the block diagram in Figure 28. Since the proposed methodology exploits real TerraSAR-X data, the two separate signals are thus simulated starting from two different parts of such an image. In particular, from the TerraSAR-X data set acquired over the Greater Munich area, Germany, four blocks (4096 x 4096 pixels) are extracted corresponding to different typical features of a SAR image: a lake in Bavaria, i.e. Lake Starnberg (Figure 29a), the Munich urban area (Figure 29b), a forest (Figure 29c) and finally a suburbs town, i.e. Germering (Figure 29d). Figure 29 displays these four scenes, extracted from the real TerraSAR-X image and employed during simulations: the complex values of such images are thus assumed to correspond to the actual complex backscatters of the corresponding scenes, in order to be able to simulate the same real scenario as a SAR system would acquire in practice. The availability of some SAR images allows simulating several scenarios, i.e. different combinations of scenes, by simply assuming different parts of the acquired TerraSAR-X image to correspond to both the useful and ambiguous signals. In particular, the sample case study in Section 5.1 has been obtained by supposing a range ambiguity, due to the Munich urban area, on the desired echo given by the lake. This scenario is not so interesting in practice, as the water backscattering is almost zero and the range ambiguity can thus be removed by simply applying a mask over the lake; however, within a simulation context, it gives a more visible information of the resulting image quality, due to the range ambiguity superimposition to the useful signal. More interesting scenarios, in practice, have been simulated, assuming the ambiguities of the same Munich urban area and of a suburbs town, i.e. Germering, on a forest, respectively, as the removal or the attenuation of the range ambiguous signal is mandatory for some interferometric and polarimetric applications, e.g. parameters retrieval.

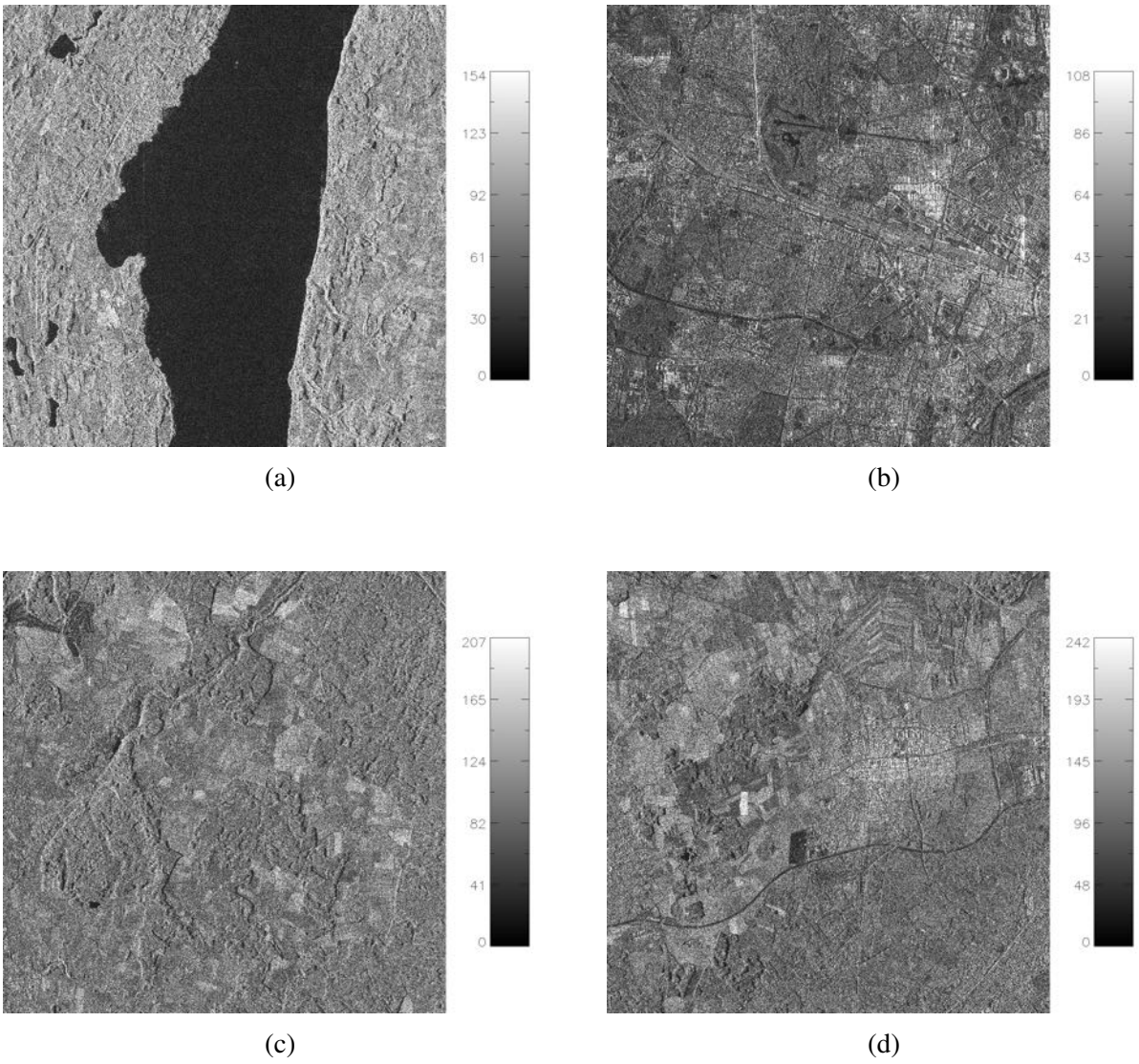

Figure 29: Data set used for the analyses. From the TerraSAR-X data set acquired over the Greater Munich area, Germany, four portions are extracted corresponding to different typical features of a SAR image: Lake Starnberg (a), the Munich urban area (b), a forest (c) and a suburbs town, i.e. Germering (d). Both the images have the same size, i.e. 4096 x 4096 pixels. The horizontal and vertical axes represent slant range and azimuth, respectively.

4.1.2 Raw Data Generation

In order to assess the range ambiguity suppression and system performance for such a waveform-encoded SAR system, simulated raw SAR data are generated using a TerraSAR-X image acquired over the Greater Munich area, Germany. From the complex backscatters of a portion of the image, e.g. the Lake Starnberg, it is possible to generate raw data as they would be acquired by a SAR system characterized by the parameters of Table 2, both without and with waveform variation [21].

Parameter	Value
Wavelength	0.229 m
Orbit height	628 km
Antenna length	9.9 m
Chirp duration	132.89474 µs
Chirp bandwidth	38 MHz
Range sampling frequency	41.8 MHz
PRF	2000 Hz
Processed Doppler bandwidth	1400 Hz
Processing window in range	Generalized Hamming, $\alpha = 0.6$
Processing window in azimuth	Generalized Hamming, $\alpha = 0.6$

Table 2: System and processing parameters [21].

In particular, a Doppler chirp modulation, combined with the azimuth antenna pattern, allows spreading each backscattering coefficient over the entire radar synthetic aperture L_s, i.e. along the azimuth direction. Then, a further chirp modulation, along the range dimension, is required in order to spread the complex backscatters of the image over the chirp duration τ, and thus to obtain simulated raw data for the SAR image assumed to correspond to the useful signal. This last operation also allows simulating both a conventional SAR, without waveform variation, and waveform-encoded SAR systems, characterized by a pulse-to-pulse variation of the transmitted waveform. This is made possible by simply considering different sequences of waveforms, i.e. conventional chirps for a conventional SAR system and cyclically-shifted chirps or an alternation between up- and down-chirps for the proposed waveform-encoded SAR system. Analogously, the complex backscatters of a different part of the image, e.g. the Munich urban area, can be used to simulate raw data for the range ambiguity, considering both the two different simulated systems, i.e. conventional SAR and waveform-encoded SAR systems, and assuming for the last one both the two waveform variation schemes described in Section 3.2. In the specific, as the range ambiguous signal corresponds to different transmitted pulses, compared to the useful one, raw SAR data are generated using different waveforms, while performing the range chirp modulation, with respect to the desired echo. Hence, they are then superimposed, through a sum operation, to the ambiguity-free raw data, thus obtaining superimposed simulated raw SAR data for such systems. In order to simulate different ambiguity strengths, the ambiguous signal raw data can be attenuated, i.e. amplitude-scaled, through an ambiguity scaling factor. Figure 30 schematically shows the raw SAR data generation methodology for both the useful and ambiguous signals, highlighting the procedure of raw data generation for the superimposed signal, resulting from the range ambiguity impact on the desired echo. In the specific, Figure 30 refers to the employment of cyclically-shifted chirps while simulating such a waveform-encoded SAR system.

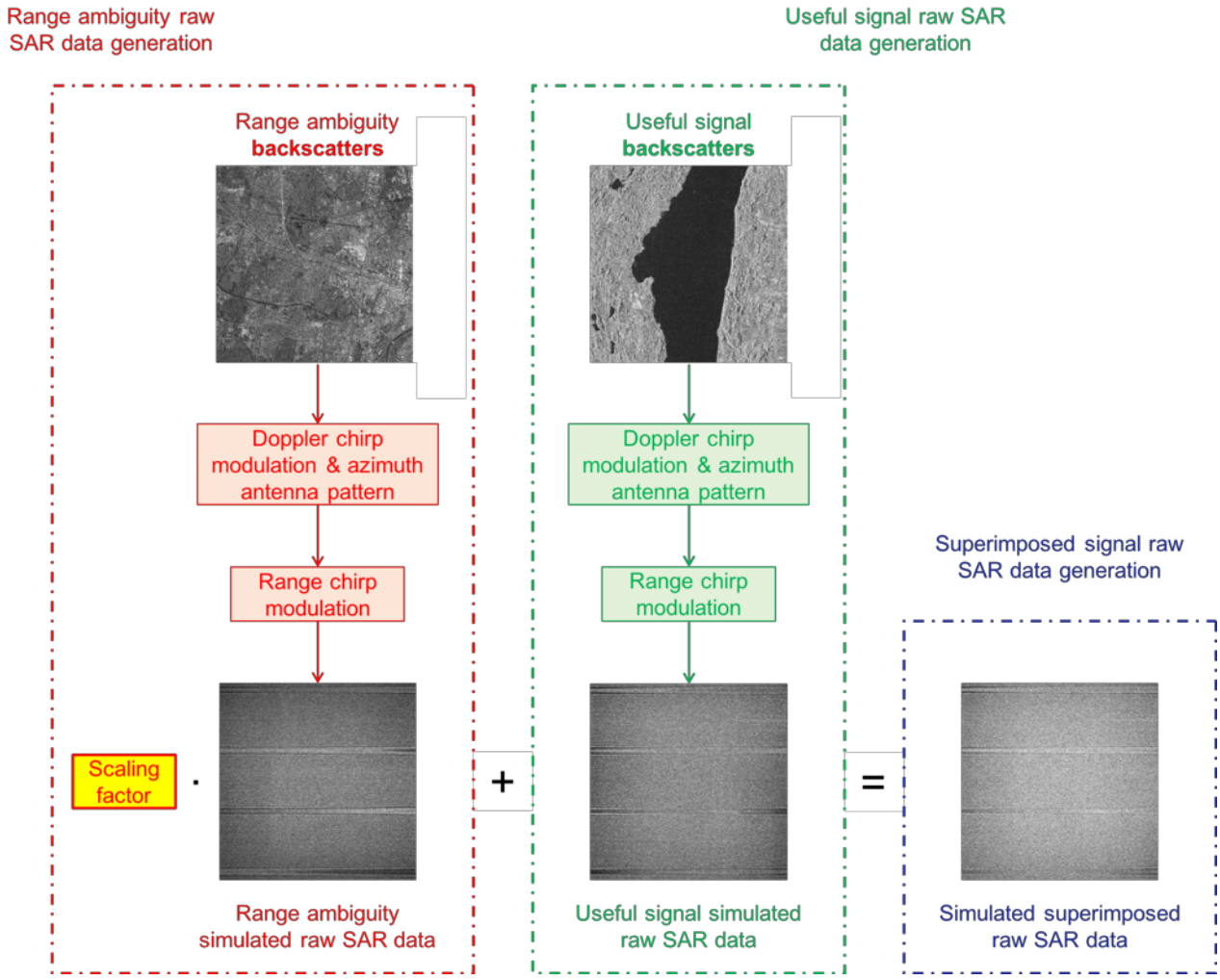

Figure 30: Schematic representation of the methodology for raw SAR data generation. In the specific, it refers to the employment of cyclically-shifted chirps while simulating the proposed waveform-encoded SAR system. The block diagram in green refers to the useful signal raw data generation, and it is analogous to the procedure of raw SAR data generation for the range ambiguity. The two range chirp modulation operations consider different transmitted waveforms, as the useful and ambiguous signals correspond to succeeding transmitted pulses. The simulated raw data corresponding to the range ambiguous signal can be amplitude-scaled through a scaling factor, in order to simulate different ambiguity strengths, and is then superimposed, through a sum operation, to the ambiguity-free one, thus obtaining the superimposed simulated raw SAR data for such a system.

4.1.3 Threshold Selection: Optimal Threshold

An assessment of the image quality, and thus of the system performance, is required for such a waveform-encoded SAR, in order to understand the behavior of the proposed contrast minimization method with reference to the best achievable performance. In particular, a total error measure can be evaluated after focusing matched to the useful signal as a function of thresholds and with reference to the ambiguity-free image, by exploiting the separate knowledge of useful and ambiguous signals within the simulation. Hence, since the presented multi-focus post-processing is performed separately for the two superimposed echoes, this error can be decomposed into two separate components, i.e. the residual ambiguous signal and the removed useful signal, and can be thus written as

$$Err_{tot} = \sum |I_{amb}|^2 + \sum |I_{sign,ref} - I_{sign}|^2 \tag{45}$$

where I_{amb} and I_{sign} identify the focused ambiguous and useful signals matched to the desired echo, respectively; in the specific, $I_{sign,ref}$ is obtained by considering the mere waveform encoding, thus without multi-focus post-processing, while I_{sign} refers to the employment of the proposed multi-focus post-processing with a thresholding and blanking approach for suppressing the range ambiguity. After focusing the superimposed raw SAR data using a filter matched to the range ambiguous signal, the removal of the ambiguity is performed by simply implementing a thresholding and blanking approach (Section 3.3.1). The simplest criterion for optimal threshold selection could be the minimization of the total error after ambiguity removal in the focused data matched to the ambiguous signal, as function of a set of thresholds; however, it leads to a sub-optimal threshold, as the error is computed not in the end of the post-processing chain, but in middle, after suppressing the ambiguous signal in the focused data matched to the range ambiguity. An optimal threshold can be thus obtained by minimizing the total error after focusing matched to the useful signal. In particular, such an error is computed after performing the proposed multi-focus post-processing for each threshold of the set used for suppressing the range ambiguity through the considered thresholding and blanking approach. This makes possible to define a total error curve as function of thresholds; as a consequence, the optimal threshold is simply obtained by minimizing the just defined total error function. However, as far as the computational load is concerned, the procedure for optimal threshold selection is quite expensive, as the entire multi-focus post-processing is required to be performed for all the possible thresholds. Figure 31 schematically shows the described procedure for optimal threshold selection, highlighting, in the bottom right red box, the total relative error curve as function of thresholds, for the sample case study of Section 5.1 and assuming cyclically-shifted chirps as transmitted waveforms.

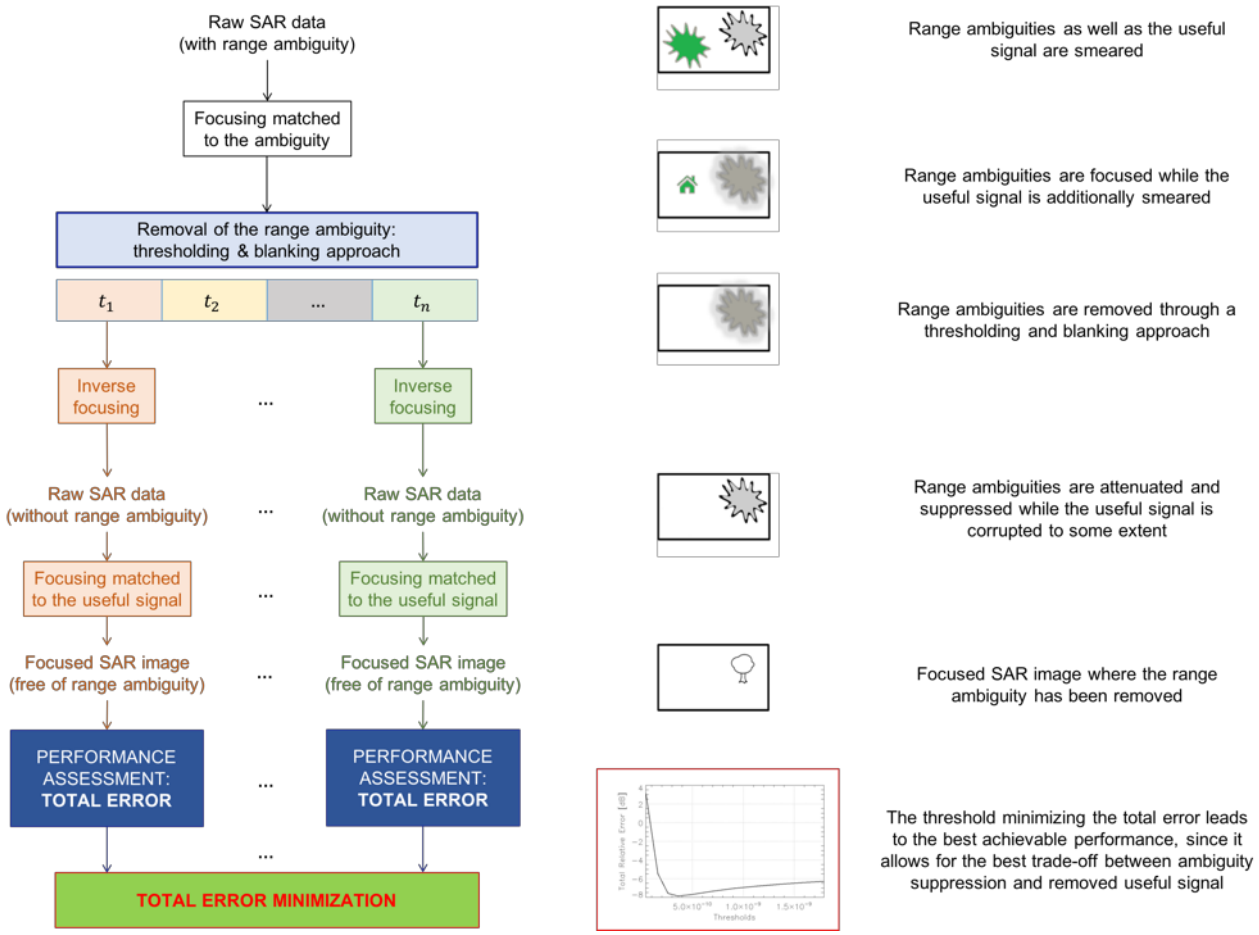

Figure 31: Schematic representation of the methodology for optimal threshold selection. The total error is evaluated for all the possible thresholds in the end of the multi-focus post-processing chain, after focusing matched to the useful signal. The plot in the bottom right red box refers to the total relative error as function of thresholds, assuming the sample case study of Section 5.1 and cyclically-shifted chirps on transmit.

The total error minimization can be used as best reference to assess the system performance, and thus the resulting image quality, as it leads to an optimal threshold allowing for the best trade-off between ambiguity suppression and removed useful signal. However, this best achievable performance, and thus the optimal threshold, cannot be obtained in practice, but only within a simulation context, as the useful and ambiguous signals are required to be separately available.

As far as block size considerations are concerned, the same image quality assessment is performed in order to evaluate the contrast minimization method, for threshold selection, with reference to the best achievable performance, for all the possible analyzed block sizes. However, only block-based sub-optimal thresholds are considered for achieving the best performance, as optimal thresholds cannot be obtained because of a too big computational load. The block-based and contrast minimization-based thresholding and blanking approach (Section 3.3.3) is thus assessed with reference to a sub-optimal performance; in the specific, this last one is made possible by minimizing the block-based total error after ambiguity removal, in the focused superimposed data matched to the ambiguous signal. The procedure presented in Section 3.3.3 is kept for the moving window implementation, so that the total error is computed on a bigger window centered on each block, while the blanking step, once the block-based sub-optimal threshold has been computed, is performed only inside the corresponding original block.

4.2 Performance Measures

In order to assess the system performance, and thus the quality of the resulting corrupted image, due to the range ambiguity, four different performance figures are evaluated after performing the proposed multi-focus post-processing. In particular, these measures are obtained by exploiting the separate knowledge of the useful and range ambiguous signals within the simulation context, thus making the system performance analysis not possible in practice, as only the sum of the two superimposed signals is available. The proposed performance measures aim to assess the just presented waveform-encoded SAR system with reference to a conventional SAR one, without waveform variation on transmit. Also, they allow evaluating the employment of a multi-focus post-processing with a thresholding and blanking approach and based on a contrast minimization method, for threshold selection, on the focused superimposed signal matched to the ambiguity, with reference to the mere waveform encoding, as well as the best achievable performance resulting from the minimization of the total error, in the end of the post-processing chain, after focusing matched to the useful signal. The main performance figure is given by the computation of the total error after focusing matched to the desired echo; it allows understanding the image quality improvement, exploiting the presented waveform-encoded SAR concept, compared to a conventional SAR system, as well as the goodness of the proposed multi-focus post-processing with a contrast minimization-based thresholding and blanking approach (to be applied in practice), with reference to both the mere waveform encoding and the best achievable performance, for different system and processing parameters, e.g. processed Doppler bandwidth and block size, and several range ambiguity strengths (Section 5.2). In the specific, the total error is defined with reference to the ambiguity-free image, as

$$Err_{tot} = \sum |I_{amb}|^2 + \sum |I_{sign,ref} - I_{sign}|^2 \tag{46}$$

and is thus given by two separate contributions, i.e. the residual ambiguous signal ($\sum |I_{amb}|^2$) and the removed useful signal ($\sum |I_{sign,ref} - I_{sign}|^2$). I_{amb} and I_{sign} identify the focused ambiguous and useful signals matched to the desired echo, respectively; in the specific, $I_{sign,ref}$ is obtained by considering the mere waveform encoding, without multi-focus post-processing, while I_{sign} refers to the employment of the proposed multi-focus post-processing with a thresholding and blanking approach for suppressing the range ambiguity. The same error can be expressed in dB and as a relative error, by scaling it through the energy of the ambiguity-free signal

$$Err_{tot,rel}[dB] = 10 \cdot \log\left(\frac{\sum |I_{amb}|^2 + \sum |I_{sign,ref} - I_{sign}|^2}{\sum |I_{sign,ref}|^2}\right) \tag{47}$$

Two further performance figures, i.e. the residual ambiguity e the removed useful signal, can be derived from the total error measure. In particular, the removed relative signal is present only if the proposed multi-focus post-processing is considered, as the mere waveform encoding allows suppressing, not only smearing, the range ambiguity without corruption of the useful signal. Analogously to the total error, these two performance measure can be written in dB and as relative errors, in order to understand their contribution on the total relative error. In the specific, the residual relative ambiguity and the removed relative signal can be expressed in dB as

$$Err_{amb,rel}[dB] = 10 \cdot \log\left(\frac{\sum |I_{amb}|^2}{\sum |I_{sign,ref}|^2}\right) \tag{48}$$

$$Err_{sign,rel}[dB] = 10 \cdot \log\left(\frac{\sum |I_{sign,ref} - I_{sign}|^2}{\sum |I_{sign,ref}|^2}\right) \tag{49}$$

respectively. In order to assess the ambiguity suppression performance, a last measure can be obtained from the residual ambiguity; however, despite the ambiguity suppression can be obtained for such

a waveform-encoded SAR system with reference to the focused ambiguous signal matched to the desired echo and assuming the mere waveform encoding, it is usually evaluated with reference to a conventional SAR system, without waveform variation, to accurately measure the range ambiguity suppression, determined by the proposed multi-focus post-processing, for the presented waveform-encoded SAR system. Therefore, it is given by

$$Suppr_{ambiguity} = \frac{E_{amb,ref}}{E_{amb}} = \frac{\sum |I_{amb,ref}|^2}{\sum |I_{amb}|^2} \tag{50}$$

where $E_{amb,ref}$ and E_{amb} are the energies of the range ambiguity, after focusing matched to the useful signal, assuming a conventional SAR system without pulse-to-pulse variation of the transmitted waveform, and the considered waveform-encoded SAR system with a multi-focus post-processing, respectively. Analogously to the previous measures, also the range ambiguity suppression is usually expressed in dB, as

$$Suppr_{ambiguity}[dB] = 10 \cdot \log\left(\frac{\sum |I_{amb,ref}|^2}{\sum |I_{amb}|^2}\right) = 10 \cdot \log\left(\sum |I_{amb,ref}|^2\right) - 10 \cdot \log\left(\sum |I_{amb}|^2\right) \tag{51}$$

The assessment of the system performance, and thus of the resulting image quality, through these four performance figures (usually three, as the residual ambiguity and the range ambiguity suppression are analogous, if knowing the energy of the focused ambiguous echo matched to the useful signal for a conventional SAR system), is performed for both the two different waveform variation schemes described in Section 3.2, i.e. the employment of cyclically-shifted chirps and an alternation of up- and down-chirps. Also, it is obtained for different system and processing parameters, e.g. processed Doppler bandwidth and block size, as well as several ambiguity strengths (Section 5.2), in order to understand the proposed system behaviour when these variables change.

5 Results

In the following, an example of implementation of the proposed technique, i.e. multi-focus post-processing with a thresholding and blanking approach, is presented together with an assessment of the range ambiguity suppression capabilities, for both the two considered waveform variation schemes described in Section 3.2. In particular, a sample case study corresponding to the range ambiguity of the Munich urban area on Lake Starnberg is assumed, in order to maximize the visible information of the resulting image quality, due to the ambiguous signal superimposition on the useful one. Specifically, the complex backscatters of these two portions, extracted from the real TerraSAR-X data set acquired over the Greater Munich area, Germany, allow simulating a typical L-band SAR system, characterized by the parameters of Table 3, both without and with waveform variation.

Parameter	Value
Wavelength	0.229 m
Orbit height	628 km
Antenna length	9.9 m
Chirp duration	132.89474 μs
Chirp bandwidth	38 MHz
Range sampling frequency	41.8 MHz
PRF	2000 Hz
Processed Doppler bandwidth	1400 Hz
Processing window in range	Generalized Hamming, α = 0.6
Processing window in azimuth	Generalized Hamming, α = 0.6

Table 3: System and processing parameters [21].

Also, several range ambiguity strengths have been simulated, as well as different combinations of scenes and different system and processing parameters, e.g. processed Doppler bandwidth and block size, in order to understand the proposed waveform-encoded SAR system performance behaviour when these variables change.

5.1 Sample Case Study: Ambiguity of an Urban Area on a Lake

In order to better understand the proposed waveform-encoded SAR concept for range ambiguity suppression, a sample case study is kept, where a range ambiguity, due to the Munich urban area, is assumed to be superimposed to a lake in Bavaria, i.e. Lake Starnberg. As described in Section 4.1.1, this scenario in not so interesting in practice, but allows obtaining a more visible information of the resulting image quality improvement due to such technique. In the following, an example of implementation of such a waveform-encoded SAR concept is presented step-by-step, together with an assessment of its range ambiguity suppression capabilities, as well as a histogram analysis of the ambiguous signal intensities. In particular, this section aims to show both the effects of transmitting different waveforms from pulse-to-pulse, i.e. both cyclically-shifted and up- and down- chirps, compared to a conventional SAR system, and the step-by-step implementation of the described thresholding and blanking-based multi-focus post-processing. As already said, in the following example the

Munich urban area (Figure 32b) is assumed to cause range ambiguity on Lake Starnberg (Figure 32a); however, the ambiguous signal is 10-dB amplitude scaled in order to simulate a very reasonable range ambiguity, despite a much higher attenuation is expected from the two-way elevation antenna pattern [21].

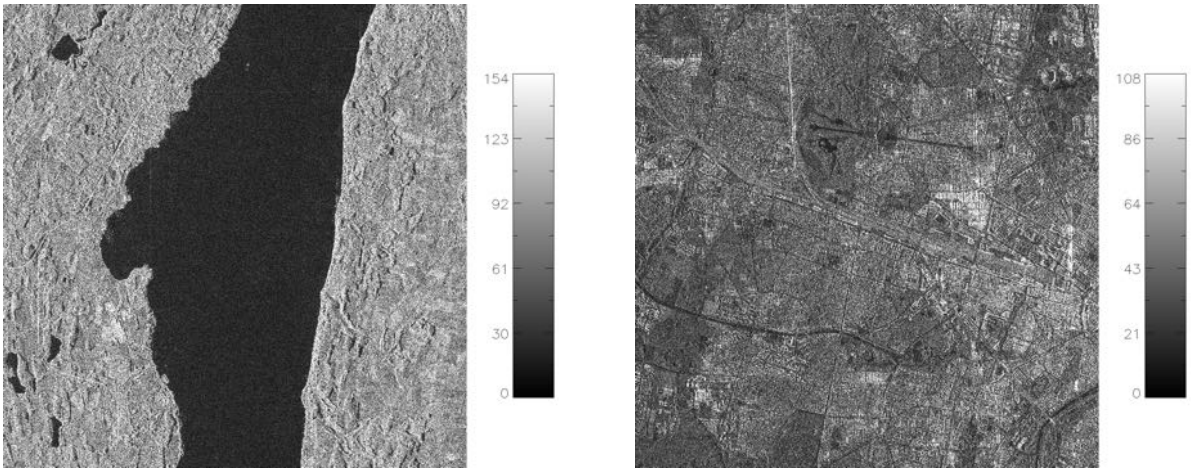

(a) (b)

Figure 32: SAR images, from the TerraSAR-X data set acquired over the Greater Munich area, Germany, used to simulate the range ambiguity, due to the Munich urban area (b), on a lake in Bavaria, i.e. Lake Starnberg (a). The ambiguous signal is then 10-dB amplitude scaled in order to simulate a very reasonable range ambiguity. Both the images have the same size, i.e. 4096 x 4096 pixels. The horizontal and vertical axes represent slant range and azimuth, respectively.

5.1.1 Waveform-Encoded SAR: Mere Waveform Encoding

In order to limit the impact of the range ambiguous signal on the useful one, and to implement the proposed waveform-encoded SAR system for range ambiguity suppression, waveform diversity must be kept on transmit, so that a different focusing can be performed for the two superimposed signals. In particular, assuming the two waveform variation schemes described in Section 3.2, i.e. cyclically-shifted and up- and down- chirps, the range ambiguity can be smeared in a different way, as well as a different ambiguity suppression can be achieved, compared to a conventional SAR system without waveform variation. First of all, a conventional SAR system has been simulated, assuming a 10-dB amplitude scaling of the range ambiguity; specifically, starting from the complex backscatters of two different portions of a real TerraSAR-X image acquired over the Greater Munich area, Germany, i.e. the Munich urban area (Figure 32b) and Lake Starnberg (Figure 32a), raw SAR data (Figures 33a, 33b, 33c) have been generated as they would have been acquired by a conventional SAR system characterized by the parameters of Table 3 and without waveform variation on transmit. Thus, they have been focused by compressing the raw data energy first along the range dimension and then along azimuth, by means of range and azimuth compression operations, respectively. Figure 33 show the detailed procedure for focusing the just simulated raw data, for both the useful, range ambiguous and superimposed signals, respectively; in particular, the focused range ambiguity in Figure 33h appears as slightly-defocused artifacts and significantly corrupts the final acquired image (Figure 33i).

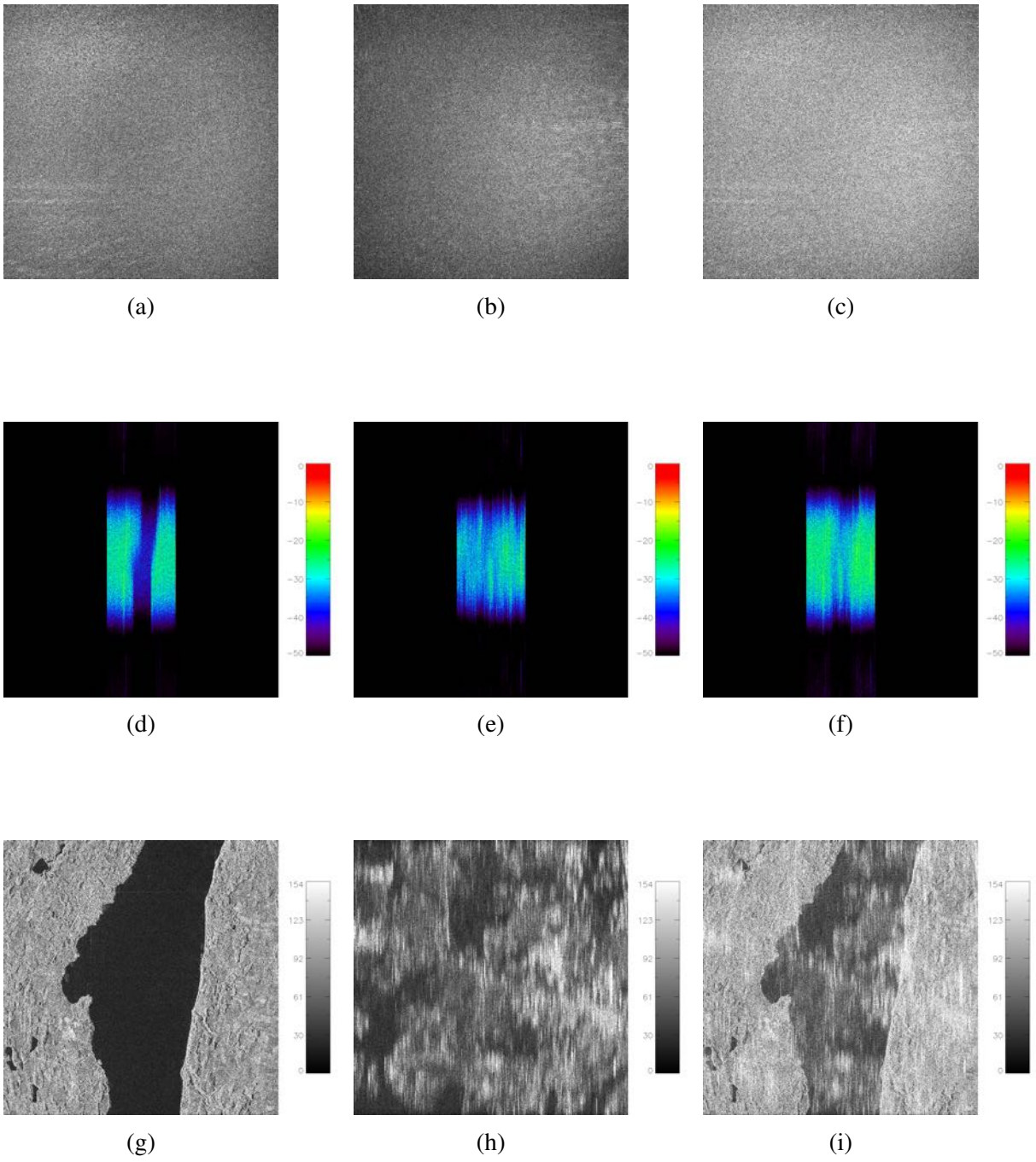

Figure 33: Focused simulated data as they would be acquired by a conventional SAR system characterized by the parameters of Table 3 and without waveform variation. The simulated raw SAR data, corresponding to both the useful (a), ambiguous (b) and superimposed (c) signals, are focused by means of range and azimuth compression operations, to obtain the focused signals in (g), (h), (i), respectively. Both the images have the same size, i.e. 4096 x 4096 pixels. The range ambiguity appears as slightly-defocused localized artifacts over the lake, strongly corrupting the final acquired image (i). (d), (e) and (f) show the range-compressed data (16384 x 16384 pixels) obtained after compressing the simulated raw data along the range dimension, corresponding to both the two separate, i.e. useful and range ambiguous, and superimposed signals, respectively. The horizontal and vertical axes represent slant range and azimuth, respectively.

Analogously, the same raw SAR data have been generated also for a waveform-encoded SAR sys-

tem characterized by a pulse-to-pulse variation of the transmitted waveform. However, in this context they are then focused using a filter matched to the useful signal, so that this one results to be properly focused and located, while the range ambiguity is smeared as well as suppressed to some extent. Specifically, as a consequence of continuously transmitting a different waveform from pulse-to-pulse, the ambiguous signal is uniformly smeared over the pulse width i.e. slant range direction, and the synthetic aperture, i.e. azimuth direction, appearing as a noise-like disturbance, as well as some ambiguous energy is suppressed. Similarly to a staggered SAR, in fact, the ambiguous energy is incoherently integrated in azimuth and spread almost uniformly across the Doppler spectrum; therefore, a part of it is filtered out during the SAR processing, if the PRF of the system is larger than its processed Doppler bandwidth [21][18]. Figure 35 and Figure 36 show the focusing procedure, starting from simulated raw data and using a filter matched to the useful signal, assuming a waveform-encoded SAR system characterized by cyclically-shifted and up- and down- chirps on transmit, respectively. As already explained, the employment of cyclically-shifted chirps as transmitted waveforms leads to the most uniform ambiguity smearing, as the range ambiguous signal, after range compression, is dislocated at different ranges and then smeared over azimuth as a consequence of azimuth compression, as well as to 1.9 dB ambiguity suppression without corruption of the useful signal. As alternative, the unfocused signal can be smeared only along the range direction, as a result of the pulse or range compression operation, if different, orthogonal waveforms are used for two succeeding transmitted pulses [21][11], i.e. up- and down-chirps alternation. Also, using up- and down- chirps implies a different spreading of the range ambiguous signal across the Doppler spectrum (Figure 34), compared to the employment of cyclically-shifted chirps, as well as a different ambiguous energy suppression (2.8 dB) without corruption of useful signal, by imposing the same processed Doppler bandwidth.

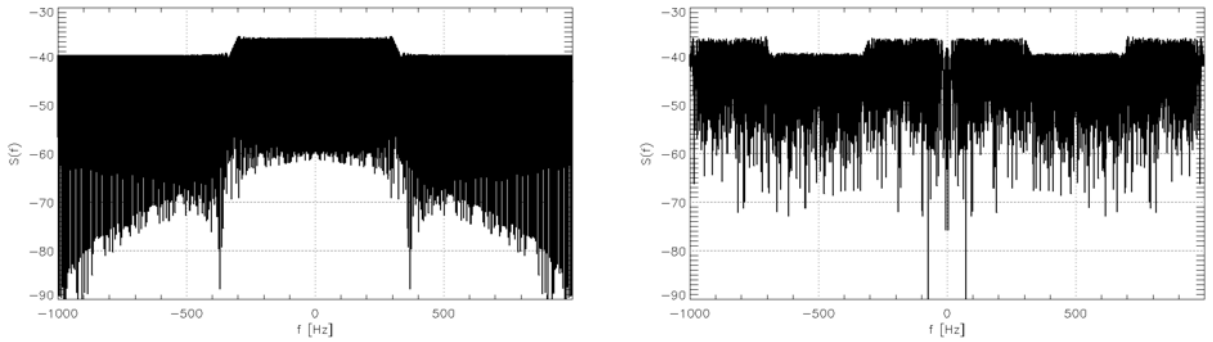

(a) (b)

Figure 34: Graphic representation of the ambiguity Doppler spectrum, if cyclically-shifted (a) or up- and down-chirps (b) are employed. By imposing the same processed Doppler bandwidth, and assuming it smaller than the considered *PRF*, a different range ambiguous energy suppression can be achieved without corruption of useful signal, for the two proposed waveform variation schemes. Specifically, for a 1400 Hz processed Doppler bandwidth, 1.9 dB (a) and 2.8 dB (b) range ambiguity suppression is achieved, assuming cyclically-shifted chirps and up- and down- chirp alternation on transmit, respectively.

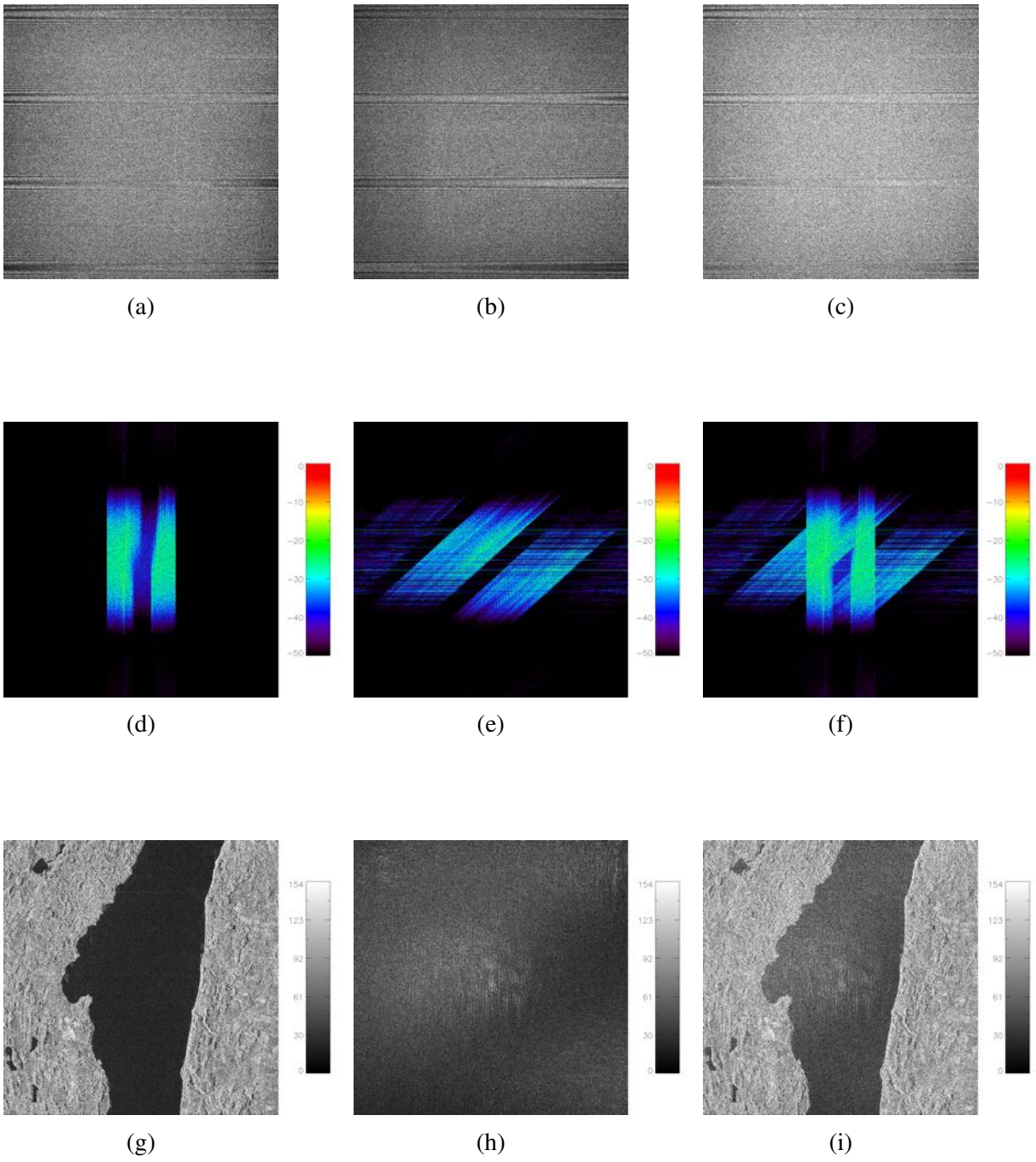

Figure 35: Focused simulated data as they would be acquired by a waveform-encoded SAR system characterized by the parameters of Table 3 and by cyclically-shifted chirps on transmit. The simulated raw SAR data, corresponding to both the useful (a), ambiguous (b) and superimposed (c) signals, are focused by means of range and azimuth compression operations, using a filter matched to the desired echo, to obtain the focused signals in (g), (h), (i), respectively. Both the images have the same size, i.e. 4096 x 4096 pixels. The range ambiguity appears as a noise-like disturbance, as well as some ambiguous energy (1.9 dB) is suppressed. (d), (e) and (f) show the range-compressed data (16384 x 16384 pixels) obtained after compressing the simulated raw data along the range dimension, corresponding to both the two separate, i.e. useful and range ambiguous, and superimposed signals, respectively. The horizontal and vertical axes represent slant range and azimuth, respectively.

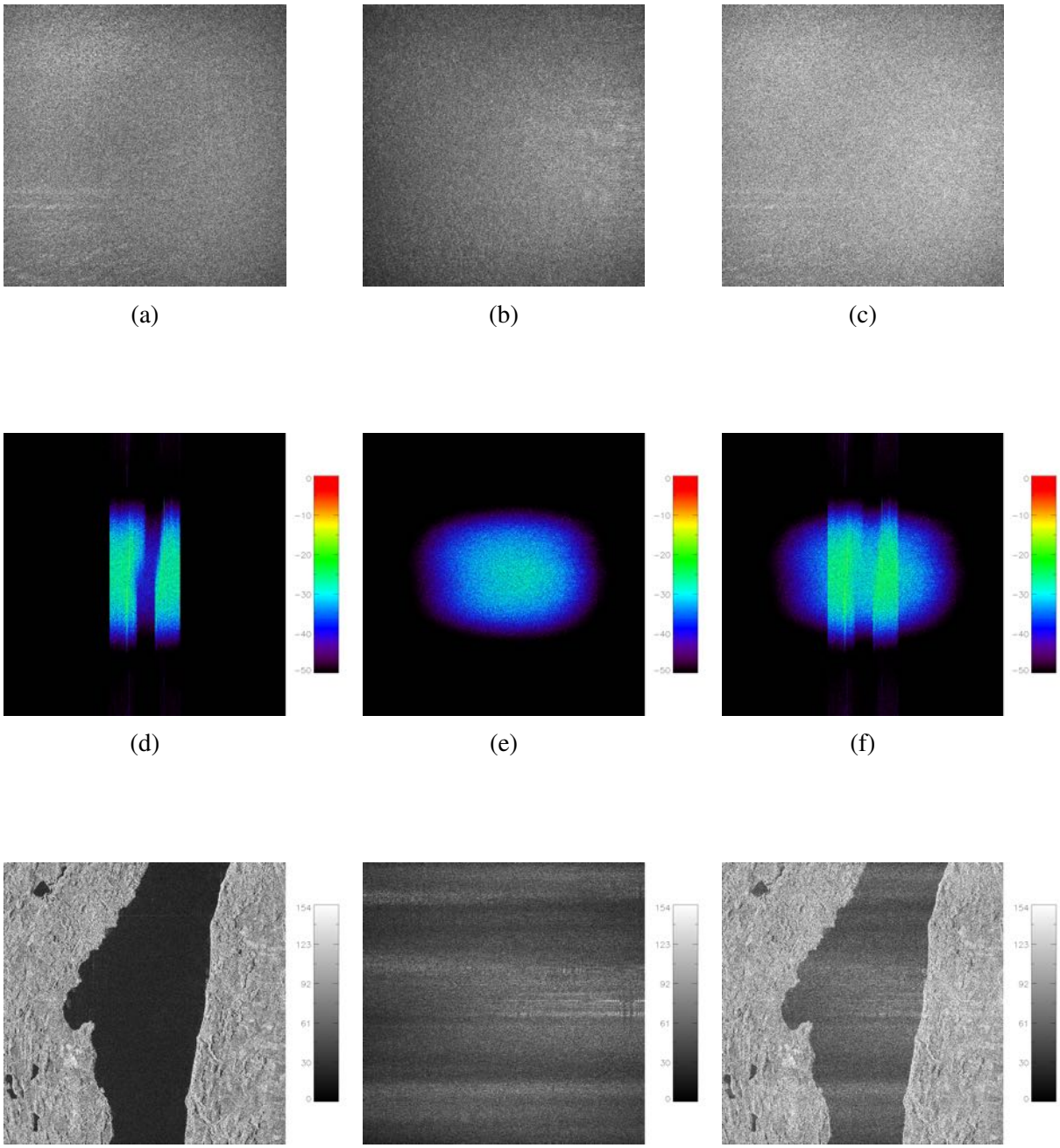

Figure 36: Focused simulated data as they would be acquired by a waveform-encoded SAR system characterized by the parameters of Table 3 and by an up- and down-chirp alternation on transmit. The simulated raw SAR data, corresponding to both the useful (a), ambiguous (b) and superimposed (c) signals, are focused by means of range and azimuth compression operations, using a filter matched to the desired echo, to obtain the focused signals in (g), (h), (i), respectively. Both the images have the same size, i.e. 4096 x 4096 pixels. The range ambiguity appears as a noise-like disturbance, as well as some ambiguous energy (2.8 dB) is suppressed. (d), (e) and (f) show the range-compressed data (16384 x 16384 pixels) obtained after compressing the simulated raw data along the range dimension, corresponding to both the two separate, i.e. useful and range ambiguous, and superimposed signals, respectively. The horizontal and vertical axes represent slant range and azimuth, respectively.

As results summary, the resulting corruption of the SAR image, i.e. Lake Starnberg, due to the

range ambiguity, i.e. the Munich urban area, is shown in Figures 37b, 37c and 37d, for a conventional SAR system without waveform variation, a SAR characterized by cyclically-shifted chirps on transmit, and a SAR system with up- and down- chirp alternation, respectively. While for a conventional SAR without waveform variation slightly-defocused artifacts can be observed over the lake, a waveform-encoded SAR system uniformly smears the range ambiguity over the pulse width and the synthetic aperture, or, as alternative, only over range, if cyclically-shifted or up- and down- chirps are used on transmit, respectively. In addition, some range ambiguous energy suppression is achieved (1.9 dB and 2.8 dB for Figure 37c and Figure 37d, respectively) by cutting the ambiguity Doppler spectrum through a processed Doppler bandwidth smaller than the considered *PRF* (Table 3).

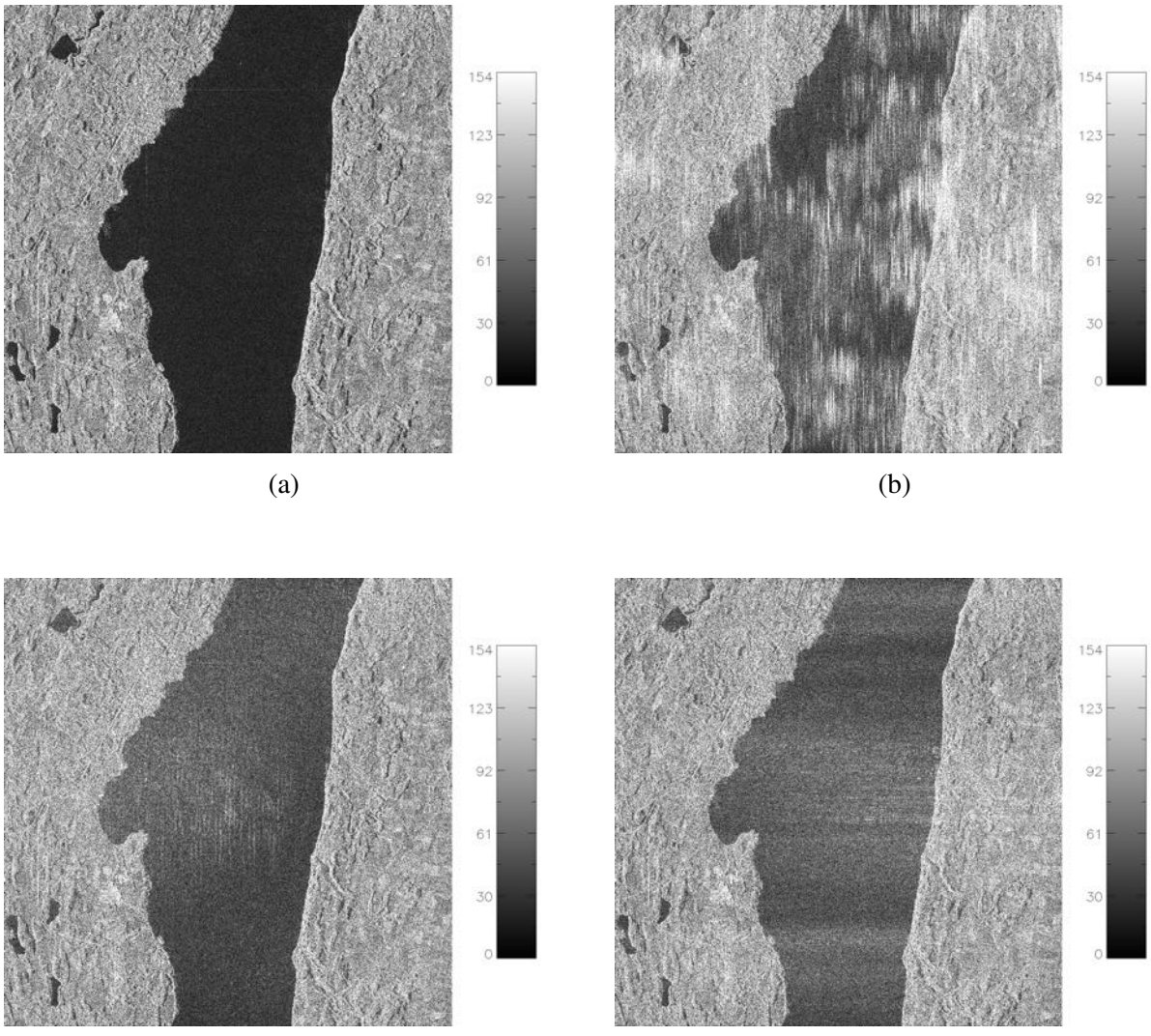

(a) (b)

(c) (d)

Figure 37: Impact of mere waveform variation on image quality using simulated data. (a) identifies the reference, ambiguity-free image, while (b), (c) and (d) show the corruption, due to a strong range ambiguity, i.e. the Munich urban area, for a conventional SAR without waveform variation and a waveform-encoded SAR system characterized by cyclically-shifted chirps on transmit, and an alternation between up- and down- chirps, respectively. In the specific, (c) and (d) present 1.9 dB and 2.8 dB ambiguity suppression, as well as an uniform smearing (the range ambiguous signal appears as a noise-like disturbance rather than localized artifacts), compared to (b). Both the images have the same size, i.e. 4096 x 4096 pixels. The horizontal and vertical axes represent slant range and azimuth, respectively.

As well as total smearing and some ambiguous energy suppression, a very interesting analysis can be performed on the intensities histogram of the range ambiguity, for both a conventional SAR and a waveform-encoded SAR system characterized by the two sequences of waveforms described in Section 3.2. Since for a conventional SAR without waveform variation the ambiguous signal appears as localized slightly-defocused artifacts, the corresponding intensities histogram (Figure 38a) shows a higher mean and standard deviation, compared to a waveform-encoded SAR system with pulse-to-pulse variation of the transmitted waveform (Figures 38b, 38c); in particular, the distribution in Figure 38a is characterized by a higher standard deviation compared to the mean (Table 4), so justifying the presence of localized artifacts. Differently, if the proposed waveform-encoded SAR system is considered, the unfocused range ambiguous signal presents an intensities distribution characterized by similar values for the mean and the standard deviation (Table 4), assuming both cyclically-shifted (Figure 38b) and up- and down- chirps (Figure 38c) on transmit. Usually, such distribution is commonly observed in noise-like disturbance; the range ambiguity can be thus modeled as noise.

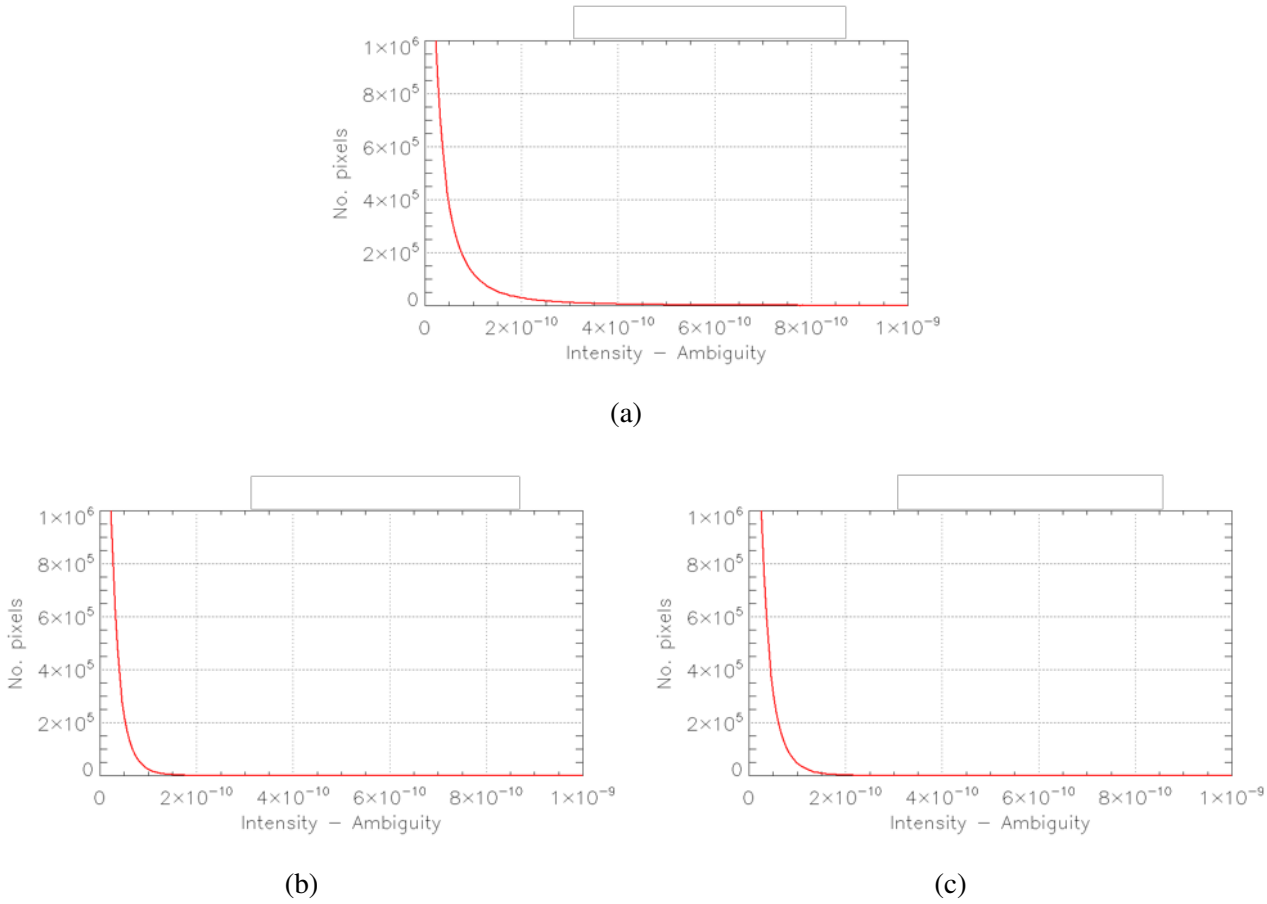

(a)

(b)

(c)

Figure 38: Histograms of intensities of the unfocused range ambiguity. (a) refers to a conventional SAR system without waveform variation, while (b) and (c) refer to the employment of cyclically-shifted and up- and down- chirps, respectively, assuming the proposed waveform-encoded SAR system.

RANGE AMBIGUITY HISTOGRAMS		Mean	Standard Deviation
Conventional SAR (a)		**6.2027948e-11**	**3.4605504e-10**
Waveform-encoded SAR Only encoding	Cyclically-shifted chirps (b)	**1.7261775e-11**	**1.9848748e-11**
	Up- and down-chirp alternation (c)	**2.1837652e-11**	**2.5064031e-11**

Table 4: Comparison between the main descriptors, i.e. mean and standard deviation, of the histograms in Figure 38.

5.1.2 Waveform-Encoded SAR: Multi-Focus Post-Processing

As well as waveform diversity on transmit, a multi-focus post-processing is required, in order to achieve a better ambiguity suppression; therefore, raw SAR data are subsequently focused with filters matched to each range ambiguous signal, in order to highlight and remove it. In this example, for simplicity, only one range ambiguity, i.e. the Munich urban area, is assumed to be superimposed to the useful signal, i.e. Lake Starnberg. Specifically, this section aims to show the step-by-step implementation of the proposed thresholding and blanking-based multi-focus post-processing, together with an assessment of its range ambiguity suppression capabilities. Simulated raw data, corresponding to both the useful, ambiguous and superimposed signals and generated for a waveform-encoded SAR system with cyclically-shifted and up- and down- chirps, are thus focused using a filter matched to the range ambiguity, so that it will be properly focused and located, while the desired echo will be smeared, dependently on the sequence of waveforms used, as a consequence of the use of a mismatched filter. Figure 39 and Figure 40 show this focusing procedure, assuming a waveform-encoded SAR system characterized by cyclically-shifted and up- and down- chirps on transmit, respectively, where simulated raw data are focused using a filter matched to the ambiguity, in order to highlight it. In particular, as already described, the employment of cyclically-shifted chirps as transmitted waveforms allows smearing the useful signal (Figure 39g) most uniformly over range and azimuth, as consequence of range and azimuth compression, respectively, while using an up- and down- chirp alternation allows smearing it (Figure 40g) only along the range direction, as a result of the pulse compression operation.

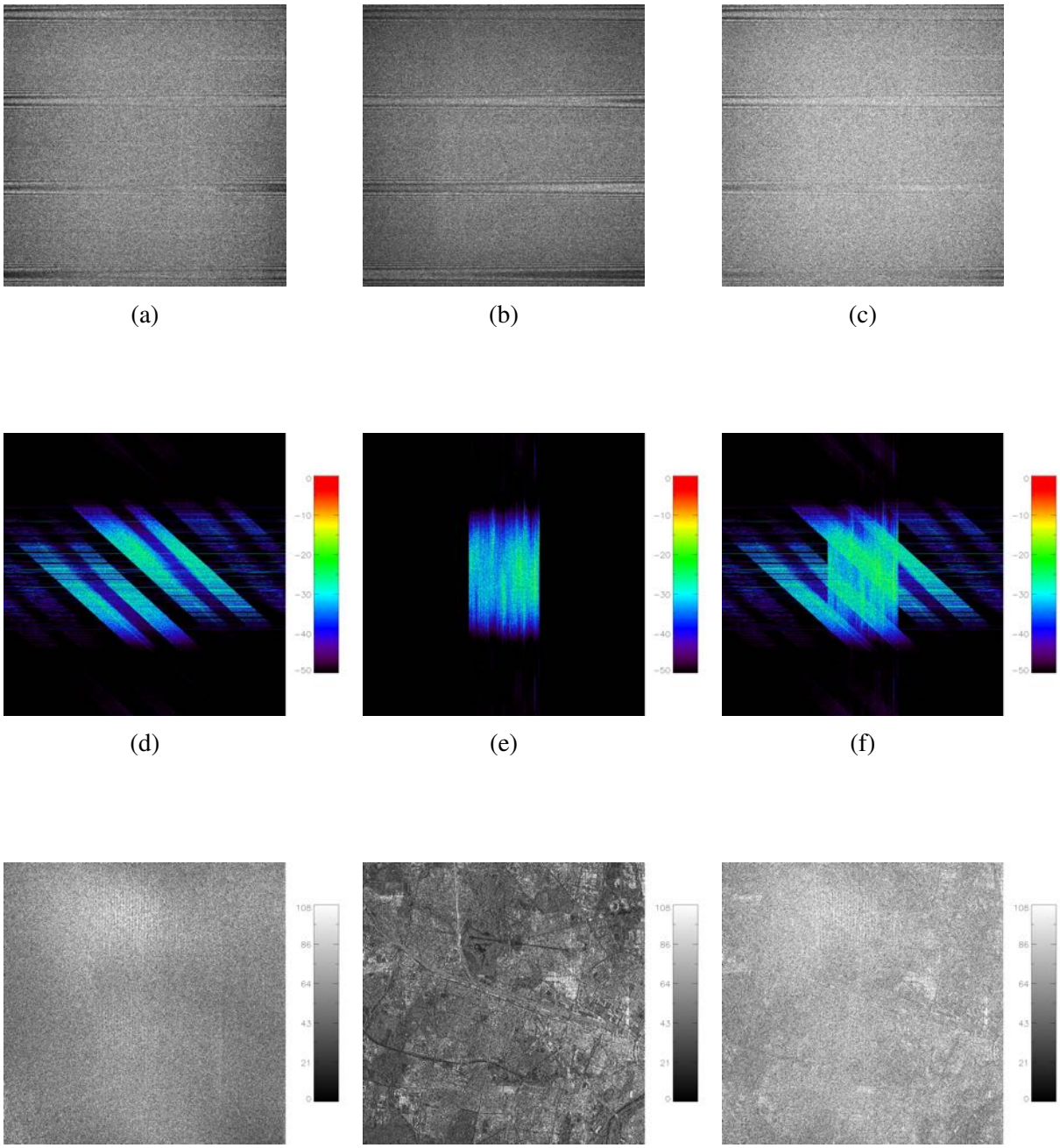

Figure 39: Focused simulated data using a filter matched to the range ambiguity, as they would be acquired by a waveform-encoded SAR system characterized by the parameters of Table 1 and by cyclically-shifted chirps on transmit. The simulated raw SAR data, corresponding to both the useful (a), ambiguous (b) and superimposed (c) signals, are focused by means of range and azimuth compression operations, using a filter matched to the range ambiguous signal, to obtain the focused images in (g), (h), (i), respectively. Both the images have the same size, i.e. 4096 x 4096 pixels. The range ambiguity (h) results to be properly focused and located, while the desired echo (g) is smeared most uniformly over range and azimuth, as consequence of compression operations along these two orthogonal directions. (d), (e) and (f) show the range-compressed data (16384 x 16384 pixels) obtained after compressing the simulated raw data along the range dimension, corresponding to both the two separate, i.e. useful and range ambiguous, and superimposed signals, respectively. The horizontal and vertical axes represent slant range and azimuth, respectively.

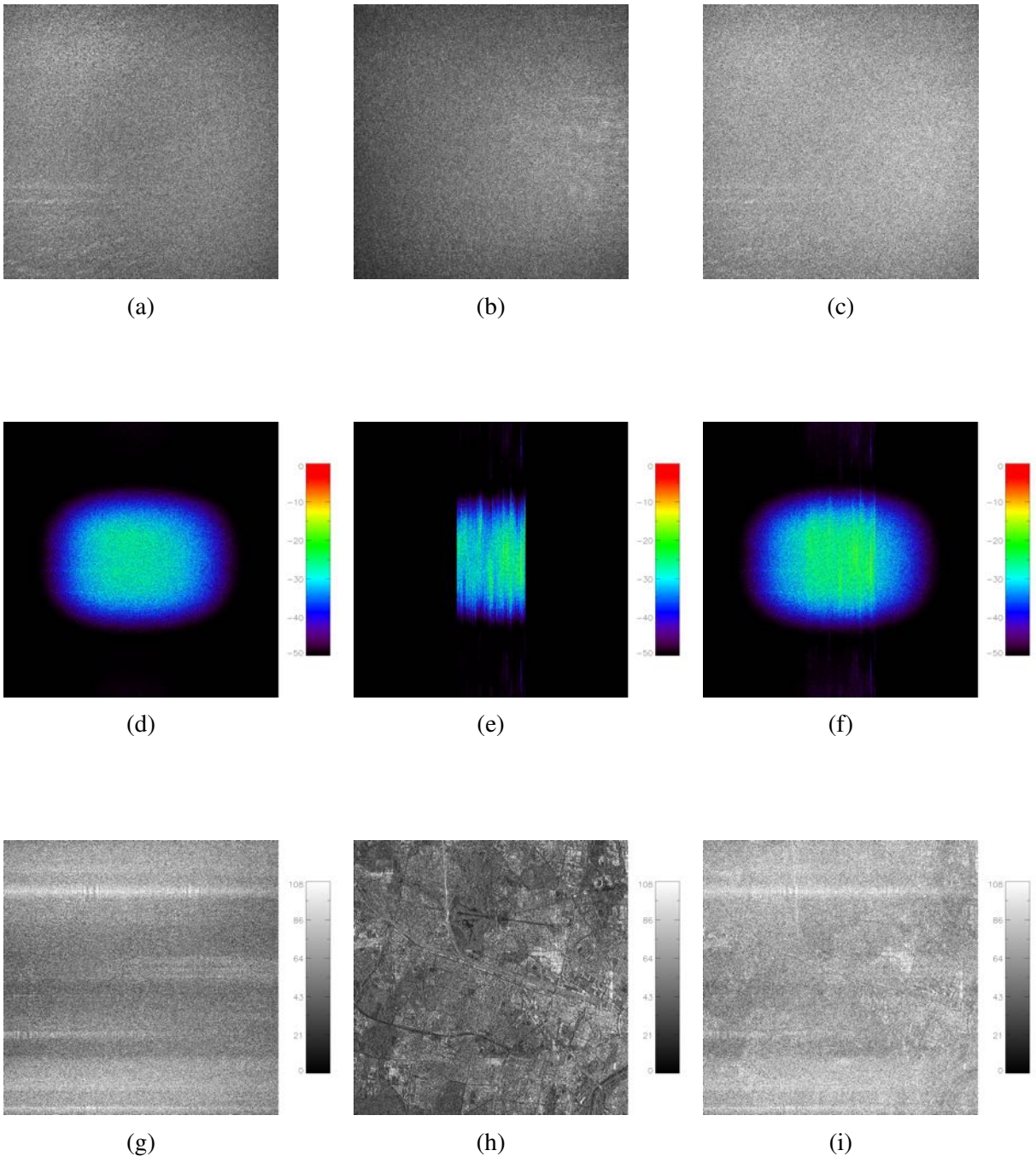

Figure 40: Focused simulated data using a filter matched to the range ambiguity, as they would be acquired by a waveform-encoded SAR system characterized by the parameters of Table 1 and by an up- and down- chirp alternation on transmit. The simulated raw SAR data, corresponding to both the useful (a), ambiguous (b) and superimposed (c) signals, are focused by means of range and azimuth compression operations, using a filter matched to the range ambiguous signal, to obtain the focused images in (g), (h), (i), respectively. Both the images have the same size, i.e. 4096 x 4096 pixels. The range ambiguity (h) results to be properly focused and located, while the desired echo (g) is only smeared along the range direction, as a result of the pulse compression operation. (d), (e) and (f) show the range-compressed data (16384 x 16384 pixels) obtained after compressing the simulated raw data along the range dimension, corresponding to both the two separate, i.e. useful and range ambiguous, and superimposed signals, respectively. The horizontal and vertical axes represent slant range and azimuth, respectively.

In order to suppress the range ambiguity, once simulated raw SAR data are focused using a filter matched to it, i.e. the ambiguous signal results to be correctly focused and properly located, while the useful signal is smeared, a thresholding and blanking approach can be applied (Section 3.3.1), by simply setting to zero all the pixels with intensity higher than a given threshold; specifically, the blanking operation is performed on both the useful, ambiguous and superimposed signals. However, the main issue while dealing with such a thresholding and blanking approach is related to the difficulty of finding an effective criterion for threshold selection. In this example, the results of the proposed contrast minimization-based thresholding and blanking approach (Section 3.3.2) are shown, while its range ambiguity suppression capabilities are evaluated with reference to the best achievable performance, referring to the use of an optimal threshold (Section 4.1.3), i.e. obtained by minimizing the total error, defined as the sum between the residual ambiguous signal and the removed useful signal. In particular, the contrast minimization is performed in the focused superimposed signal matched to the range ambiguity, as only it is available in practice. Figure 41 and Figure 42 show the ambiguity removal procedure based on contrast minimization, for the proposed waveform-encoded SAR system with cyclically-shifted chirps, and the inverse focusing operation, through which the latter focused data, where the range ambiguity has been removed, are transformed back into raw SAR data, respectively.

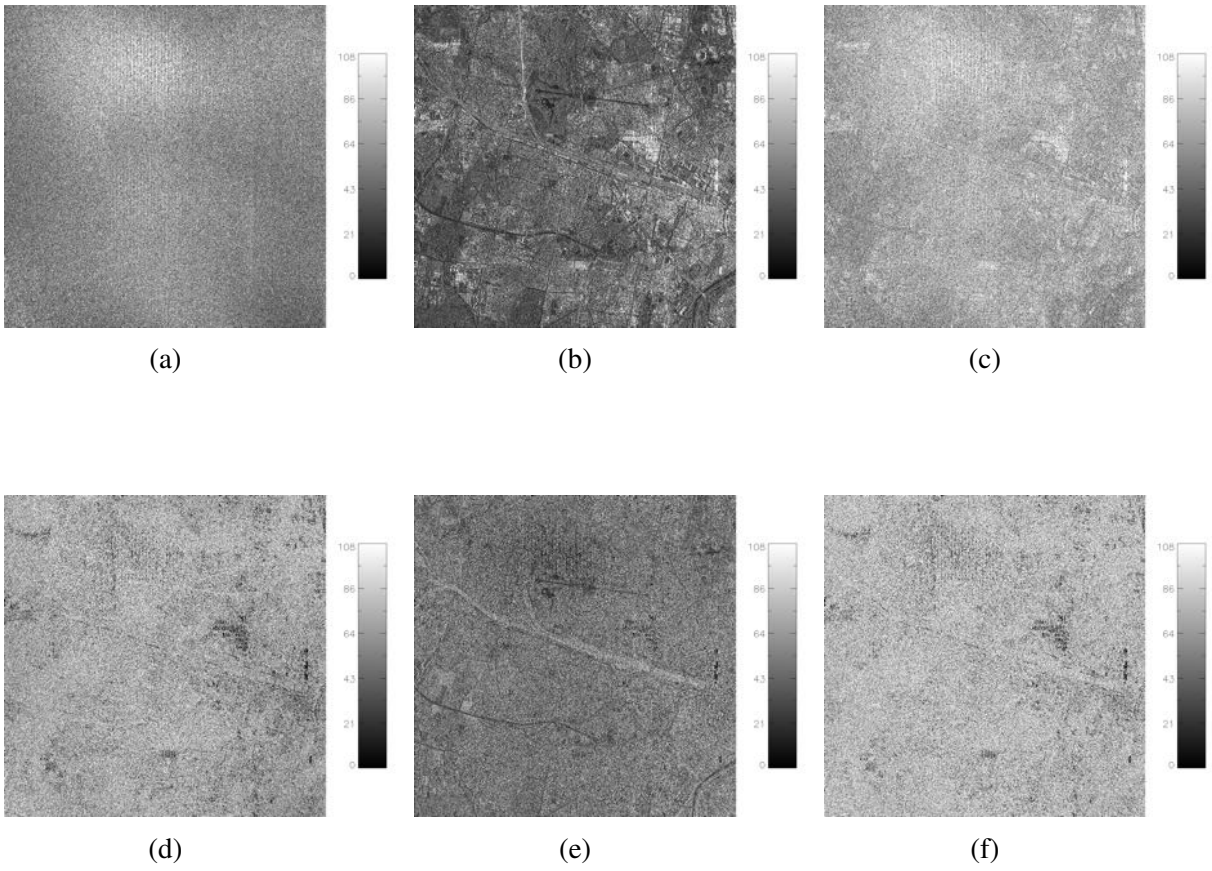

(a) (b) (c)

(d) (e) (f)

Figure 41: Range ambiguity removal through a contrast minimization-based thresholding and blanking approach, assuming a waveform-encoded SAR system with cyclically-shifted chirps on transmit. Despite the contrast minimization is performed on the superimposed focused signal matched to the ambiguity (c), pixels are blanked, i.e. set to zero, on both the useful (d), ambiguous (e) and superimposed (f) images. Both the images have the same size, i.e. 4096 x 4096 pixels. The horizontal and vertical axes represent slant range and azimuth, respectively.

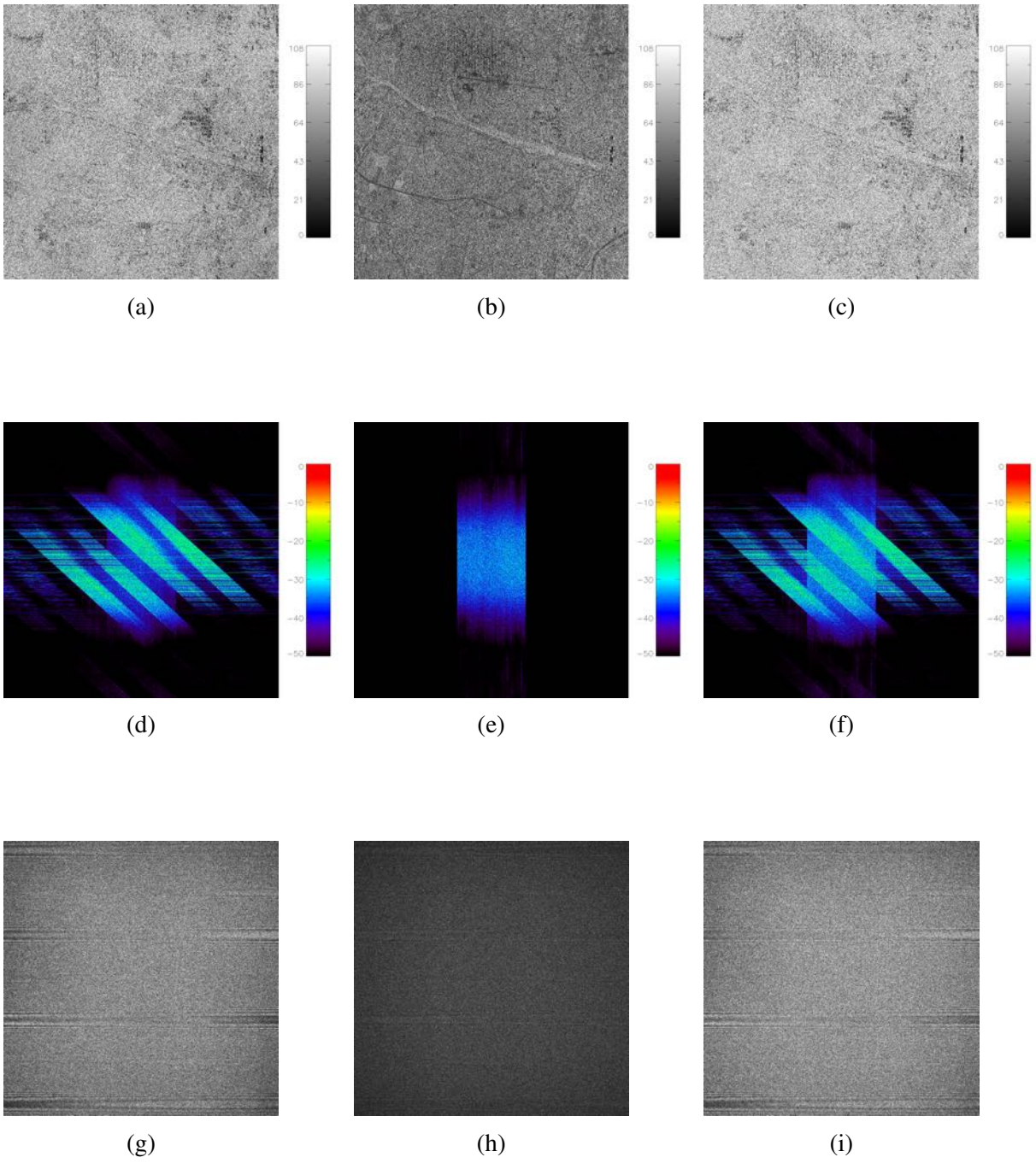

Figure 42: Inverse focusing procedure, assuming a waveform-encoded SAR system with cyclically-shifted chirps on transmit. The latter focused data matched to the range ambiguity, i.e. useful (a), ambiguous (b) and superimposed (c) signals, in which the range ambiguity has been removed, are transformed back into raw SAR data, i.e. (g), (h) and (i), respectively. Both the images have the same size, i.e. 4096 x 4096 pixels. (d), (e) and (f) show the range-decompressed images (16384 x 16384 pixels), obtained as a result of range decompression, corresponding to both the two separate, i.e. useful and range ambiguous, and superimposed signals, respectively. The horizontal and vertical axes represent slant range and azimuth, respectively.

In the following, the same procedures, i.e. range ambiguity removal through a contrast minimization-based thresholding and blanking approach (Figure 43) and the inverse focusing operation (Figure 44), respectively, are shown also for a waveform-encoded SAR system characterized by an up- and down-

chirp alternation on transmit, thus highlighting the impact of transmitting a different sequence of waveforms while performing the inverse focusing, in particular in the range-decompressed data.

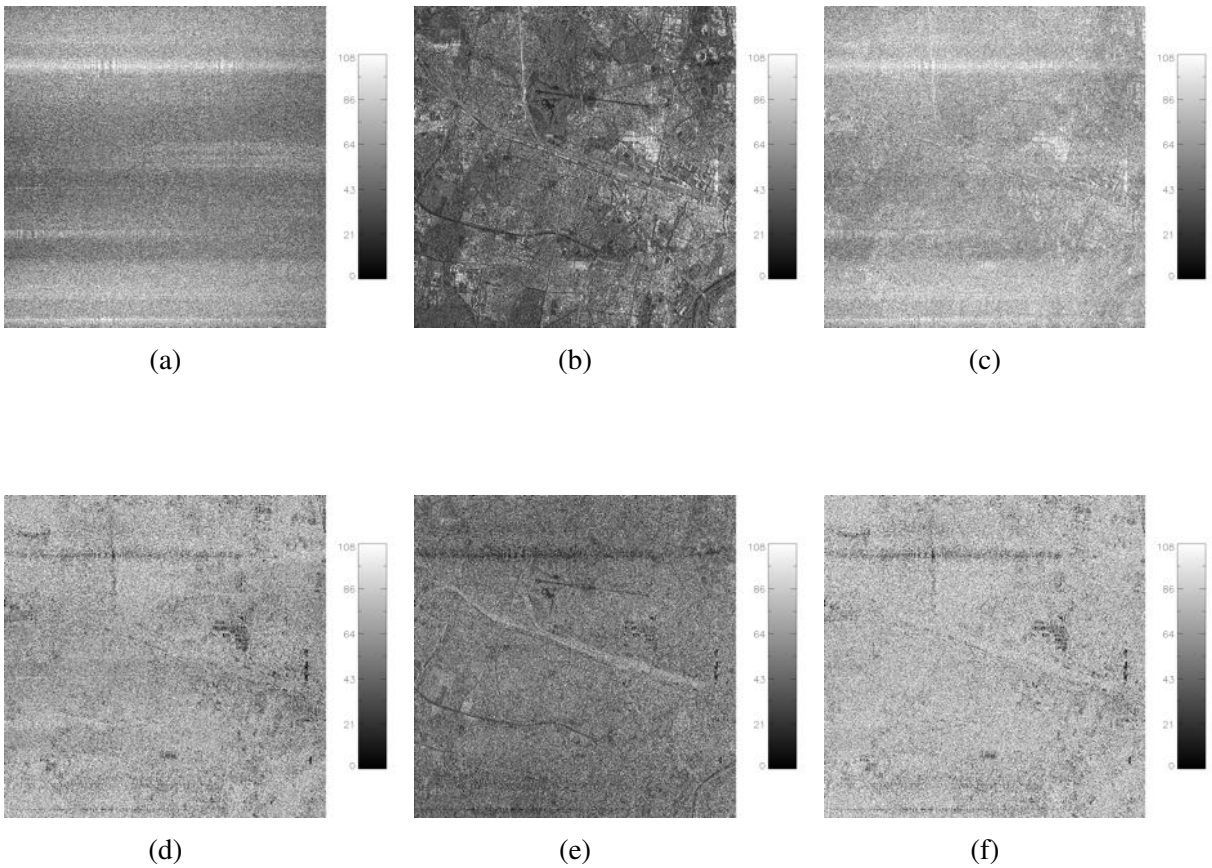

(a) (b) (c)

(d) (e) (f)

Figure 43: Range ambiguity removal through a contrast minimization-based thresholding and blanking approach, assuming a waveform-encoded SAR system with an up- and down- chirp alternation on transmit. Despite the contrast minimization is performed on the superimposed focused signal matched to the ambiguity (c), pixels are blanked, i.e. set to zero, on both the useful (d), ambiguous (e) and superimposed (f) images. Both the images have the same size, i.e. 4096 x 4096 pixels. The horizontal and vertical axes represent slant range and azimuth, respectively.

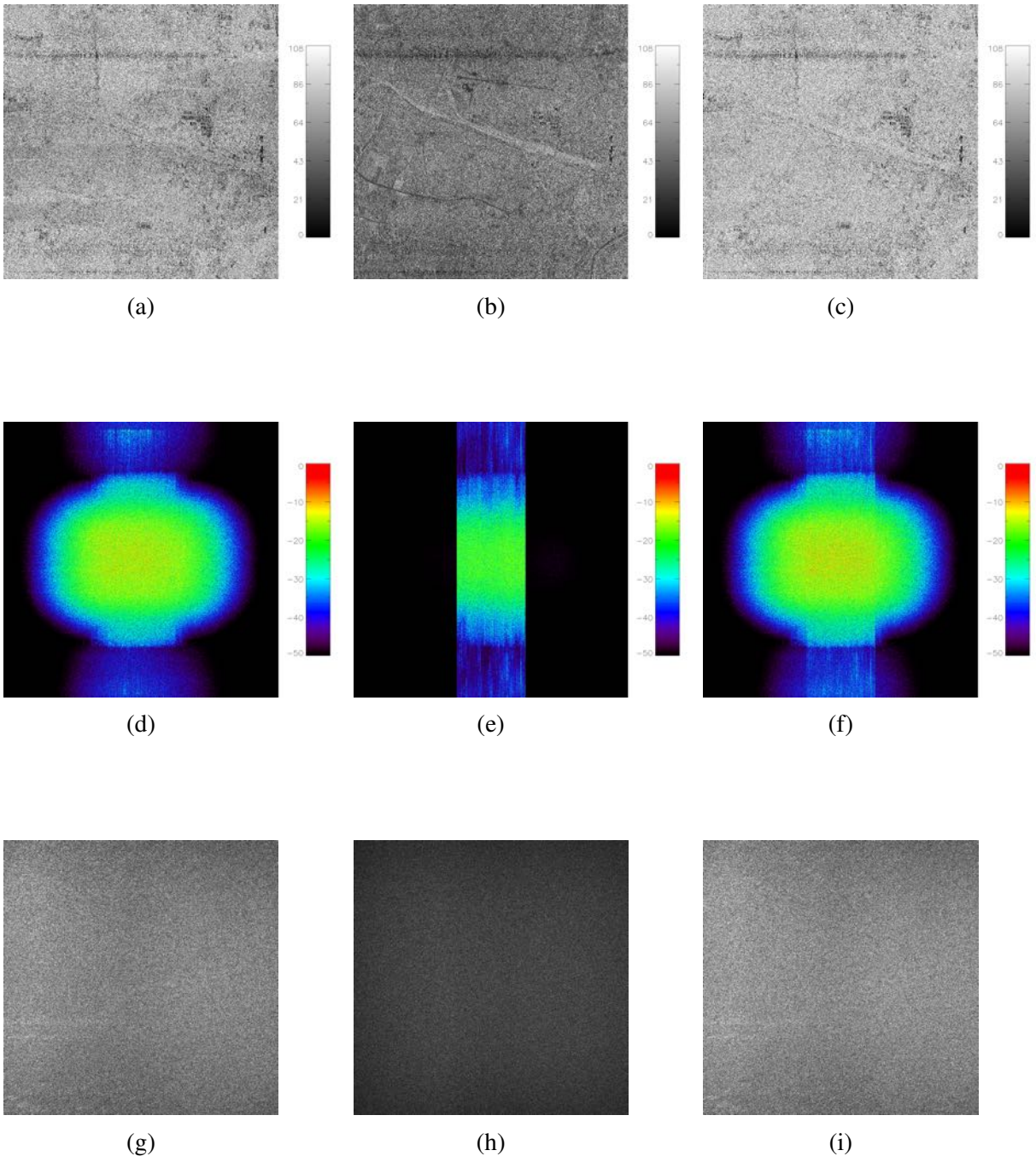

Figure 44: Inverse focusing procedure, assuming a waveform-encoded SAR system with an up- and down- chirp alternation on transmit. The latter focused data matched to the range ambiguity, i.e. useful (a), ambiguous (b) and superimposed (c) signals, in which the range ambiguity has been removed, are transformed back into raw SAR data, i.e. (g), (h) and (i), respectively. Both the images have the same size, i.e. 4096 x 4096 pixels. (d), (e) and (f) show the range-decompressed images (16384 x 16384 pixels), obtained as a result of range decompression, corresponding to both the two separate, i.e. useful and range ambiguous, and superimposed signals, respectively. The horizontal and vertical axes represent slant range and azimuth, respectively.

Once the focused images matched to the range ambiguity, in which the ambiguous signal has been removed, are transformed back to raw SAR data, a further focusing, using a filter matched to the useful signal, is required in order to finally obtain a focused image, where the range ambiguity is significantly

attenuated, while the desired echo is only minimally affected. In particular, the focusing procedure is the same as described in Section 5.1.1, assuming a waveform-encoded SAR system with both cyclically-shifted and up- and down- chirps. Specifically, the useful signal will result to be correctly focused and properly located, despite few energy will be smeared, as consequence of removal of few pixels, while the residual range ambiguity will be smeared uniformly over range and azimuth, or only along the range dimension, if cyclically-shifted or up- and down- chirps are employed on transmit, respectively. Figure 45 and Figure 46 show this last multi-focus post-processing step, i.e. focusing using a filter matched to the useful signal, starting from raw data obtained as a result of the inverse focusing operation, after suppressing the range ambiguity in the focused data matched to the ambiguous signal; in particular, Figure 45 and Figure 46 refer to the proposed waveform-encoded SAR system, if cyclically-shifted and up- and down- chirps are employed as transmitted waveforms, respectively.

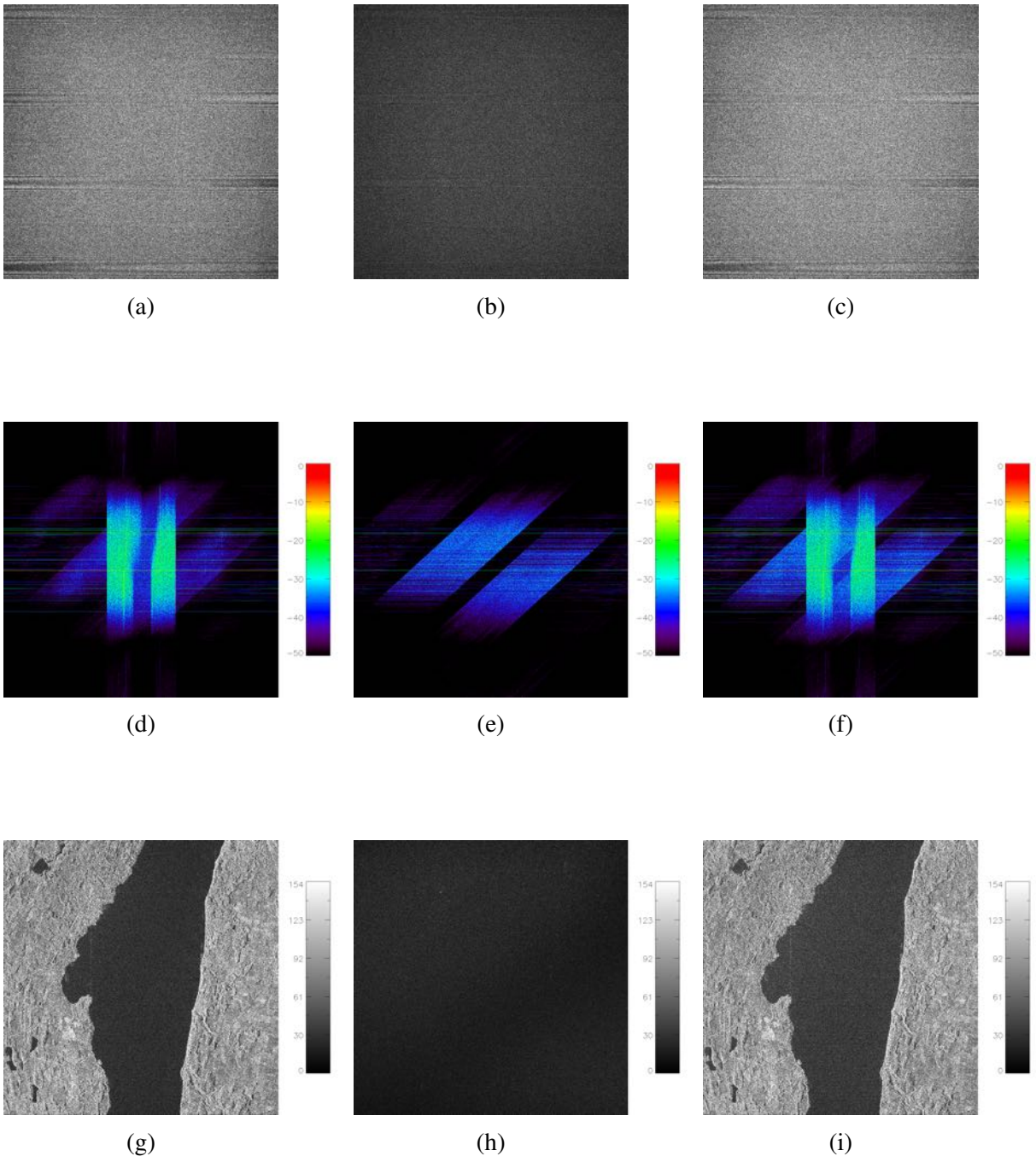

Figure 45: Focused simulated data after applying a contrast minimization-based thresholding and blanking approach, assuming a waveform-encoded SAR system characterized by the parameters of Table 3 and by cyclically-shifted chirps on transmit. The simulated raw SAR data obtained after performing the inverse focusing operation on the focused data matched to the range ambiguity, in which the ambiguous signal has been removed, and corresponding to both the useful (a), ambiguous (b) and superimposed (c) signals, are focused by means of range and azimuth compression operations, using a filter matched to the desired echo, to obtain the focused signals in (g), (h), (i), respectively. Both the images have the same size, i.e. 4096 x 4096 pixels. (d), (e) and (f) show the range-compressed data (16384 x 16384 pixels) obtained after compressing the simulated raw data along the range dimension, corresponding to both the two separate, i.e. useful and range ambiguous, and superimposed signals, respectively. The horizontal and vertical axes represent slant range and azimuth, respectively.

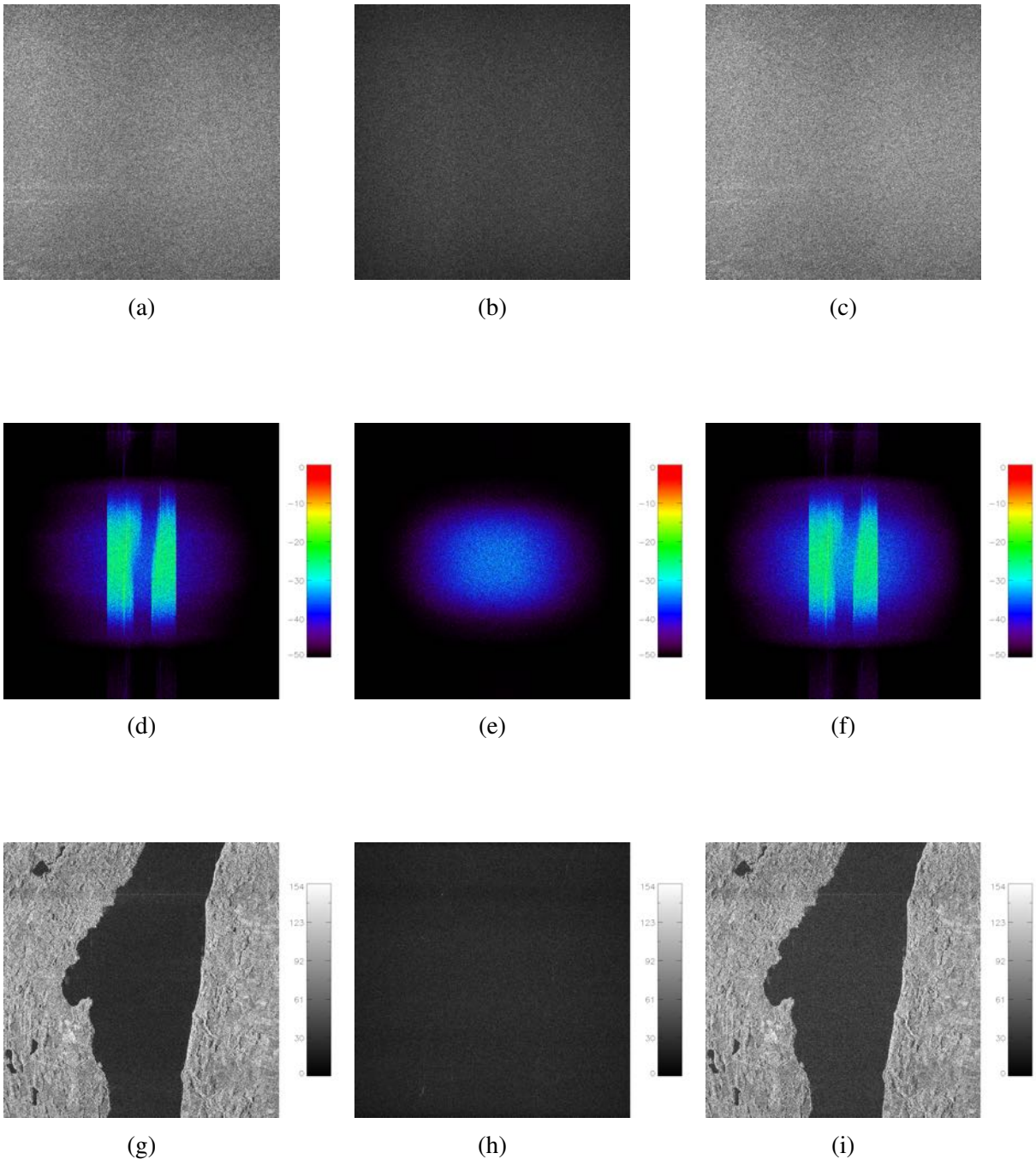

Figure 46: Focused simulated data after applying a contrast minimization-based thresholding and blanking approach, assuming a waveform-encoded SAR system characterized by the parameters of Table 3 and by an up- and down- chirp alternation on transmit. The simulated raw SAR data obtained after performing the inverse focusing operation on the focused data matched to the range ambiguity, in which the ambiguous signal has been removed, and corresponding to both the useful (a), ambiguous (b) and superimposed (c) signals, are focused by means of range and azimuth compression operations, using a filter matched to the desired echo, to obtain the focused signals in (g), (h), (i), respectively. Both the images have the same size, i.e. 4096 x 4096 pixels. (d), (e) and (f) show the range-compressed data (16384 x 16384 pixels) obtained after compressing the simulated raw data along the range dimension, corresponding to both the two separate, i.e. useful and range ambiguous, and superimposed signals, respectively. The horizontal and vertical axes represent slant range and azimuth, respectively.

In the following, the resulting corruption of the SAR image, corresponding to Lake Starnberg, due to the range ambiguity, i.e. the Munich urban area, is shown in Figure 47a and Figure 47b, for a waveform-encoded SAR characterized by cyclically-shifted chirps on transmit and considering the mere waveform encoding and the implementation of a multi-focus post-processing with a contrast minimization-based thresholding and blanking approach, respectively. Specifically, in this example, the proposed multi-focus post-processing (Section 3.3) with the described contrast minimization approach (Section 3.3.2) leads to 8.2 dB ambiguity suppression, with a negligible corruption of useful signal, i.e. additional 6.3 dB in comparison to the mere waveform encoding. Figure 47 shows the focused images (up) and the residual ambiguous signals (down) for the considered waveform-encoded SAR with cyclically-shifted chirps as transmitted waveforms, highlighting the improvement due to the proposed multi-focus post-processing (right), compared to the mere waveform encoding (left).

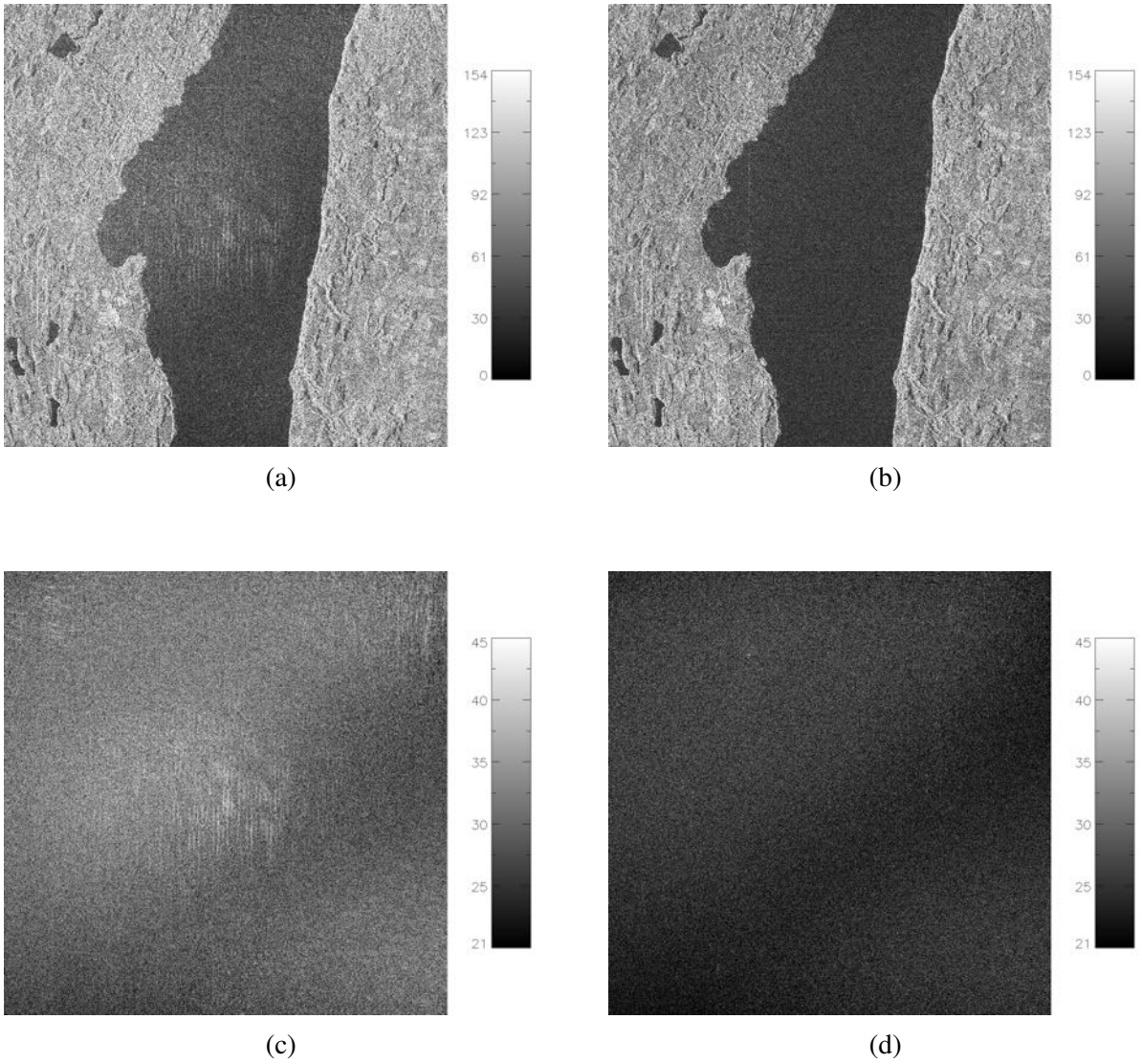

Figure 47: Focused images (up) and residual ambiguous signals (down) for a waveform-encoded SAR system, assuming cyclically-shifted chirps as transmitted waveforms, in case of mere waveform encoding (left) and a multi-focus post-processing with a contrast minimization-based thresholding and blanking approach (right). Both the images have the same size, i.e. 4096 x 4096 pixels. The horizontal and vertical axes represent slant range and azimuth, respectively.

In particular, the improvement in the range ambiguity suppression, due to the proposed multi-

focus post-processing with a contrast minimization-based thresholding and blanking approach, can be clearly observed also in the histograms of intensities in Figure 48, corresponding to the ambiguous signal. Specifically, Figure 48 shows the histogram of the ambiguous signal intensities assuming a multi-focus post-processing with a contrast minimization-based thresholding and blanking approach (blue curve), once the range ambiguity has been removed and after focusing data using a filter matched to the desired echo, thus highlighting the improvement in the range ambiguity suppression compared to a conventional SAR system without waveform variation (black curve) and to the proposed waveform-encoded SAR with cyclically-shifted chirps on transmit, assuming the mere waveform encoding (red curve), respectively. Moreover, the three different histograms are quantitatively described in Table 5 through mean and standard deviation.

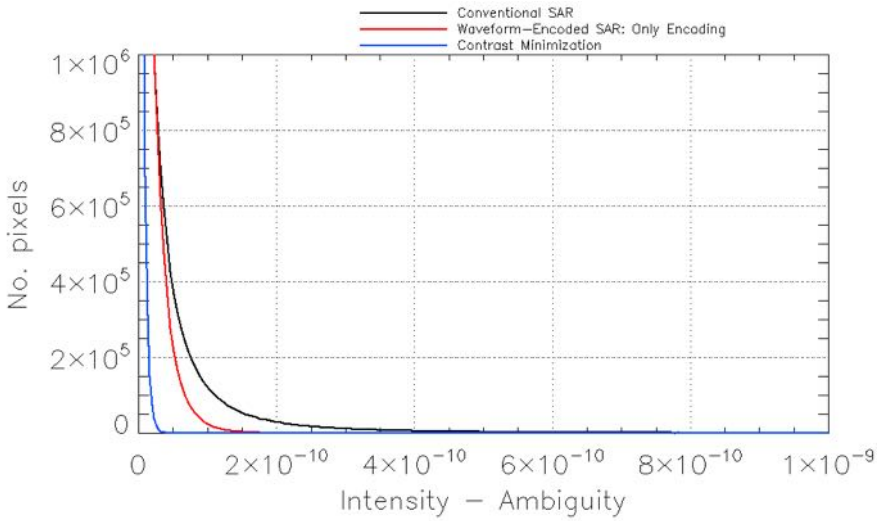

Figure 48: Comparison between intensities histograms of the unfocused range ambiguity. Specifically, the curve referred to the employment of a multi-focus post-processing with a contrast minimization-based thresholding and blanking approach (blue), assuming a waveform-encoded SAR characterized by cyclically-shifted chirps on transmit, is compared to those ones obtained assuming a conventional SAR system without waveform variation (black) and the mere waveform encoding (red), respectively.

RANGE AMBIGUITY HISTOGRAMS		Mean	Standard Deviation
Conventional SAR		6.2027948e-11	3.4605504e-10
Waveform-encoded SAR	Only encoding (cyclically-shifted chirps)	1.7261775e-11	1.9848748e-11
	Multi-focus post-processing (contrast minimization-based thresholding and blanking)	3.6228501e-12	9.9434615e-12

Table 5: Comparison between the main descriptors, i.e. mean and standard deviation, of the histograms in Figure 48.

In order to assess the range ambiguity suppression capabilities for such a thresholding and blanking-based multi-focus post-processing, the best achievable performance, due to the employment of an optimal threshold, obtained by minimizing the total error, i.e. the sum between the residual ambiguity and the removed signal, is used as best reference, as it leads to the best trade-off between ambiguity suppression and removed useful signal. In particular, Table 6 quantitatively shows the already described results, assuming a waveform-encoded SAR with cyclically-shifted chirps on transmit, together with the best achievable performance, in terms of total relative error, ambiguity suppression and removed signal.

			Total relative error [dB]	Ambiguity suppression [dB]	Removed signal [dB]
Conventional SAR			-1.4 [dB]	0 [dB]	0 [dB]
Waveform-encoded SAR	Only encoding		-3.3 [dB]	1.9 [dB]	0 [dB]
	Multi-focus post-processing (thresholding & blanking)	Contrast minimization	-5.5 [dB]	8.2 [dB]	-35.9 [dB]
		Optimal threshold	-7.8 [dB]	6.9 [dB]	-45.7 [dB]

Table 6: Quantitative results, assuming the proposed waveform-encoded SAR system with cyclically-shifted chirps as transmitted waveforms.

In the following, the same results as described for the case of cyclically-shifted chirps are shown also assuming a waveform-encoded SAR system with an up- and down- chirp alternation on transmit. In particular, the resulting corruption of the useful signal, i.e. Lake Starnberg, due to the range ambiguity, i.e. the Munich urban area, is shown assuming the mere waveform encoding (Figure 49a) and a multi-focus post-processing with a contrast minimization-based thresholding and blanking approach (Figure 49b), respectively. In the specific, the proposed multi-focus post-processing, with the described contrast minimization technique, leads to 9.4 dB ambiguity suppression compared to a conventional SAR system without waveform variation, i.e. additional 6.6 dB with respect to the mere waveform encoding. Figure 49 shows the focused images (up) and the residual ambiguous signals (down) for the considered waveform-encoded SAR with up- and down- chirps as transmitted waveforms, highlighting the improvement due to the proposed multi-focus post-processing (right), compared to the mere waveform encoding (left).

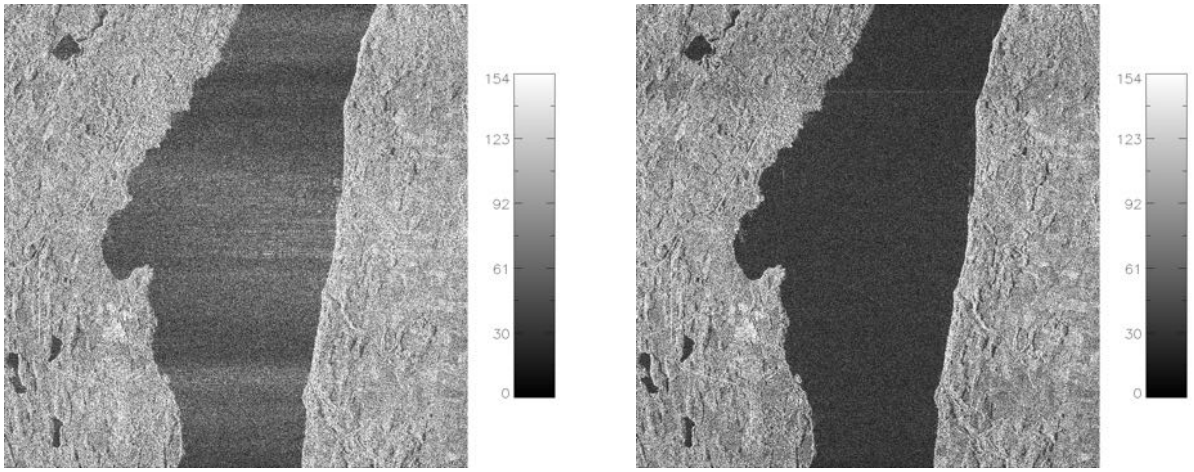

(a) (b)

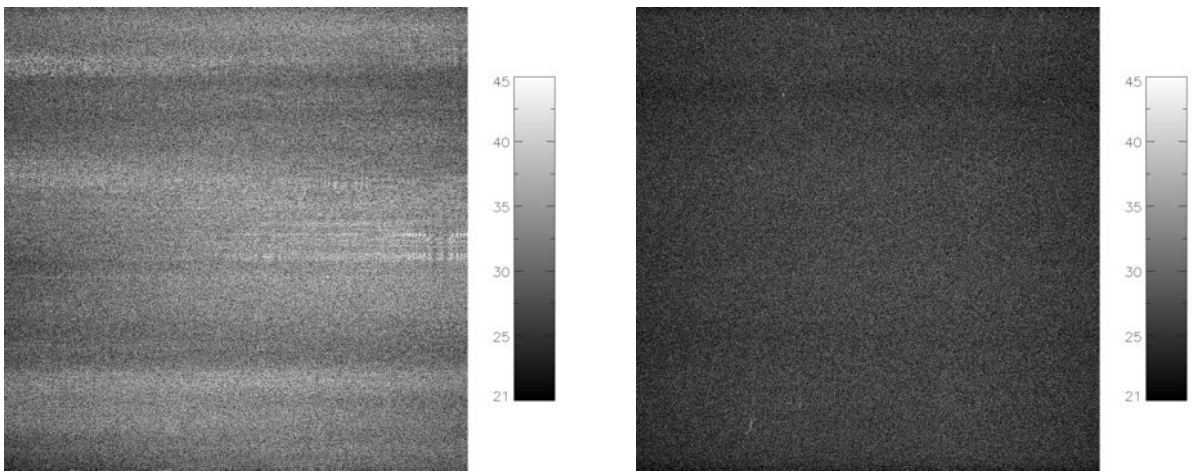

(c) (d)

Figure 49: Focused images (up) and residual ambiguous signals (down) for a waveform-encoded SAR system, assuming up- and down- chirps as transmitted waveforms, in case of mere waveform encoding (left) and a multi-focus post-processing with a contrast minimization-based thresholding and blanking approach. Both the images have the same size, i.e. 4096 x 4096 pixels. The horizontal and vertical axes represent slant range and azimuth, respectively.

As previously shown for the case of cyclically-shifted chirps, the improvement in the range ambiguity suppression, due to a multi-focus post-processing with the proposed contrast minimization-based thresholding and blanking approach, is presented also in terms of intensities histogram, for a waveform-encoded SAR system characterized by up- and down- chirps. Specifically, Figure 50 displays the histogram of the ambiguous signal intensities, once the range ambiguity has been removed through the already described contrast minimization-based thresholding and blanking technique and after focusing data using a filter matched to the desired echo (blue curve), together with the visualization of the ambiguity suppression improvement, compared to a conventional SAR system without waveform variation (black curve) and to the proposed waveform-encoded SAR with an up- and down-chirp alternation on transmit, assuming the mere waveform encoding (red curve), respectively. Moreover, the three different histograms are quantitatively described in Table 7 through mean and standard deviation.

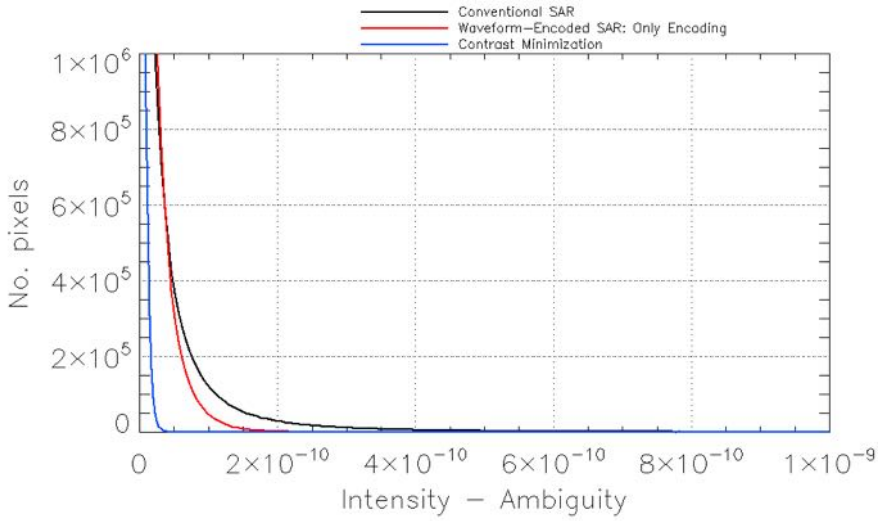

Figure 50: Comparison between intensities histograms of the unfocused range ambiguity. Specifically, the curve referred to the employment of a multi-focus post-processing with a contrast minimization-based thresholding and blanking approach (blue), assuming a waveform-encoded SAR characterized by an up- and down- chirp alternation on transmit, is compared to those ones obtained assuming a conventional SAR system without waveform variation (black) and the mere waveform encoding (red), respectively.

RANGE AMBIGUITY HISTOGRAMS		Mean	Standard Deviation
Conventional SAR		6.2027948e-11	3.4605504e-10
Waveform-encoded SAR	Only encoding (up- and down-chirp alternation)	2.1837652e-11	2.5064031e-11
	Multi-focus post-processing (contrast minimization-based thresholding and blanking)	4.2612708e-12	6.2381299e-12

Table 7: Comparison between the main descriptors, i.e. mean and standard deviation, of the histograms in Figure 50.

In order to assess the system performance, and thus the resulting image quality, for such a waveform-encoded SAR with up- and down- chirps, the obtained results are evaluated with reference to the best achievable one, due to an optimal threshold employment, as it leads to the best trade-off between range ambiguity suppression and removed useful signal. Table 8 quantitatively shows the results of the proposed waveform-encoded SAR with up- and down- chirps on transmit, together with the optimal performance, in terms of total relative error, ambiguity suppression and removed signal.

			Total relative error [dB]	Ambiguity suppression [dB]	Removed signal [dB]
Conventional SAR			-1.4 [dB]	0 [dB]	0 [dB]
Waveform-encoded SAR	Only encoding		-4.2 [dB]	2.8 [dB]	0 [dB]
	Multi-focus post-processing (thresholding & blanking)	Contrast minimization	-8 [dB]	9.4 [dB]	-39.5 [dB]
		Optimal threshold	-8.7 [dB]	8 [dB]	-45.3 [dB]

Table 8: Quantitative results, assuming the proposed waveform-encoded SAR system with up- and down- chirps as transmitted waveforms.

5.2 Dependency of Performance Measures on Local Ambiguity-to-Signal Ratio, Processed Doppler Bandwidth and Block Size

The achievable ambiguity suppression depends in general on the scene and the ambiguity level itself, i.e. the higher the range ambiguity level, the better the ambiguity suppression capability. Thus, several range ambiguity strengths have been simulated, as well as different combinations of scenes and different system and processing parameters, e.g. processed Doppler bandwidth and block size, in order to understand the proposed waveform-encoded SAR system performance behaviour when these variables change. In particular, the range ambiguity impact on the useful signal has been quantitatively measured by using a parameter, i.e. local ambiguity-to-signal ratio, which is strictly related to the already described ambiguity scaling factor. In addition, different scenarios have been considered, i.e. the ambiguities of both the Munich urban area and a suburbs town (Germering) on a forest, respectively, in order to understand how much the proposed waveform-encoded SAR system performance depends on the considered scenes. As far as some system and processing parameters are concerned, e.g. processed Doppler bandwidth and block size, this section also presents an analysis of the performance measures dependency, assuming the sample case study in Section 5.1 for both cyclically-shifted and up- and down- chirps, respectively.

5.2.1 Local Ambiguity-to-Signal Ratio

In the following, the proposed waveform-encoded SAR system performance is assessed for several range ambiguity strengths, as well as different combinations of scenes. Specifically, as described in Section 4.1.2, the simulated raw SAR data corresponding to the ambiguous signal is amplitude-scaled by means of an ambiguity scaling factor, in order to simulate reasonable ambiguities and different impacts on the useful signal. Therefore, a parameter, i.e. local ambiguity-to-signal ratio, is required in order to quantify the range ambiguity, with reference to the useful signal. In particular, it is strictly related to the ambiguity scaling factor, as this last one is used for amplitude-scaling the ambiguous signal, and is thus defined for a conventional SAR system without waveform variation, with reference to the desired echo, as

$$RASR_{local} = \frac{E_{amb,ref}}{E_{sign,ref}} = \frac{\sum |I_{amb,ref}|^2}{\sum |I_{sign,ref}|^2} \tag{52}$$

where $E_{amb,ref}$ and $E_{amb,ref}$ are the energies of the range ambiguity ($I_{amb,ref}$) and the useful signal ($I_{sign,ref}$), respectively, after focusing using a filter matched to the desired echo and assuming a conventional SAR system without pulse-to-pulse variation of the transmitted waveform. Also, the local ambiguity-to-signal ratio can be defined in dB as

$$RASR_{local}[dB] = 10 \cdot \log\left(\frac{\sum |I_{amb,ref}|^2}{\sum |I_{sign,ref}|^2}\right) = 10 \cdot \log\left(\sum |I_{amb,ref}|^2\right) - 10 \cdot \log\left(\sum |I_{sign,ref}|^2\right) \tag{53}$$

Additionally, different scenarios are simulated, in order to test the proposed waveform-encoded SAR system for more interesting cases, in practice, and to quantitatively analyze the performance measures dependency on the considered scenes. Specifically, two others scenarios are simulated, assuming the ambiguities of the same Munich urban area as before and of a suburbs town, i.e. Germering, on a forest, respectively, as the removal or the attenuation of the range ambiguous signal is mandatory for some interferometric and polarimetric applications, e.g. parameters retrieval. Figure 51 and Figure 52 show the total relative error as function of local ambiguity-to-signal ratio, assuming a waveform-encoded SAR system characterized by cyclically-shifted and up- and down- chirps on transmit, respectively. In particular, Figure 51a and Figure 52a refers to the impact of a range ambiguity, due to the Munich urban area, on Lake Starnberg, Figure 51b and Figure 52b assumes the same urban area as before on a forest, while in Figure 51c and Figure 52c the same forest is corrupted by a range ambiguous signal due to a suburbs town, i.e. Germering. It can be noticed that the system performances,

in terms of total relative error and as function of local ambiguity-to-signal ratio, are very similar from each other, assuming the three different simulated scenarios and both cyclically-shifted chirps and an up- and down- chirp alternation, respectively. Specifically, for the black line, corresponding to the performance of a conventional SAR system without waveform variation on transmit, the total relative error is analogous to local ambiguity-to-signal ratio, as the two measures are computed in the same way.

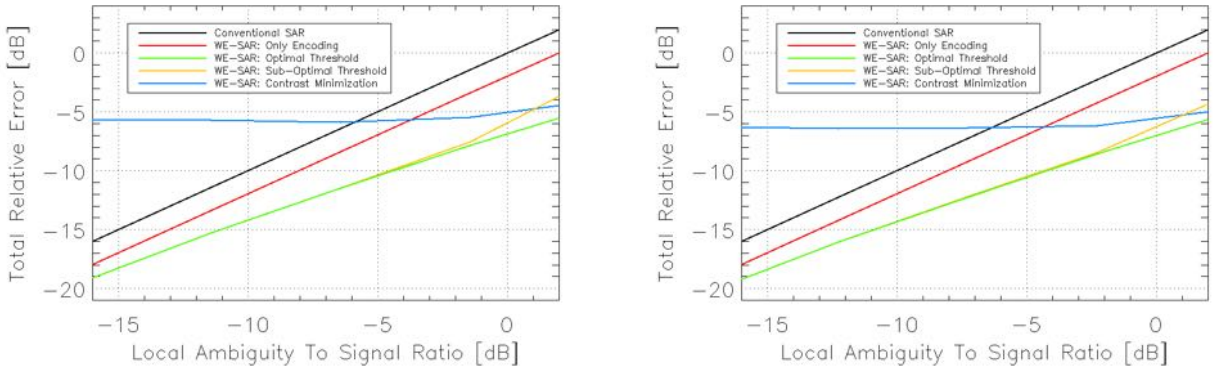

(a) (b)

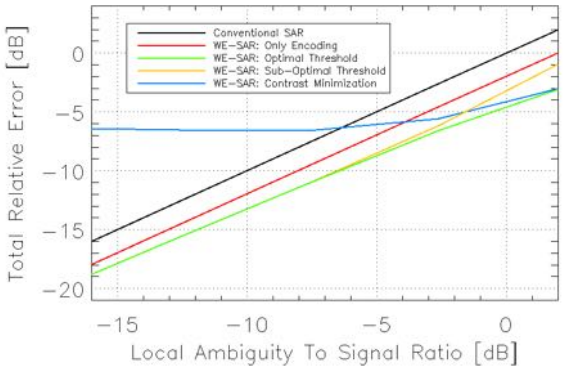

(c)

Figure 51: Total relative error as function of local ambiguity-to-signal ratio, assuming a waveform-encoded SAR system characterized by cyclically-shifted chirps on transmit. (a) refers to the impact of a range ambiguity, due to the Munich urban area, on Lake Starnberg, (b) assumes the same urban area as before on a forest, while in (c) the same forest is corrupted by a range ambiguity due to a suburbs town, i.e. Germering.

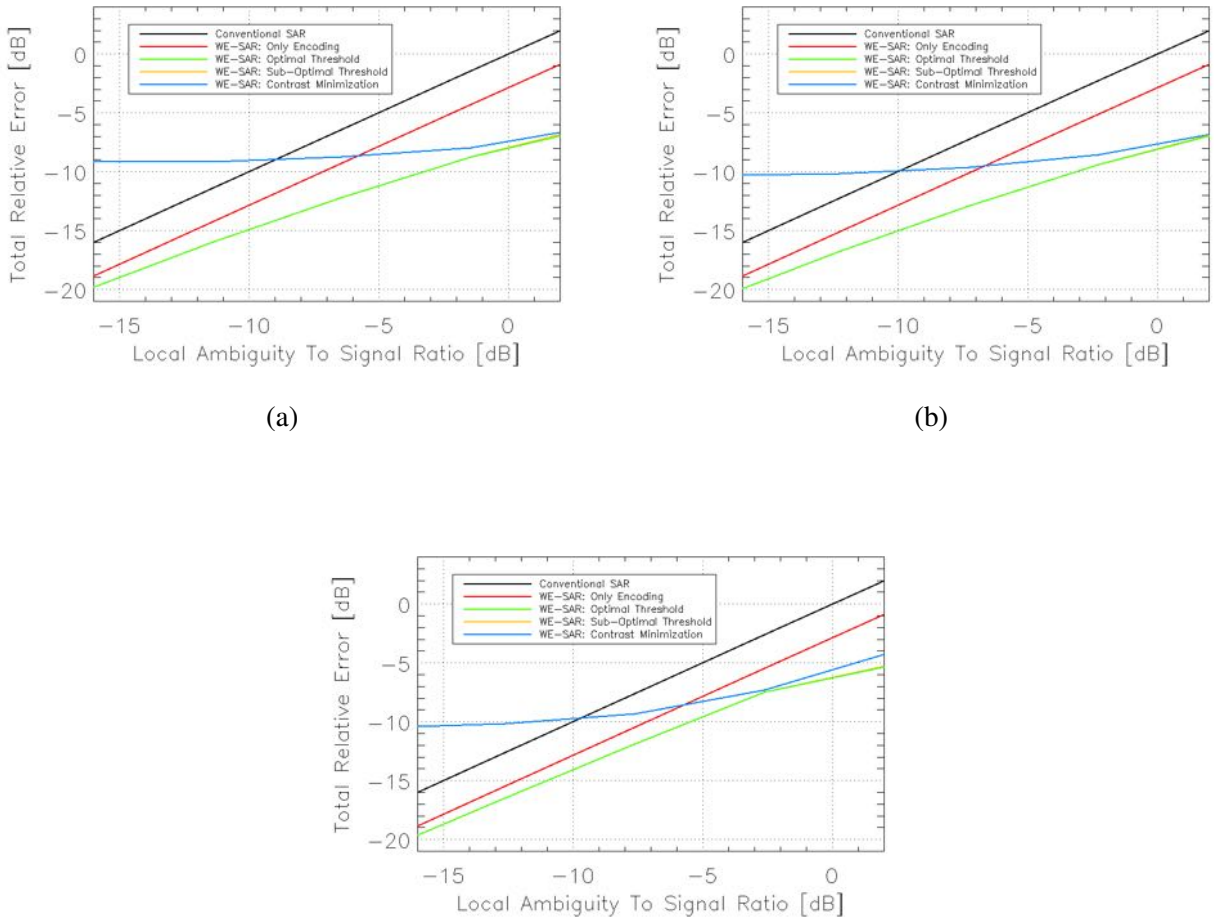

(a)

(b)

(c)

Figure 52: Total relative error as function of local ambiguity-to-signal ratio, assuming a waveform-encoded SAR system characterized by an up- and down- chirp alternation on transmit. (a) refers to the impact of a range ambiguity, due to the Munich urban area, on Lake Starnberg, (b) assumes the same urban area as before on a forest, while in (c) the same forest is corrupted by a range ambiguity due to a suburbs town, i.e. Germering.

Also, the mere waveform encoding (red line) leads to 1.9 dB and 2.8 dB range ambiguity suppression without removal of useful signal, assuming a waveform-encoded SAR system with cyclically-shifted (Figures 53a, 53c, 53e) and up- and down- (Figures 54a, 54c, 54e) chirps as transmitted waveforms, respectively, for both the three different scenarios. In particular, the suppression is higher transmitting an up- and down- chirp alternation rather than cyclically-shifted chirps, despite using only two orthogonal waveforms allows smearing and suppressing to some extent only odd range ambiguities (Section 3.2.2). As previously described, a further range ambiguity suppression, thus an image quality improvement, can be achieved by means of a multi-focus post-processing with a thresholding and blanking approach: using an optimal threshold (green line) allows for the best trade-off between ambiguity suppression and removed signal, thus allowing suppressing more ambiguous energy without significant removal of useful signal, compared to the mere waveform encoding, despite the computational load is very high. A sub-optimal threshold (orange line) can be thus obtained by minimizing the total error after removing the range ambiguity, in the focused data matched to the ambiguous signal, in order to decrease and limit the processing computational burden. As it can be noticed in Figure 51 and Figure 52, the performance due to a sub-optimal threshold perfectly approximates the optimal one, assuming up- and down- chirps on transmit (Figure 52), while it diverges for

very strong ambiguities, if cyclically-shifted chirps are employed as transmitted waveforms (Figure 51). However, since the sub-optimal and optimal thresholds cannot be of course obtained in practice, as the separate knowledge of the useful and ambiguous signals is needed, a contrast minimization method (blue line)(Section 3.3.2) can be exploited. In particular, it can still leads to a further range ambiguity suppression, but with a significant removal of useful signal for low local ambiguity-to-signal ratios, making sense to use it only for suppressing strong ambiguities. Also, the proposed waveform-encoded SAR system performance is better if up- and down- chirps are employed on transmit, thus allowing applying this processing also to slightly weaker range ambiguities (comparison between Figures 51 and 52). Figure 53 and Figure 54 show the range ambiguity suppression (left) and the removed relative signal (right), assuming the proposed waveform-encoded SAR system with cyclically-shifted and up- and down- chirps on transmit, respectively, for both the three different scenarios, i.e. the Munich urban area on Lake Starnberg (up) and on a forest (middle), and a suburbs town, i.e. Germering, on the same forest as before (down).

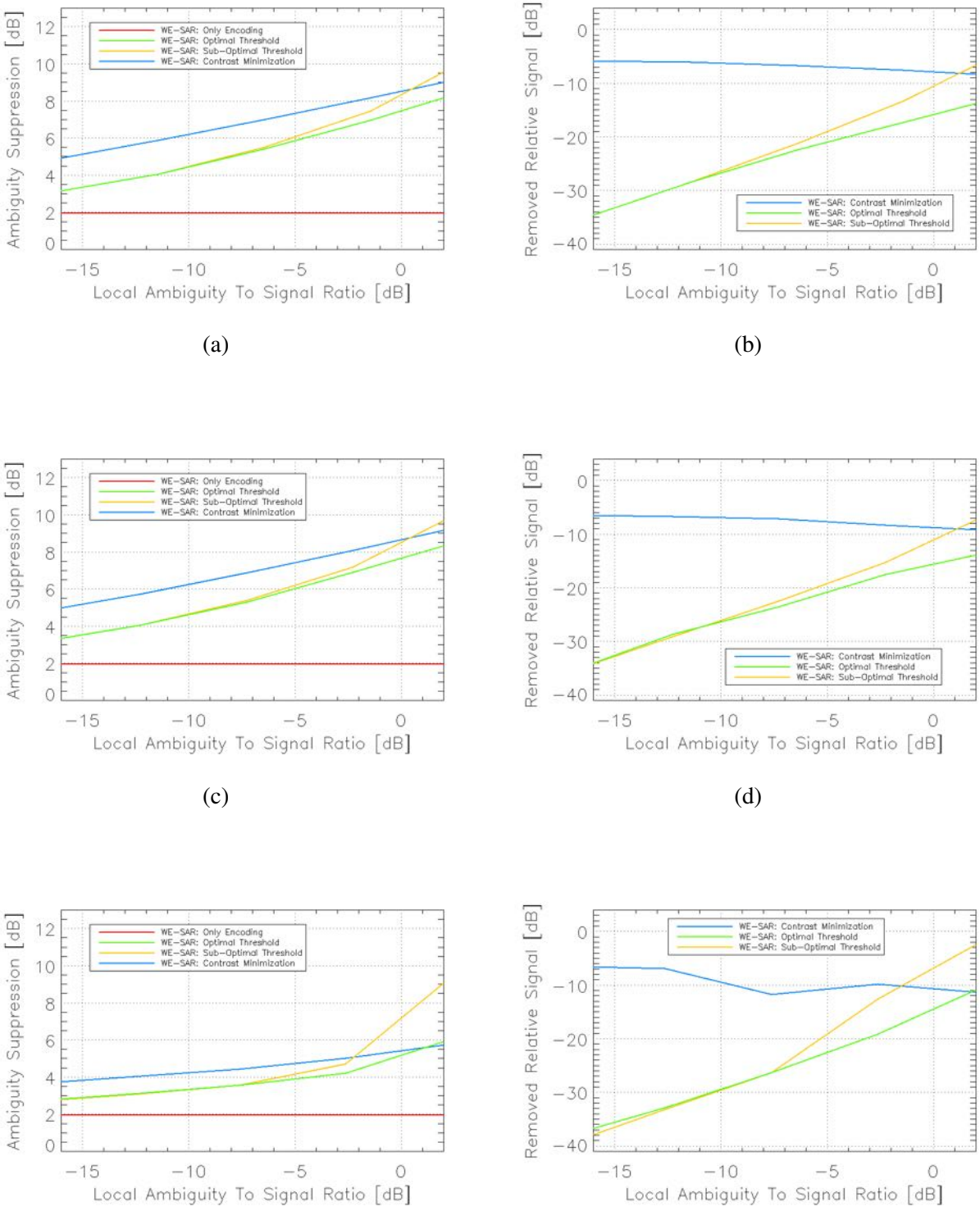

Figure 53: Range ambiguity suppression (left) and removed relative signal (right) as function of local ambiguity-to-signal ratio, assuming a waveform-encoded SAR system characterized by cyclically-shifted chirps on transmit. (a) and (b) refer to the impact of a range ambiguity, due to the Munich urban area, on Lake Starnberg, (c) and (d) assume the same urban area as before on a forest, while in (e) and (f) the same forest is corrupted by a range ambiguity due to a suburbs town, i.e. Germering.

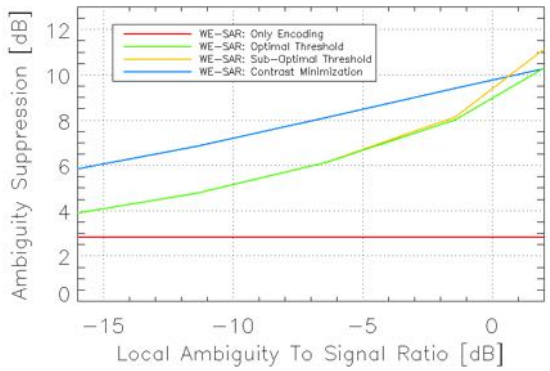

(a)

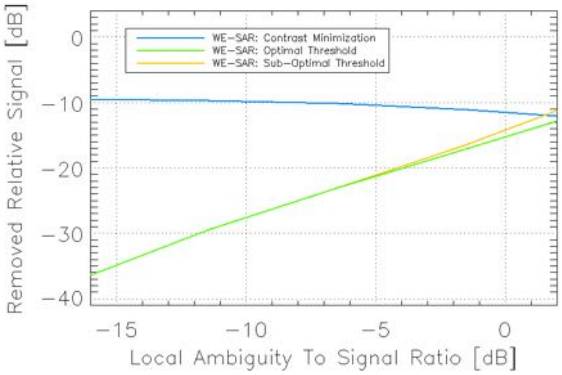

(b)

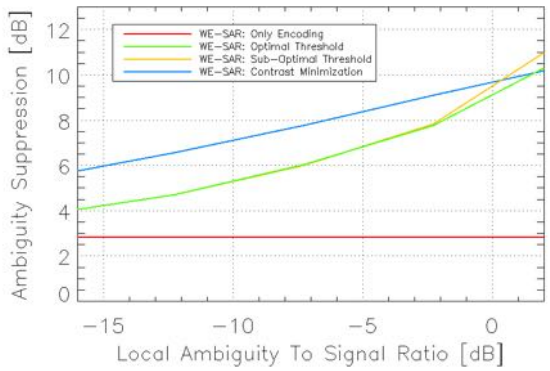

(c)

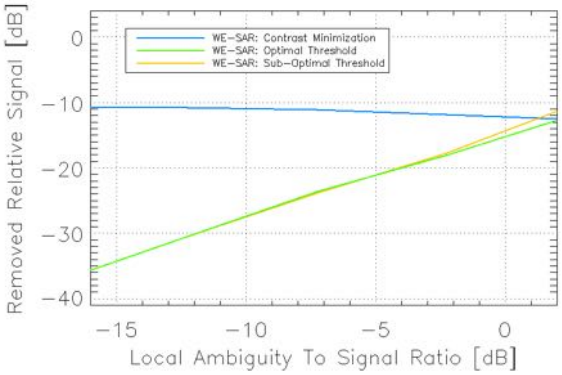

(d)

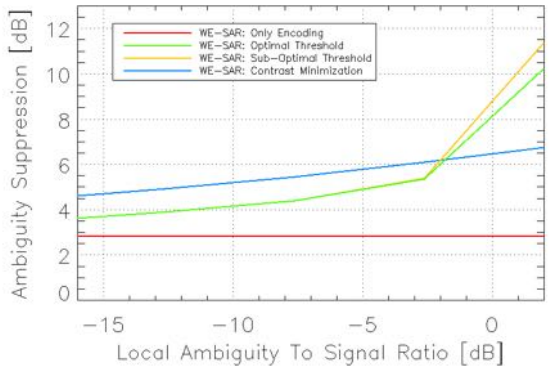

(e)

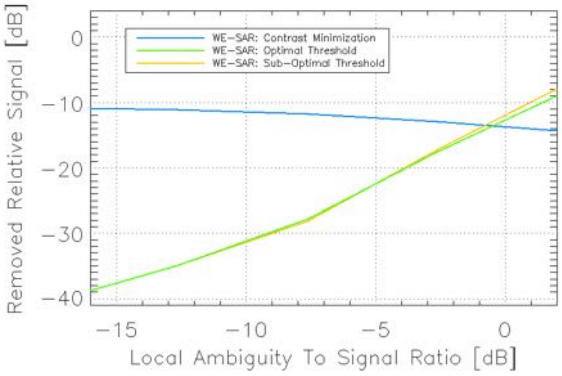

(f)

Figure 54: Range ambiguity suppression (left) and removed relative signal (right) as function of local ambiguity-to-signal ratio, assuming a waveform-encoded SAR system characterized by an up- and down- chirp alternation on transmit. (a) and (b) refer to the impact of a range ambiguity, due to the Munich urban area, on Lake Starnberg, (c) and (d) assume the same urban area as before on a forest, while in (e) and (f) the same forest is corrupted by a range ambiguity due to a suburbs town, i.e. Germering.

Therefore, as shown in this paragraph, the performance of the different methods depends of course on local ambiguity-to-signal ratio, thus on the range ambiguity strength with reference to the useful signal, and is almost independent from the scenes.

5.2.2 Processed Doppler Bandwidth

The proposed waveform-encoded SAR system performance has been assessed also as function of the processed Doppler bandwidth, assuming the sample case study in Section 5.1, i.e. range ambiguity due to the Munich urban area on Lake Starnberg, for both cyclically-shifted and up- and down-chirps on transmit, respectively. Specifically, as described in Section 3.3, as a consequence of continuously transmitting a different waveform from pulse-to-pulse, the ambiguous signal is uniformly smeared over the pulse width, i.e. slant range direction, and the synthetic aperture, i.e. azimuth direction, appearing as a noise-like disturbance, as well as some ambiguous energy is suppressed. In particular, the ambiguous energy is incoherently integrated in azimuth and spread almost uniformly across the Doppler spectrum; thus, it is filtered out during the SAR processing, by assuming a processed Doppler bandwidth smaller than the considered *PRF* [21][18]. As a consequence, different processed Doppler bandwidths allow obtaining different system performances, in terms of range ambiguity suppression and assuming the mere waveform encoding, since the Doppler spectrum is cut at several frequencies. Also, if the presented multi-focus post-processing with a thresholding and blanking approach (Section 3.3.1) is exploited, a different ambiguity suppression capability, i.e. a different system performance and image quality, is expected dependently on the considered processed Doppler bandwidth, assuming both the contrast and total error minimization methods, respectively. As it can be expected, the range ambiguity suppression increases as the processed Doppler bandwidth becomes smaller, since the Doppler spectrum is more cut, due to a smaller frequency. Analogously, also the proposed waveform-encoded SAR system performance increases as a result of smaller processed Doppler bandwidths, assuming a multi-focus post-processing with both a contrast and total error minimization-based thresholding and blanking approaches. Figure 55 show the system performance, i.e. total relative error (up), range ambiguity suppression (middle) and removed relative signal (down), as function of the processed Doppler bandwidth, assuming a waveform-encoded SAR system characterized by cyclically-shifted chirps (left) and an up- and down- chirp alternation (right) on transmit, respectively. Specifically, the mere waveform encoding is considered, as well as the employment of a multi-focus post-processing with a thresholding and blanking approach. As it can be noticed, the presented multi-focus post-processing results follow the mere waveform encoding ones, assuming both the contrast and total error minimization methods for threshold selection, i.e. the performance curves seem to be almost parallel; this can allow predicting the system performance, in terms of total relative error and range ambiguity suppression, due to the proposed multi-focus post-processing implementation, starting from the knowledge of the mere waveform encoding one behaviour. Also, the performance achieved by using a sub-optimal threshold, i.e. obtained as a result of total error minimization in the focused data matched to the ambiguity, once the range ambiguous signal has been removed, perfectly approximates the optimal one, assuming up- and down- chirps as transmitted waveforms, while it leads to slightly worse results, in terms of total relative error, compared to the best achievable ones, if cyclically-shifted chirps are employed on transmit. In particular, this is due to a much higher removed relative signal, assuming the employment of a sub-optimal threshold compared to the optimal one, despite a slightly better range ambiguity suppression is achieved.

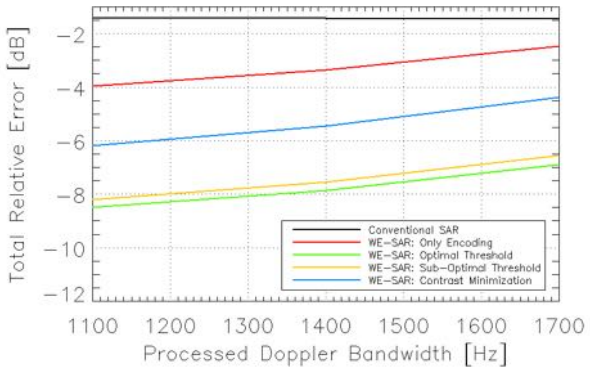

(a)

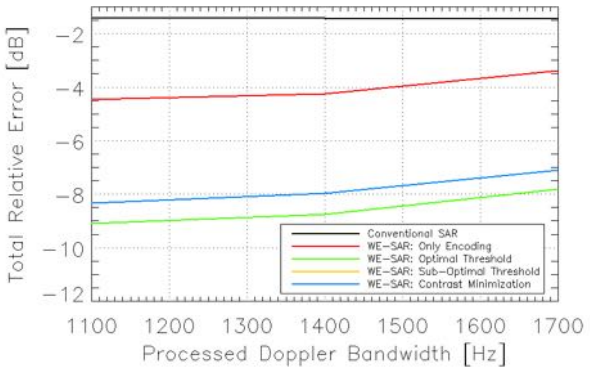

(b)

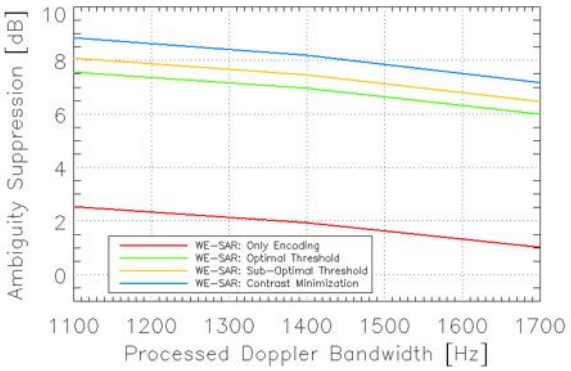

(c)

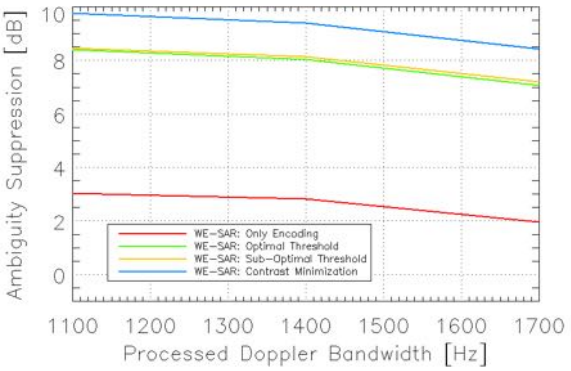

(d)

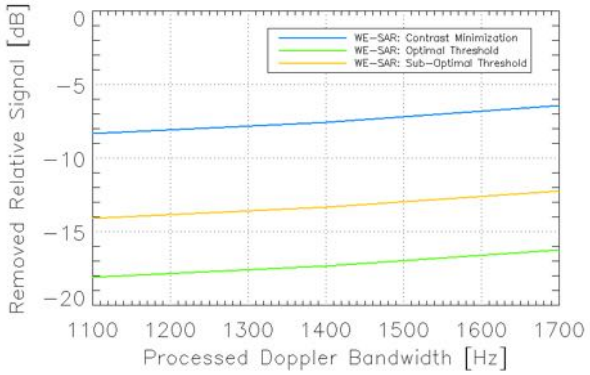

(e)

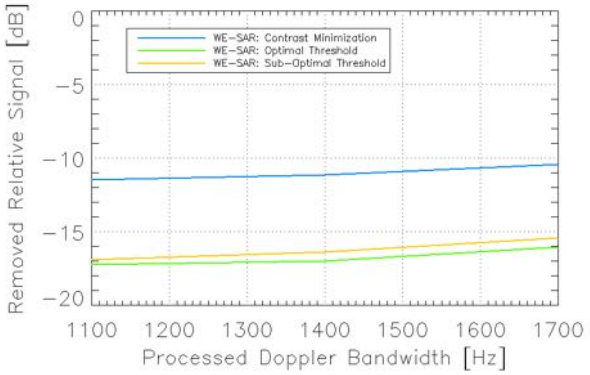

(f)

Figure 55: System performance of the proposed waveform-encoded SAR as function of the processed Doppler bandwidth, assuming cyclically-shifted chirps (left) and an up- and down- chirp alternation (right) on transmit. In particular, (a) and (b) show the total relative error dependency on the processed Doppler bandwidth, (c) and (d) refer to the range ambiguity suppression while (e) and (f) displays the removed relative signal as function of this system and processing parameter.

5.2.3 Final Considerations on Block Size

Generally, the acquired data is characterized by a very large image size, both in range and azimuth directions; thus, a block-based image processing is required in order to limit the computational burden. Consequently, the analysis of the system performance dependency on block size is required, as an optimum block size could improve the proposed waveform-encoded SAR processing performance. Specifically, better results, in terms of range ambiguity suppression and total relative error, could be achieved by exploiting a spatially variant threshold. In particular, the implementation of a moving window, as described in Section 3.3.3, could lead to a performance improvement, as a consequence of block-adaptive thresholds, which allow removing the range ambiguity depending on the block-based behaviour of the useful and ambiguous signals. In the following, the proposed waveform-encoded SAR processing performance is evaluated as function of block size, as a block processing is mandatory in practice, because of a too big dimension of the acquired data, assuming the sample case study in Section 5.1 for both cyclically-shifted chirps and an up- and down- chirp alternation on transmit. Also, the block-based contrast minimization method (Section 3.3.3), for thresholds selection, assuming a multi-focus post-processing with the presented thresholding and blanking approach, is assessed with reference to the employment of block-based sub-optimal thresholds, as the optimal ones cannot be obtained because of a too big computational load; thus, it is evaluated with reference to a sub-optimal performance, corresponding to the minimization of the block-based total error, after range ambiguity removal, in the focused data matched to the ambiguous signal. Figure 56 show the proposed waveform-encoded SAR system performance, i.e. total relative error (up), range ambiguity suppression (middle) and removed relative signal (down), as function of block size and assuming both cyclically-shifted (left) and up- and down- (right) chirps on transmit, if a block-based multi-focus post-processing with the presented thresholding and blanking approach is considered. Despite better results could be expected using a very small block size, in order to account for small intensities variations, especially in the range ambiguous signal, since the desired echo appears as a noise-like disturbance, the processing performance, in terms of total relative error, results to be almost block-independent, making no sense to perform a detailed analysis on the optimum block size. Specifically, reducing the block size allows reduce the total relative error up to 0.5-1 dB, assuming both the two different sequences of waveforms proposed in Section 3.2, i.e. cyclically-shifted and up- and down- chirps. However, while generally for sub-optimal thresholds the error reduces as the block gets smaller, although it is not totally proved in Figure 56a, assuming the contrast minimization method for thresholds selection there is a minimum block size, i.e. 16 x 16 and 32 x 32 for cyclically-shifted and up- and down- chirps, respectively, after which the error slightly increases again, because of block-based contrast computation. Nevertheless, the proposed considerations on block size depend of course on the considered system parameters, i.e. synthetic aperture L_s and chirp duration τ. In particular, since while focusing the superimposed raw SAR data using a filter matched to the range ambiguity the defocused useful signal, after range compression, is dislocated at different ranges, as a consequence of an uniform smearing over the pulse width τ, i.e. the slant range direction, and is then incoherently integrated in azimuth, i.e. over the synthetic aperture L_s, and spread almost uniformly across the Doppler spectrum, because of azimuth compression, the proposed considerations on block size are thus strictly related to these two system parameters, and can be reformulated if different synthetic aperture and pulse duration integration windows are considered.

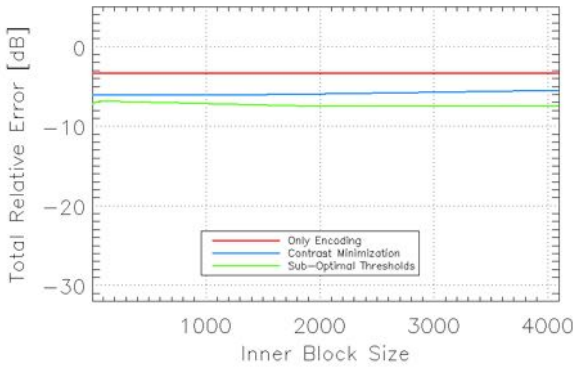

(a)

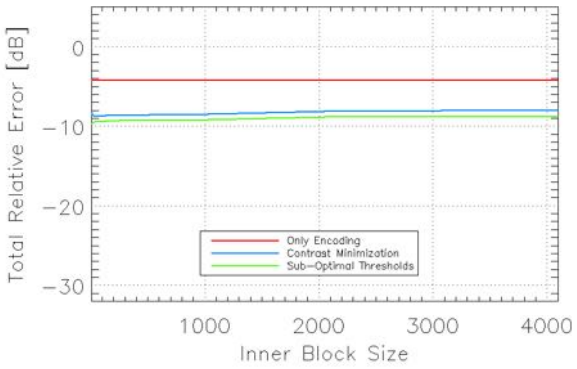

(b)

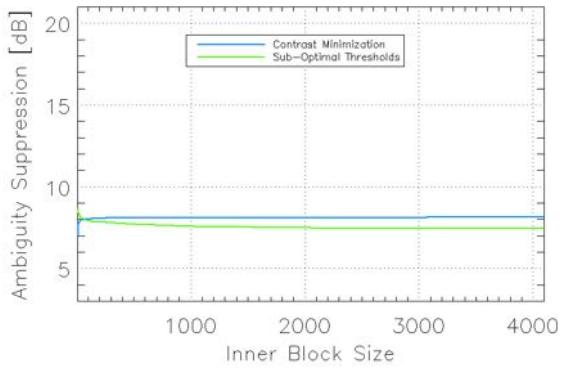

(c)

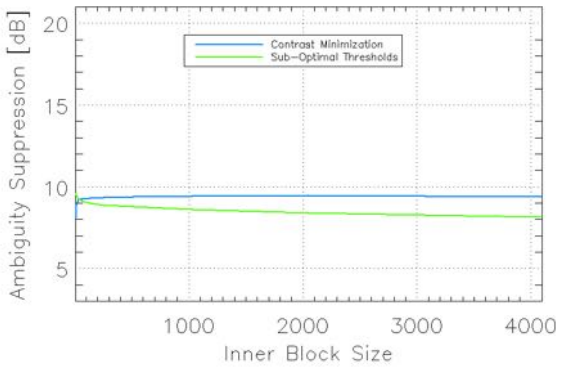

(d)

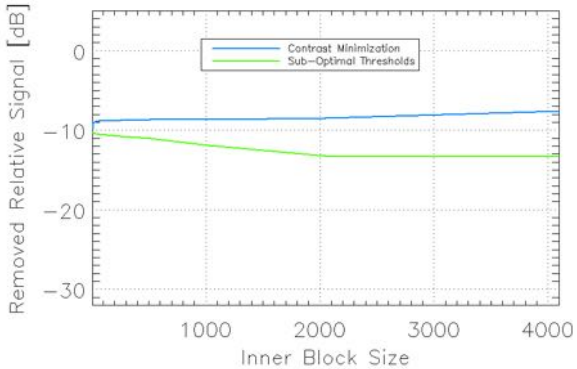

(e)

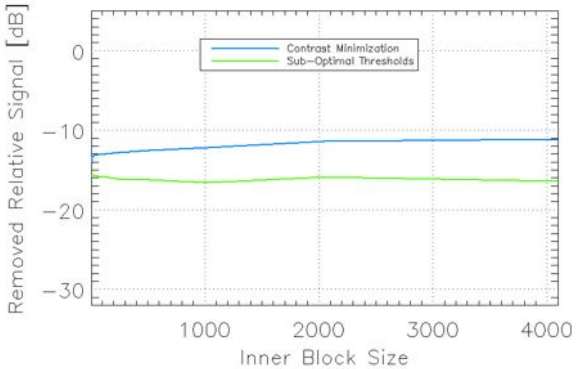

(f)

Figure 56: Processing performance of the proposed waveform-encoded SAR system as function of block size, assuming the presented block-based multi-focus post-processing and cyclically-shifted (left) and up- and down- chirps (right) on transmit. In particular, (a) and (b) show the total relative error dependency on block size, (c) and (d) refer to the range ambiguity suppression while (e) and (f) displays the removed relative signal as function of this processing parameter.

6 Conclusions

This work analyzes in detail a novel SAR concept, i.e. waveform-encoded SAR, which allows suppressing, not only smearing, range ambiguities by continuously changing the transmitted waveform, in combination with a multi-focus post-processing, and proposes an assessment of the resulting image quality, as well as its range ambiguity suppression capabilities. In the following, the overall work is discussed and the results are listed; also, an outlook for further research is provided.

6.1 Discussion

Synthetic Aperture Radar (SAR) remote sensing can provide a significant contribution in understanding the dynamic processes within the Earth system, since it allows high resolution imaging independently of weather conditions and sunlight illumination. The effective long ”synthetic” antenna generated by the coherent reception of the radar echoes allows an improvement of the resolution, while the use of microwaves makes possible all weather imaging independently of clouds, fog and precipitations.

However, when speaking about SAR, one important limitation has to be considered (Section 2.2). As a consequence of the pulsed operation and side-looking geometry, some undesirable echoes coming from different transmitted pulses return back to the radar at the same time of the echos of interest, during the acquisition process. The most common ambiguity corresponds to the nadir returns, i.e. the echoes propagating from the closest point to the radar, corresponding to a null incidence angle, which typically limit both the swath width and the ambiguity performance of a SAR system, since they may be stronger than the desired ones. As well as nadir returns, also the so-called range ambiguities may significantly affect the quality of the acquired SAR image; they correspond to antecedent and subsequent echoes arriving back at the the radar simultaneously with the desired swath signal, thus strongly affecting the quality of the acquired data. This phenomenon is mainly relevant for spaceborne SAR systems, as several pulses are transmitted after a given pulse before receiving its echo. These limitations typically constrain the PRF selection, as well as conventional SAR systems design (Section 2.3), making it not a trivial task, as several parameters and requirements have to be considered.

Waveform-encoded SAR (Section 3.1) is a novel SAR concept which allows suppressing, not only smearing, nadir returns and range ambiguities by continuously changing the transmitted waveform, in combination with a dual/multi-focus post-processing, respectively. Specifically, the continuous pulse-pulse variation of the transmitted waveform allows focusing the nadir echo and the range ambiguities and suppressing them through the dual/multi-focus post-processing proposed in Section 3.3. This technique is born for nadir echo suppression, exploiting the continuous variation of waveforms on transmit and the use of different matched filters in the processing, but in this dissertation it is extended to the case of range ambiguities suppression, yielding to a significant improvement in the image quality, with remarkable benefits in the design of novel SAR systems, as an increased system design flexibility can be achieved at the reasonable cost of employing different waveforms on transmit.

Nevertheless, the assessment of the ambiguity suppression performance (Section 4) for such a system is not trivial, as the processing involves a non-linear thresholding and blanking approach (Section 3.3.1). This work proposes a novel methodology, which exploits real TerraSAR-X data to accurately simulate the effect of the range ambiguity on the useful signal and allows for a quantitative assessment of the image quality of such a waveform-encoded SAR system. The analysis has considered different waveform variation schemes (Section 3.2), i.e. cyclically-shifted and up- and down- chirps, and a contrast-minimization technique (Section 3.3.2) for threshold selection, as well as the best achiev-

able performance (Section 4.1.3), i.e. optimal threshold. Also, the proposed waveform-encoded SAR system has been evaluated assuming several range ambiguity strengths, as well as different scenarios and different system and processing parameters, e.g. processed Doppler bandwidth and block size, in order to understand the performance behaviour of such a system when these variables change.

The results of this work further highlight the potentialities of the waveform-encoded SAR concept and allow accounting for its ambiguity suppression capability in the design of novel SAR systems. In particular, since it could increase the SAR system design flexibility at the reasonable cost of employing different waveforms on transmit, it could be extended also to the case of high-resolution wide-swath SAR systems.

6.2 Summary of Results

In the following, the results achieved within this work are listed in detail.

As already explained, While for a conventional SAR without waveform variation slightly-defocused artifacts can be observed over the desired signal, the waveform-encoded SAR concept allows suppressing, not only smearing, range ambiguities by continuously transmitting a different waveform from pulse-to-pulse, together with the implementation of a multi-focus post-processing. In particular, exploiting waveform diversity on transmit allows focusing raw SAR data using different matched filters in the processing, in order to separately highlight both the two superimposed signals, i.e. desired echo and range ambiguity. Specifically, while focusing raw data using a filter matched to the useful signal, it results to be properly focused and located, while the range ambiguity is uniformly smeared over the pulse width i.e. slant range direction, and the synthetic aperture, i.e. azimuth direction, appearing as a noise-like disturbance, as well as some ambiguous energy is suppressed. Similarly to a staggered SAR, in fact, it is incoherently integrated in azimuth and spread almost uniformly across the Doppler spectrum; therefore, a part of it is filtered out during the SAR processing, if the PRF of the system is larger than its processed Doppler bandwidth (Section 5.1.1).

As a result, the employment of cyclically-shifted chirps as transmitted waveforms leads to the most uniform ambiguity smearing, as the range ambiguous signal, after range compression, is dislocated at different ranges and then smeared over azimuth as a consequence of azimuth compression, as well as to 1.9 dB ambiguity suppression, without corruption of useful signal, assuming a 1400 Hz processed Doppler bandwidth.

As alternative, the unfocused signal can be smeared only along the range direction, as a result of the pulse or range compression operation, if different, orthogonal waveforms are used for two succeeding transmitted pulses, i.e. up- and down-chirps alternation. However, using up- and down-chirps allows smearing and suppressing only odd range ambiguities, as the even ones correspond to the same waveforms as the useful signal. Also, it implies a different spreading of the range ambiguity across the Doppler spectrum, compared to cyclically-shifted chirps, as well as a different ambiguous energy suppression (2.8 dB) without corruption of useful signal, by imposing the same processed Doppler bandwidth.

As it can be noticed in Section 5.2.2, the range ambiguity suppression depends of course on the processed Doppler bandwidth, and increases as it becomes smaller, since more energy is filtered out from the Doppler spectrum, due to a smaller cut frequency.

As shown with simulations based on real TerraSAR-X data, a further range ambiguity suppression can be achieved by means of a multi-focus post-processing with a thresholding and banking approach (Section 3.3.1). Specifically, a simple but effective criterion for threshold selection, in practice, can be obtained by minimizing the image contrast (Section 3.3.2), after focusing matched to each range ambiguity. In fact, as the ambiguous signal is properly focused, it is thus characterized by a high image contrast; on the contrary, the useful signal appears as a noise-like disturbance, thus characterized by a low contrast, as consequence of the use of a mismatched filter during the processing. As the threshold decreases, the image contrast decreases as a consequence of the removal of strong and

focused ambiguous features; however, once the range ambiguity has been removed, a further decrease of the threshold determines an increase in the contrast, as a consequence of a significant removal of useful signal. Also, a quantitative assessment of the ambiguity suppression capabilities, and thus of the resulting image quality, of such a processing, i.e. contrast minimization-based thresholding and blanking approach, has been performed by assuming as reference the best achievable performance (Section 4.1.3), due to the employment of an optimal threshold, i.e. obtained by minimizing the total error after focusing matched to the useful signal, once the range ambiguity has been removed.

Specifically, several scenarios have been considered, i.e. the ambiguities due to the Munich urban area and a suburbs town (Germering) on both Lake Starnberg and a forest, as well as several range ambiguity strengths have been simulated by means of an ambiguity scaling factor. In particular, one parameter, i.e. local ambiguity-to-signal ratio (Section 5.2.1), has been defined, in order to quantify the ambiguous signal with reference to the desired one.

As shown in Section 5.2.1 from simulations based on real TerraSAR-X data, an optimal threshold leads to a further ambiguity suppression, i.e. higher suppression for higher local ambiguity-to-signal ratios, without significant removal of useful signal, compared to the mere waveform encoding, as it allows for the best trade-off between ambiguous energy suppression and removed signal. Differently, the contrast minimization method still leads to a further range ambiguity suppression, i.e. it is greater as the ambiguous signal becomes stronger, but with a significant removal of useful signal for low local ambiguity-to-signal ratios, making sense to use it only for suppressing strong ambiguities, e.g. cross-pol data in quad-pol acquisitions. Also, the proposed waveform-encoded SAR system performance is better if up- and down- chirps are employed on transmit, compared to cyclically-shifted chirps, thus allowing applying the described multi-focus post-processing also to slightly weaker range ambiguities. Therefore, the performance of the different methods depend of course on local ambiguity-to-signal ratio, thus on the ambiguity strength, despite it has been proved to be quite independent from the scenes.

In practice, as the acquired data is typically characterized by a very large image size, both in range and azimuth directions, a block-based image processing is required (Section 3.3.3). Specifically, better results could be achieved by exploiting spatially, i.e. block-adaptive, variant thresholds, as they allow removing the range ambiguity depending on the block-based behaviour of the useful and ambiguous signals. However, despite better results could be expected using a very small block size, in order to account for small intensities variations, especially in the range ambiguity, since the desired echo appears as a noise-like disturbance, the processing performance results to be almost block-independent; in particular, reducing the block size allows reduce the total relative error up to 0.5-1 dB. While generally for sub-optimal thresholds, i.e. reference for performance assessment, if a block-based multi-focus post-processing is considered, the error reduces as the block gets smaller, assuming the contrast minimization method for thresholds selection there is a minimum block size, i.e. 16 x 16 and 32 x 32 for cyclically-shifted and up- and down- chirps, respectively, after which the error slightly increases again, because of block-based contrast computation. Nevertheless, the proposed considerations on block size depend of course on the considered system parameters, i.e. synthetic aperture L_s and chirp duration τ, and can be reformulated if different synthetic aperture and pulse duration integration windows are considered.

The results obtained in Section 5.2, from simulations based on real TerraSAR-X data, further highlight the potentialities of such a waveform-encoded SAR concept, allowing accounting for its range ambiguity suppression capability in the design of novel SAR systems, as the performance of the different methods, for threshold selection, have been proved to be quite independent from the scenes.

6.3 Outlook

In this thesis, a preliminary study on the waveform-encoded SAR concept capabilities has been presented, based on pulse-to-pulse variation of the transmitted waveform as well as on the implementation of a multi-focus post-processing, which allows suppressing, not only smearing, nadir returns and range ambiguities. Further developments, however, could lead to even better performance, thus increasing the flexibility in the design of novel SAR systems, at the reasonable cost of employing different waveforms on transmit.

In particular, the azimuth phase coding technique can be applied, which allows eliminating nadir returns and range ambiguities in SAR images using an azimuth filter, after having applied an azimuth phase modulation to the transmitted pulses and a corresponding demodulation to the received pulses. Specifically, this technique excels by actually eliminating the ambiguities, with a negligible implementation complexity, rather than just defocusing them as most other techniques do, making it applicable to distributed targets [4].

Also, more complex alternatives to the thresholding and blanking approach, as well as to the contrast minimization method, can be looked for, in order to achieve a further ambiguity suppression with a negligible removal of useful signal, also assuming weak range ambiguities.

Furthermore, looking for other different sequences of waveforms could be of great interest, which allow for a different smearing of the range ambiguous energy across the Doppler spectrum, and thus for different ambiguity suppression capabilities. Specifically, the Doppler spectrum behaviour has to be investigated while looking for other waveform variation schemes, as alternatives to the already described cyclically-shifted and up- and down- chirps. In this context, a further analysis, of course, has to be performed on cyclically-shifted chirps, in order to reduce the number of different waveforms, as in practice transmitting a too big number of them is not recommended because of the complexity of the problem.

Finally, the range ambiguity suppression capability of the proposed waveform-encoded SAR concept has to be accounted in the design of novel SAR systems; in particular, such a concept could be applied also to the case of high-resolution wide-swath SAR systems, as it could lead to an improvement of the system design flexibility, at the reasonable cost of employing different waveforms on transmit.

Bibliography

[1] Delphine Cerutti-Maori, Ishuwa Sikaneta, Jens Klare, and Christoph H Gierull. Mimo sar processing for multichannel high-resolution wide-swath radars. *IEEE Transactions on Geoscience and Remote Sensing*, 52(8):5034–5055, 2014.

[2] John C Curlander and Robert N McDonough. Synthetic aperture radar- systems and signal processing(book). *New York: John Wiley & Sons, Inc, 1991.*, 1991.

[3] L Cutrona, W Vivian, E Leith, and G Hall. Synthetic aperture radars: A paradigm for technology evolution. *IRE Trans. Military Electron*, pages 127–131, 1961.

[4] Jørgen Dall and Anders Kusk. Azimuth phase coding for range ambiguity suppression in sar. In *Geoscience and Remote Sensing Symposium, 2004. IGARSS'04. Proceedings. 2004 IEEE International*, volume 3, pages 1734–1737. IEEE, 2004.

[5] Anthony Freeman. On ambiguities in sar design. 2006.

[6] Nicolas Gebert, Gerhard Krieger, and Alberto Moreira. Digital beamforming on receive: Techniques and optimization strategies for high-resolution wide-swath sar imaging. *IEEE Transactions on Aerospace and Electronic Systems*, 45(2):564–592, 2009.

[7] Scientific SAR User's Guide. Alaska sar facility scientific sar user's guide. *Analyst*, 1993.

[8] G Krieger, M Younis, N Gebert, S Huber, F Bordoni, A Patyuchenko, and A Moreira. Advanced concepts for high-resolution wide-swath sar imaging. In *8th European Conference on Synthetic Aperture Radar*, pages 1–4. VDE, 2010.

[9] Gerhard Krieger, Nicolas Gebert, and Alberto Moreira. Multidimensional waveform encoding: A new digital beamforming technique for synthetic aperture radar remote sensing. *IEEE Transactions on Geoscience and Remote Sensing*, 46(1):31–46, 2008.

[10] FK Li and WTK Johnson. Ambiguities in spacebornene synthetic aperture radar systems. *IEEE Transactions on Aerospace and Electronic Systems*, (3):389–397, 1983.

[11] Josef Mittermayer and J Márquez Martínez. Analysis of range ambiguity suppression in sar by up and down chirp modulation for point and distributed targets. In *Geoscience and Remote Sensing Symposium, 2003. IGARSS'03. Proceedings. 2003 IEEE International*, volume 6, pages 4077–4079. IEEE, 2003.

[12] A Moreira and T Misra. On the use of the ideal filter concept for improving sar image quality. *Journal of electromagnetic waves and applications*, 9(3):407–420, 1995.

[13] Alberto Moreira, Pau Prats-Iraola, Marwan Younis, Gerhard Krieger, Irena Hajnsek, and Konstantinos P Papathanassiou. A tutorial on synthetic aperture radar. *IEEE Geoscience and remote sensing magazine*, 1(1):6–43, 2013.

[14] Chris Oliver and Shaun Quegan. *Understanding synthetic aperture radar images*. SciTech Publishing, 2004.

[15] R Keith Raney and G Julius Princz. Reconsideration of azimuth ambiguities in sar. *IEEE Transactions on Geoscience and Remote Sensing*, (6):783–787, 1987.

[16] Martin Süß, Bernhard Grafmüller, and Rolf Zahn. A novel high resolution, wide swath sar system. In *IGARSS 2001. Scanning the Present and Resolving the Future. Proceedings. IEEE 2001 International Geoscience and Remote Sensing Symposium (Cat. No. 01CH37217)*, volume 3, pages 1013–1015. IEEE, 2001.

[17] Michelangelo Villano. *Staggered synthetic aperture radar*. DLR, Deutsches Zentrum für Luft- und Raumfahrt, 2016.

[18] Michelangelo Villano, Gerhard Krieger, Marc Jäger, and Alberto Moreira. Staggered sar: Performance analysis and experiments with real data. *IEEE Transactions on Geoscience and Remote Sensing*, 55(11):6617–6638, 2017.

[19] Michelangelo Villano, Gerhard Krieger, and Alberto Moreira. Staggered sar: High-resolution wide-swath imaging by continuous pri variation. *IEEE Transactions on Geoscience and Remote Sensing*, 52(7):4462–4479, 2014.

[20] Michelangelo Villano, Gerhard Krieger, and Alberto Moreira. Nadir echo removal in synthetic aperture radar via waveform diversity and dual-focus postprocessing. *IEEE Geoscience and Remote Sensing Letters*, 15(5):719–723, 2018.

[21] Michelangelo Villano, Gerhard Krieger, and Alberto Moreira. Waveform-encoded sar: A novel concept for nadir echo and range ambiguity suppression. In *EUSAR 2018; 12th European Conference on Synthetic Aperture Radar*, pages 1–6. VDE, 2018.

[22] CA Willey. Synthetic aperture radars–a paradigm for technology evolution. *IEEE Trans. Aerospace Elec. Sys*, 21:440–443, 1985.